UNIVERSITÉ DU QUÉBEC À MONTRÉAL

HISTOIRE TECTONO-MÉTAMORPHIQUE DE LA ZONE DE CISAILLEMENT TAUREAU ORIENTALE ET SES IMPLICATIONS POUR L'EXHUMATION DE LA CROÛTE MOYENNE DANS LA PROVINCE DE GRENVILLE

MÉMOIRE

PRÉSENTÉ

COMME EXIGENCE PARTIELLE

DE LA MAÎTRISE EN SCIENCES DE LA TERRE

PAR

RENAUD SOUCY LA ROCHE

JANVIER 2014

REMERCIEMENTS

Je voudrais tout d'abord remercier mes directeur et co-directeur Alain Tremblay (UQÀM) et Félix Gervais (École Polytechnique de Montréal) pour leur soutien, leurs commentaires constructifs et l'aide précieuse qu'ils m'ont offerte tout au long de ma maîtrise. Jim Crowley (Boise State University) et Gilles Ruffet (Géosciences Rennes), mes co-auteurs pour le manuscrit du chapitre 2, sont aussi remerciés pour leur assistance essentielle lors de l'acquisition et de l'interprétation des données de géochronologie et de thermochronologie, respectivement. J'aimerais de plus remercier les évaluateurs externes Alexandre Zagorevski (Commission Géologique du Canada – Ottawa) et Léopold Nadeau (Commission Géologique du Canada – Québec) qui ont contribué à améliorer ce mémoire.

Je voudrais aussi remercier Morgann Perrot et Xavier Vasseaud pour leur assistance sur le terrain. Lang Shi, du laboratoire de microsonde électronique de l'université McGill est grandement remercié pour toute l'aide apportée lors de l'acquisition de la composition chimique des minéraux utilisés en thermobarométrie. Finalement, je voudrais remercier Michelle Laithier pour ses conseils précieux et utiles pour la conception de figures et l'élaboration d'affiches pour les conférences où j'ai présenté des résultats préliminaires.

J'ai reçu du soutien financier de la part du Conseil de Recherche en Sciences Naturelles et en Génie (CRSNG) lors de ma première année de maîtrise (2011-2012) tandis que le Fonds de recherche du Québec – Nature et Technologies (FRQNT) m'a offert une bourse d'études graduées lors de ma deuxième année (2012-2013). Le projet a aussi été financé par un financement du programme de subventions à la découverte (individuelles) du CRSNG octroyé à Alain Tremblay (PG 105669) et par le financement interne de l'École Polytechnique de Montréal octroyé à Félix Gervais.

TABLE DES MATIÈRES

LISTE DES FIGURES

Figure Page

LISTE DES TABLEAUX

LISTE DES ABRÉVIATIONS

Alm	almandine
Ann	annite
An	anorthite
Ap	apatite
Bt	biotite
Cal	calcite
Cpx	clinopyroxène
Di	diopside
Dol	dolomite
FeTr	trémolite ferrifère
Gr	graphite
Grt	grenat
Grs	grossulaire
Hbl	hornblende
Ilm	ilménite
Kfs	feldspath potassique
Mnz	monazite
Ol	olivine
Opx	orthopyroxène
Phl	phlogopite
Pl	feldspath plagioclase
Prp	pyrope
Qtz	quartz
Rt	rutile
Scp	scapolite
Sil	sillimanite
Spl	spinelle
Sps	spessartine
Srp	serpentine
Tr	trémolite
Ts	tschermakite
Ttn	titanite
Tur	tourmaline
Zrn	zircon

Abbréviations des minéraux d'après Kretz (1983)

RÉSUMÉ

Cette étude examine les mécanismes d'exhumation des unités de la croûte moyenne au sein d'une orogénèse collisionnelle. L'histoire tectono-métamorphique de la région de la Mauricie, dans la Province géologique du Grenville, a été étudiée afin de comprendre comment le domaine de Mékinac-Taureau, un dôme métamorphique de haut-grade, a été amené au niveau d'exposition actuel. Les études macro- et micro-structurales ont révélé le sens de cisaillement vers l'est-sud-est de la zone de cisaillement Taureau orientale, une structure d'extension majeure responsable de l'exhumation du domaine de Mékinac-Taureau. Suite à une analyse pétrographique et une caractérisation de la zonation chimique des minéraux, les conditions métamorphiques prograde et rétrograde ont été calculées sur cinq échantillons de métapélite et un échantillon d'amphibolite du domaine de Mékinac-Taureau et du domaine sus-jacent de Shawinigan. Deux pegmatites ont été analysées par géochronologie U-Pb sur zircon pour déterminer l'âge de la déformation et, par extension, l'âge du métamorphisme et de l'exhumation. Le pic métamorphique dans le domaine de Mékinac-Taureau a atteint des conditions de ~1075 MPa et ~825°C avant 1084 ± 18 Ma. Cet évènement métamorphique est considéré comme le résultat d'un chevauchement dirigé vers le nord-ouest et de l'épaississement crustal à l'échelle régionale. Des conditions de métamorphisme rétrograde variant de 800 à 700 MPa et de 775 à 675°C ont été enregistrées dans les niveaux structuraux supérieurs du domaine de Mékinac-Taureau. Le domaine de Shawinigan a enregistré des conditions de pression et de température variant de 850 à 625 MPa et de 775 à 700°C, des valeurs qui sont équivalentes ou légèrement inférieures à celles obtenues avec les échantillons rétrogressés des niveaux structuraux supérieurs du domaine de Mékinac-Taureau. La zone de cisaillement Taureau orientale était active autour de 1064 ± 12 Ma, pendant et/ou après le métamorphisme rétrograde documenté dans le domaine de Mékinac-Taureau. Selon les données de thermochronologie $^{40}Ar/^{39}Ar$ sur amphibole et biotite, la région a refroidi sous 550-600°C à ~1000-1030 Ma et sous 450°C à ~900-970 Ma. Les caractéristiques structurales et métamorphiques de la Mauricie sont similaires à celles observées dans les niveaux structuraux inférieurs des dômes métamorphiques extensifs formés lors de l'effondrement orogénique post-convergent. Les domaines de Mékinac-Taureau et de Shawinigan ont donc probablement été exhumés par un processus similaire. Cette étude appuie le modèle d'effondrement orogénique récemment proposé pour expliquer l'exhumation de dômes métamorphiques de la Province de Grenville. Le fait que cette phase d'exhumation soit synchrone avec la phase de compression Ottawan enregistrée ailleurs demeure énigmatique.

Mots clés : Province de Grenville, zone de cisaillement Taureau orientale, exhumation de la croûte moyenne, géochronologie, thermobarométrie

INTRODUCTION

Le terme «orogénèse» réfère à la formation de régions montagneuses à la surface de la Terre suite à la déformation de la lithosphère terrestre associée à des frontières de plaques tectoniques convergentes ou divergentes (Ring et al. 1999). Dans les orogénèses convergentes (collisionnelles), l'exhumation (i.e. le déplacement des roches vers la surface de la Terre; England and Molnar, 1990) de roches de haut grade métamorphique au sein des zones internes des orogénèses convergentes est commune, mais les mécanismes impliqués sont variés et sujets à de nombreux débats (ex : Ring et al. 1999; Gapais et al. 2009, Gervais et Brown, 2011). L'exhumation d'unités de la croûte moyenne a, par exemple, été expliquée par un fluage chenalisé syn-convergent (ex : Beaumont et al. 2001, 2006), par un effondrement gravitaire post-convergent (ex : Dewey, 1988; Rey et al. 2001) associé au développement de dômes métamorphiques extensifs (ex : Brun et al. 1994; Tirel, 2004; Tirel et al. 2004, 2006, 2008; Rey et al. 2009) et par diapirisme (e.g. Calvert et al. 1999; Teyssier and Whitney, 2002; Gervais et al. 2004).

La Province de Grenville, qui représente la frontière sud-est du paléo-continent protérozoïque Laurentia, est considérée comme le résultat d'une large orogénèse, chaude et de longue durée (selon la classification de Beaumont et al. 2006) caractérisée par une période prolongée d'épaississement crustal (>100 m.y) affectant une région de plus de 600 km de largeur (Rivers, 2008, 2009, 2012; Hynes and Rivers, 2010). Suivant l'idée de Dewey et Burke (1973), Rivers (2008) a d'ailleurs proposé l'existence d'un plateau orogénique de type Himalayen et d'une croûte ayant été doublement épaissie dans les zones internes de cette province géologique. Dans un tel contexte, la croûte moyenne est typiquement affaiblie par des phénomènes de fusion partielle et peut fluer latéralement (Rosenberg and Handy, 2005), un processus connu sous le nom de fluage chenalisé (*channel flow*; ex : Beaumont et al. 2006) qui mènerait à un effondrement syn-orogénique (e.g. Godin, 2006). L'importance du fluage chenalisé au sein de la croûte moyenne lors de l'orogénèse grenvillienne a été récemment évaluée (Jamieson et al. 2007, 2010; Rivers, 2008, 2009), mais toutes les caractéristiques typiques du fluage chenalisé n'ont pas encore été reconnues dans le Grenville. Toutefois, les

travaux récents ont aussi montré que la Province de Grenville est constituée de segments de la croûte profonde, moyenne et supérieure (Rivers, 2008, 2012 et références inclues), ce qui contraste avec l'interprétation traditionnelle de ces roches comme représentant une tranche homogène à travers la croûte moyenne. La reconnaissance de niveaux crustaux variés dans la Province de Grenville a donc favorisé la recherche sur les mécanismes d'exhumation responsables de son architecture actuelle (ex : Indares et al. 1998; Selleck et al. 2005, Jamieson et al. 2007, 2010 and Rivers, 2008, 2009, 2012). Un modèle récent de Rivers (2008, 2012) présente la Province de Grenville dans son ensemble comme une série de dômes métamorphiques extensifs de haut-grade recouverts par des fragments de la croûte supérieure, une architecture résultant de l'effondrement d'un plateau orogénique. Plusieurs régions de la Province de Grenville exposent des failles normales et des zones de cisaillement en extension qui juxtaposent donc des dômes métamorphiques de la croûte moyenne à des segments de la croûte supérieure (Rivers, 2008, 2009, 2012). Ces régions incluent de grandes parties du nord-est de la Province de Grenville, du sud-est de la *Composite Arc Belt*, du nord-ouest de la *Frontenac-Adirondack Belt* et de plus petites régions telles que le domaine de Natashquan et la région de la Mauricie (Fig. 2.1). Finalement, le diapirisme a été proposé comme mécanisme d'exhumation de dômes métamorphiques pour de rares localités de la Province de Grenville (e.g. Gervais et al. 2004)

Ce mémoire présente de nouvelles données structurales, métamorphiques et géochronologiques des roches grenvilliennes de la région de la Mauricie qui sont essentielles à la compréhension de l'exhumation d'un dôme de roches métamorphiques de haut-grade exposant de la croûte moyenne et connu sous le nom de domaine de Mékinac-Taureau (Nadeau and Brouillette, 1994, 1995). Des analyses macro- et micro-structurales permettent de contraindre l'histoire cinématique de la zone de cisaillement Taureau orientale (nouveau nom), une structure régionale majeure responsable de l'exhumation du domaine de Mékinac-Taureau. La thermobarométrie classique a été employée sur une série d'échantillons de la région afin d'évaluer les conditions de pression et température (P-T) du pic métamorphique ainsi que l'évolution métamorphique rétrograde des domaines de Mékinac-Taureau et de Shawinigan. Étant donné les difficultés d'acquisition de données fiables de thermobarométrie

dans des roches de si haut grade métamorphique, les précautions nécessaires ont été prises lors de la sélection des minéraux analysés, et les résultats ont été interprétés consciencieusement. Enfin, les contraintes temporelles du pic métamorphique et de l'exhumation ont été obtenues par la géochronologie U-Pb effectuées sur deux échantillons de pegmatite, alors que la thermochronologie $^{40}Ar/^{39}Ar$ sur amphiboles et biotites a permis d'estimer l'âge et la durée du refroidissement post-métamorphique dans la région. L'ensemble de ces contraintes structurales, thermobarométriques, géochronologiques et thermochronologiques a permis de proposer un mécanisme d'exhumation probable pour le domaine de Mékinac-Taureau.

Le mémoire de maîtrise est constitué de trois chapitres. Le premier chapitre présente les travaux antérieurs effectués sur les roches métamorphiques du Grenville dans la région de Shawinigan, la problématique, les objectifs spécifiques du projet et la méthodologie de recherche. Le deuxième chapitre présente l'essentiel des travaux effectués sous la forme d'un manuscrit d'article (rédigé en anglais) en voie d'être soumis pour publication. Finalement, le troisième chapitre regroupe et discute brièvement les résultats de la recherche qui n'ont pas été inclus (principalement par manque d'espace et/ou de pertinence) dans le chapitre 2.

CHAPITRE I

CONTEXTE DU PROJET

1.1 Travaux antérieurs et problématique

Le terrain d'étude est situé dans les régions de Shawinigan et de Rivière-Mékinac (feuillets SNRC 31 I/10 et 31 I/15 au 1 :50,000), à quelques dizaines de kilomètres au nord de la ville de Trois-Rivières en Mauricie (Québec). Cette recherche comporte toutefois des implications s'appliquant à une région beaucoup plus vaste, puisqu'elle concerne le domaine de Mékinac-Taureau en entier. Les travaux antérieurs cités dans ce chapitre concernent spécifiquement le secteur étudié ou sont particulièrement pertinents en ce qui concerne l'évolution tectonique de cette région. La cartographie initiale a été effectuée par Béland (1961) et par Rondot (1962) sur les feuillets 31 I/10 and 31 I/15, respectivement. Par la suite, Fergusson (1974), Martignole et Nantel (1982), Herd et al. (1986), Nadeau et Corrigan, (1991), Nadeau et al. (1992), Corrigan (1995), Lévesque (1995), Corrigan et van Breemen (1997) ainsi que Martignole et Friedman (1998) ont effectué des travaux sur l'histoire tectonique et métamorphique de la région. Une compilation cartographique à l'échelle 1 : 250 000 a été réalisée par Nadeau et Brouillette (1995) pour la grande région de Trois-Rivières (feuillet SNRC 31I). Enfin, une compilation géologique à l'échelle 1 : 125 000 a été produite par Nadeau et al (2009), celle-ci concerne spécifiquement les régions de Shawinigan et de Rivière-Mékinac, en plus d'inclure certains feuillets au 1 : 50 000 situés au nord et à l'est (feuillets SNRC 31P/01, 32P/02, 31 I/09, 31 I/16).

Ces différents travaux montrent que la région de la Mauricie peut être séparée en trois grands domaines lithotectoniques (Fig. 2.1). (1) le domaine de Mékinac-Taureau forme un dôme de roches métamorphisées au faciès granulite et représente le niveau structural le plus profond. Il est en contact tectonique avec (2) le terrain de Morin le long de la zone de cisaillement Taureau. Le terrain de Morin est principalement exposée sur le flanc ouest du domaine de Mékinac-Taureau, bien qu'une mince bande de ce terrain, dénommée le domaine de Shawinigan, s'étend jusque sur la bordure est du domaine de Mékinac-Taureau. Les unités

du terrain de Morin ont été métamorphisées au faciès granulite, mais le domaine de Shawinigan est dominé par le faciès amphibolite supérieur, quoique possiblement le résultat du métamorphisme rétrograde. Enfin, (3) le domaine de Portneuf-Mauricie, structuralement le plus élevé, repose en contact tectonique le long de la zone de cisaillement de Tawachiche avec le domaine de Shawinigan. La zone de cisaillement de Tawachiche est une zone d'extension oblique considérée comme ayant été active autour de 1080-1040 Ma (Lemieux, 1992; Corrigan et van Breemen, 1997).

Sur le flanc ouest du domaine de Mékinac-Taureau, la zone de cisaillement Taureau a été interprétée comme un chevauchement oblique actif jusqu'à ~1074 Ma (Martignole et Friedman, 1998). Par contraste, les études métamorphiques effectuées sur le flanc est (Martignole et Nantel, 1982; Herd et al.; 1986; Corrigan, 1995; Lévesque, 1995) indiquent une probable diminution du grade métamorphique entre le mur du cisaillement (domaine de Mékinac-Taureau au faciès granulite) et le toit du cisaillement (domaine de Shawinigan au faciès amphibolite supérieur) qui serait plutôt compatible avec un sens de cisaillement normal (Nadeau et al. 2008). Toutefois, un contraste métamorphique net entre les deux domaines n'avait pas été établi puisque les études antérieures ne comparaient pas systématiquement des échantillons du mur et du toit du cisaillement. De plus, ni la cinématique du cisaillement, ni l'âge de la déformation n'avaient encore été clairement établis. Ce travail de maîtrise vise principalement à déterminer l'évolution tectono-métamorphique de la zone de cisaillement Taureau orientale en utilisant des techniques modernes et d'en discuter les implications en termes d'exhumation des terrains de haut grade métamorphique au sein de l'orogène de Grenville.

1.2 Méthodes de travail

La majeure partie du travail de terrain a été effectué durant l'été 2011 pendant une période de 5 semaines. Il s'agissait principalement de caractériser macroscopiquement les différentes unités lithologiques de la région d'étude, d'évaluer leur état de déformation finie (type de tectonite, orientation d'éléments structuraux, etc.), de déterminer la cinématique de

la zone de cisaillement Taureau orientale, et d'effectuer un échantillonnage systématique pour les analyses géochimiques et géochronologiques subséquentes. Un séjour de 2 semaines supplémentaires a été effectué au courant de l'été 2012 afin de confirmer et/ou vérifier certaines données structurales, de vérifier des hypothèses de travail et récolter des échantillons supplémentaires. Au total, environ 200 affleurements ont été visités et plus de 80 échantillons ont été collectés. Quarante lames minces ont été produites. Les observations pétrographiques ont été effectuées dans le laboratoire de microscopie de l'Université du Québec à Montréal (UQÀM) afin de décrire les paragenèses métamorphiques dans le but de déterminer qualitativement le degré de métamorphisme auquel ont été soumises les roches des domaines de Mékinac-Taureau et de Shawinigan. Ces observations ont aussi permis de sélectionner les six échantillons les plus prometteurs pour les analyses thermobarométriques quantitatives. Les analyses à la microsonde électronique ont été effectuées à l'Université McGill. La composition chimique de certains minéraux analysés a ainsi permis d'établir quantitativement les conditions de température et de pression du métamorphisme grâce au logiciel de thermobarométrie TWEEQU (Berman, 1991). Deux échantillons ont ensuite été envoyés au *Isotope Geology Laboratory* de Boise State University (Idaho, États-Unis d'Amérique) où ont été effectué des datations U-Pb par spectrométrie de masse à source plasma couplée à une source laser (LA-ICPMS – *laser ablation inductively coupled plasma mass spectrometry*). Les dates obtenues ont été essentielles afin de contraindre la fin du pic métamorphique dans la région d'étude et la chronologie de la zone de cisaillement Taureau orientale. Enfin, six autres échantillons ont été analysés au laboratoire de spectrométrie des gaz rares de Géosciences Rennes (France) pour la thermochronologie $^{40}Ar/^{39}Ar$. Ces dernières analyses ont permis d'évaluer l'âge du refroidissement post-pic métamorphique et ainsi compléter notre documentation de l'évolution tectonique de la région.

1.3 Contribution des différents coauteurs du manuscrit du chapitre 2

Le manuscrit présenté au chapitre 2 de ce mémoire de maîtrise est signé par quatre coauteurs : Alain Tremblay (directeur de maîtrise, UQAM), Félix Gervais (codirecteur de maîtrise, Polytechnique Montréal), Jim Crowley (Boise State University, Idaho, États-Unis) et

Gilles Ruffet (Géosciences Rennes, France). Je veux donc spécifier ici les contributions respectives de chaque coauteur afin de mettre l'accent sur le travail que j'ai réalisé moi-même dans le cadre de cette maîtrise.

Au début de l'été 2011, j'ai observé quelques affleurements-clés de la région d'étude en compagnie de mes directeurs de recherche afin de me familiariser avec la géologie régionale. Les travaux de terrains subséquents ont été réalisés par moi-même avec l'aide d'une ou d'un assistant de terrain (Morgann Perrot et Xavier Vasseaud). Les visites occasionnelles de mon directeur et de mon codirecteur m'ont évidemment permis de bonifier mes observations et de discuter certaines hypothèses.

Les résultats et interprétations présentés dans ce mémoire sont principalement le fruit de mes réflexions personnelles. Je n'ai toutefois évidemment pas réalisé moi-même toutes les manipulations de laboratoire pour les analyses géochronologiques. Pour la géochronologie U-Pb, Jim Crowley s'est occupé de la préparation des échantillons, de l'acquisition des données isotopiques et géochimiques et de la rédaction de la section 2.6.2 de ce mémoire. Je me suis cependant personnellement occupé de l'échantillonnage, de l'interprétation des données et de l'intégration des résultats dans le mémoire final. Les analyses $^{40}Ar/^{39}Ar$ ont été réalisées par Gilles Ruffet, qui a aussi grandement contribué aux sections 2.7.1 et 2.7.2 du mémoire. J'ai collecté moi-même les échantillons analysés, ai interprété les âges $^{40}Ar/^{39}Ar$ et les ai intégrés aux autres données récoltées durant cette étude.

Les premières versions du chapitre 2 sont donc essentiellement le produit de mes travaux et réflexions personnelles, excluant les exceptions mentionnées ci-haut. J'ai par la suite évidemment bénéficié des révisions et commentaires critiques de mes coauteurs en fonction de leur domaine d'expertise respectif, mais j'assume l'entière responsabilité de l'ensemble des résultats et interprétations présentés de ce mémoire.

CHAPITRE II

TECTONO-METAMORPHIC HISTORY OF THE EASTERN TAUREAU SHEAR ZONE, MAURICIE AREA : ITS IMPLICATIONS FOR THE EXHUMATION OF MID-CRUSTAL UNITS OF THE GRENVILLE PROVINCE

Abstract

This study investigates the exhumation mechanisms of mid-crustal units in a collisional orogen. The tectono-metamorphic history of the Mauricie area, central Grenville Province, was studied to understand how the Mékinac-Taureau domain, a high-grade metamorphic dome, was brought to the current level of exposure. Macro- and micro-structural analysis reveal the top-down-to-the-ESE sense of shear on the eastern Taureau shear zone, a major extensional structure that exhumed the Mékinac-Taureau domain and juxtaposes it with the lower grade Shawinigan domain. Following petrographical analysis and characterization of the chemical zoning of minerals, prograde and retrograde metamorphic conditions were determined on five samples of metapelite and one of amphibolite of the Mékinac-Taureau and overlying Shawinigan domains. Two pegmatites were analyzed by U-Pb geochronology on zircon to determine the age of deformation and, by extension, the age of metamorphism and exhumation. Peak metamorphism in the Mékinac-Taureau domain attained P-T conditions of ~1075 MPa and ~825°C prior to 1084 ± 18 Ma. This metamorphic event is inferred to be the result of northwestward thrusting and regional crustal thickening. Retrograde conditions varying from 775 to 675°C and from 800 to 700 MPa were registered in the upper structural levels of the Mékinac-Taureau domain. The Shawinigan domain records P-T conditions varying from 850 to 625 MPa and from 775 to 700°C, P-T values that are equivalent or of a slightly lower metamorphic grade as compared with retrogressed samples from the margin of the Mékinac-Taureau domain. The eastern Taureau shear zone was active at 1064 ± 12 Ma, during and/or after retrograde metamorphism documented in the Mékinac-Taureau domain. On the basis of $^{40}Ar/^{39}Ar$ thermochronology on amphibole and biotite, the area cooled below 550-600°C at ~1000-1030 Ma and below 450°C at ~900-970 Ma. Structural and metamorphic characteristics of the Mauricie area are similar to those expected from the

structurally lower levels of a metamorphic core complex formed during post-convergence orogenic collapse. The Mékinac-Taureau and Shawinigan domains were thus probably exhumed by a similar process. Our study supports the orogenic collapse model recently proposed to explain the exhumation of mid-crustal metamorphic core complexes in the Grenville Province. The fact that this exhumation phase is synchronous with the Ottawan compressive phase registered elsewhere remains enigmatic.

2.1 Introduction

Orogens refer to any mountainous area of the Earth's surface ensuing from localized deformation, which can be associated with convergent or divergent plate boundary setting (Ring et al. 1999). In convergent (collisional) orogens, exhumation (i.e. the displacement of rocks towards Earth's surface; England and Molnar, 1990) of high-grade rocks in the hinterland of convergent orogens is common, but the exact mechanisms are subject to many debates (e.g. Ring et al. 1999; Gapais et al. 2009; Gervais and Brown, 2011). Exhumation of mid-crustal units for instance has been explained by syn-convergent channel flow (e.g. Beaumont et al. 2001, 2006), by post-convergent gravitational collapse (e.g. Dewey, 1988; Rey et al. 2001) and associated metamorphic core complexes (MCC) development (e.g. Brun et al. 1994; Tirel, 2004; Tirel et al. 2004, 2006, 2008; Rey et al. 2009) and by buoyancy-driven rise of migmatitic diapirs (e.g. Calvert et al. 1999; Teyssier and Whitney, 2002; Gervais et al. 2004).

The Grenville Province represents the southeastern boundary of Proterozoic Laurentia and is considered as a large hot long-duration orogen (classification of Beaumont et al. 2006) characterized by a prolonged period of heating and crustal thickening (>100 m.y.) affecting a >600 km large area (Rivers, 2008, 2009, 2012; Hynes and Rivers, 2010). Following the idea of Dewey and Burke (1973), Rivers (2008) suggested the presence of a Himalayan-type orogenic plateau in the hinterland of the orogeny that resulted from thickening of the continental crust. In such setting, the mid-crust is typically weakened by partial melting at depth and may flow laterally (Rosenberg and Handy, 2005), a process known as "channel flow" (e.g.

Beaumont et al. 2006) leading to orogenic collapse (e.g. Godin, 2006). The importance of ductile flow in the mid-crust of the Grenville orogen was assessed recently (Jamieson et al. 2007, 2010; Rivers, 2008, 2009), but all the characteristics of a channel flow were not recognized yet. However, recent work demonstrated that the Grenville Province is composed of lower, mid and upper crustal segments (Rivers, 2008, 2012 and references therein), contrasting with the long-lasting interpretation of this province as a homogeneous slice through the mid-crust. The recognition of various crustal levels in the Grenville Province therefore promoted research about the mechanisms of exhumation responsible for the current architecture of the orogen (e.g. Indares et al. 1998; Selleck et al. 2005, Jamieson et al. 2007, 2010 and Rivers, 2008, 2009, 2012). A recent model of Rivers (2008, 2012) presents the Grenville Province as a series of high-grade mid-crustal core complexes overlaid by fragments of the upper crust resulting from the collapse of an orogenic plateau. Multiple regions of the Grenville Province that exhibit normal-sense faults and shear zones juxtaposing the potential mid-crustal core complexes with upper crustal segments were recognized in Rivers (2008, 2009, and 2012). These regions include large parts of the northeastern Grenville Province, the southeastern Composite Arc Belt, the northwestern Frontenac-Adirondack Belt and smaller areas such as the Natashquan domain and the Mauricie area (Fig. 2.1). Finally, diapirism was proposed in rare localities of the Grenville Province to explain the exhumation of high grade gneiss domes (e.g. Gervais et al. 2004)

This contribution presents new data from the Mauricie area that is essential to understand the exhumation of a mid-crustal high-grade dome known as the Mékinac-Taureau domain (Nadeau and Brouillette, 1994, 1995). Detailed macro- and micro-structural analysis reveal the kinematic history of the eastern Taureau shear zone, a major regional structure, responsible for the exhumation of the Mékinac-Taureau domain. Classical thermobarometry was also applied to six selected samples in order to evaluate the peak pressure and temperature (P-T) conditions and the retrograde path of the Mékinac-Taureau and overlying Shawinigan domains. Considering the difficulty to acquire reliable thermobarometric data in such high grade rocks, great precautions were taken in the selection of analyzed minerals and results were carefully interpreted. Finally, the timing of peak metamorphism and exhumation

was assessed via U-Pb geochronology on two pegmatites, whereas $^{40}Ar/^{39}Ar$ thermochronology on amphibole and biotite from six samples provided precise timing constrains for the cooling of this area. These structural, thermobarometric, geochronologic and thermochronologic constraints were compared to different characteristics observed in type localities of well known orogenies or predicted by analog/numerical modeling of different exhumation processes. The most relevant process was then proposed for the Mauricie area.

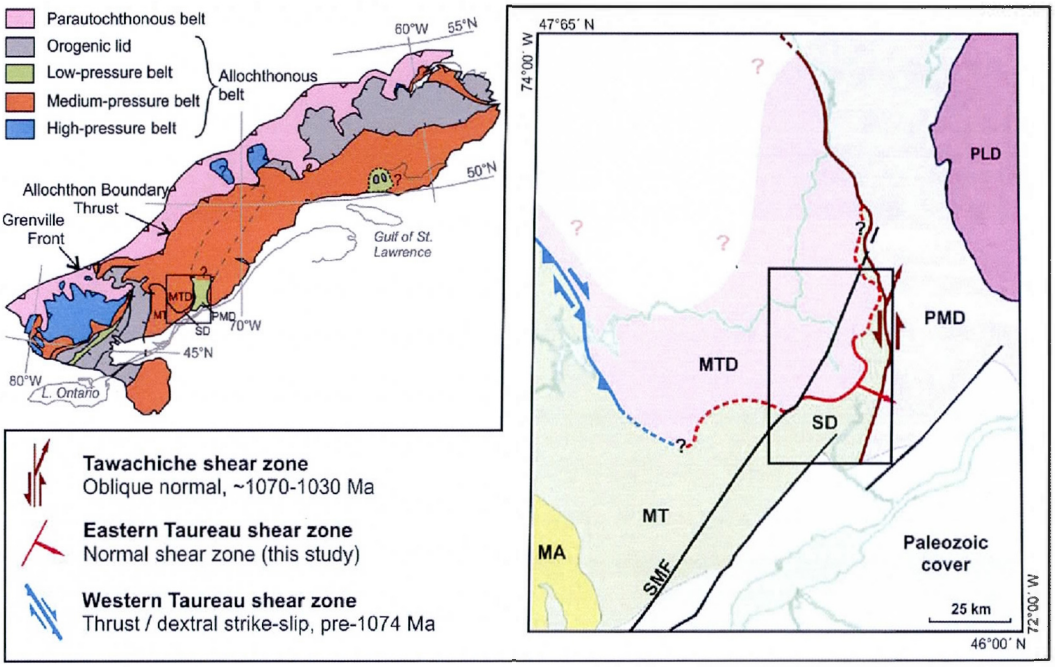

Fig. 2.1 Simplified geologic map of the Mauricie area (modified from Nadeau and Brouillette, 1995). Black rectangle represents study area shown on figure 2.2. Inset shows the simplified tectonic subdivisions of the Grenville Province (modified from Rivers, 2008) with the location of the Mauricie area (black rectangle). MT—Morin terrane, MTD—Mékinac–Taureau domain, SD—Shawinigan domain, PMD—Portneuf–Mauricie domain, PLD—Parc des Laurentides domain, MA—Anorthosite, SMF—St. Maurice fault.

2.2 Geological setting

The Grenville Province comprises rocks of southeastern Laurentia that were affected by multiple orogenic events from late Paleoproterozoic until early Neoproterozoic (Rivers, 1997,

Hynes and Rivers, 2010). Paleoproterozoic events include the ~1970-1700 Ma Penokean-Makkovikian orogenies and the ~1710-1600 Ma Labradorian orogeny. Early to Middle Mesoproterozoic events include the ~1520-1450 Ma accretionary Pinwarian orogeny, the ~1400 Ma accretion of the Montauban island arc and the ~1245-1220 Ma Elzevirian accretionary orogeny (Hynes and Rivers, 2010 and references therein). Subsequently, tectonic setting evolved into a continent-continent collision comprising the ~1190-1140 Ma Shawinigan orogeny and the ~1090-980 Ma Grenvillian orogeny (e.g. Rivers et al. 1989; McLelland et al. 1996; Rivers, 1997, 2008). The Grenvillian orogeny can be separated into two main phases according to their age and spatial extent (Rivers et al. 1997, Rivers, 2008). The Ottawan phase affected the hinterland of the Grenville Province during a first pulse of compression from 1090 to 1020 Ma. The rocks affected by this orogenic phase are far-travelled with respect to the Laurentian margin and are referred to as allochthonous belts. This contrasts with the structurally underlying parautochthonous belt, located to the northwest, which comprises rocks of the Laurentian margin that can be correlated with the Grenvillian foreland developed in the adjacent Archean and Proterozoic Superior provinces. The latter belt was deformed and metamorphosed during a second phase of compression, known as the Rigolet, between 1000 and 980 Ma. The allochthonous and the parautochthonous belts are separated by the Allochthon Boundary Thrust (ABT), whereas the northwestern limit of the Grenville Province is delineated by the Grenville Front (GF; Rivers et al. 1989). Both tectonic boundaries are crustal-scale, gently to moderately southeast-dipping shear zones that can be recognized on magnetic maps or in the field throughout the whole length of the Grenville Province (Fig. 2.1).

Rivers (2008, 2012) subdivided the allochthonous hinterland affected by the Ottawan orogeny into four belts according to their relative position in the crust (Fig. 2.1). From base to top, (1) the allochthonous high-pressure belt (aHP Belt) comprises nappes of relict eclogitic material overprinted by granulite-facies metamorphism. The aHP belt is directly underlain by the ABT in two areas of the western and central Grenville Province. It represents pieces of the base of the doubly-thickened orogenic crust that have been incorporated into the mid crust during their exhumation. (2) The allochthonous medium-pressure belt (aMP Belt) is the most

extensive belt, extending along the whole length of the Grenville Province. It is composed of amphibolite- to granulite-facies mid-crustal units of various compositions that are commonly migmatitic. The upper crust is preserved as (3) the allochthonous low-pressure belt (aLP Belt) and (4) the Ottawan Orogenic Lid (OOL). The aLP Belt is exposed only in small areas of the southeastern, central and western Grenville Province. It consists of greenschist to amphibolite-facies rocks that were juxtaposed to the aMP Belt via extensional shear zones. Finally, the structurally overlying OOL occupies large zones of the northeast and southwest Grenville Province. It comprises units that escaped penetrative Ottawan metamorphism and deformation, although they may have been subjected to older tectono-metamorphic episodes.

2.3 Regional geology

The present study is located in the Mauricie area, central Grenville Province, comprising rocks of the aMP and aLP belts that have been subdivided into three main lithotectonic domains (Fig. 2.1 and 2.2; Nadeau and Corrigan, 1991; Nadeau and Brouillette, 1994, 1995). The Mékinac-Taureau domain is the structurally lowest domain and forms a dome that extends for more than 80 km from the St. Maurice River to the Taureau Reservoir. Its northern boundary is not yet recognized, but it is in tectonic contact to the west, south and south-east with the overlying Morin Terrane along the Taureau shear zone. The Morin Terrane is principally exposed on the western side of the Mékinac-Taureau domain, but a thin slice of this terrane extends towards the east and is referred to as the Shawinigan domain (e.g. Corrigan, 1995; Corrigan and van Breemen, 1997; Rivers, 2008). The elongated, north-south striking Portneuf-Mauricie domain structurally overlies the two other domains along the Tawachiche shear zone. These three lithotectonic domains can be distinguished according to their lithology, age, structural style and magnetic signature (Fig. 2.3, Nadeau and Corrigan, 1991; Nadeau and Brouillette, 1994, 1995, Corrigan, 1995).

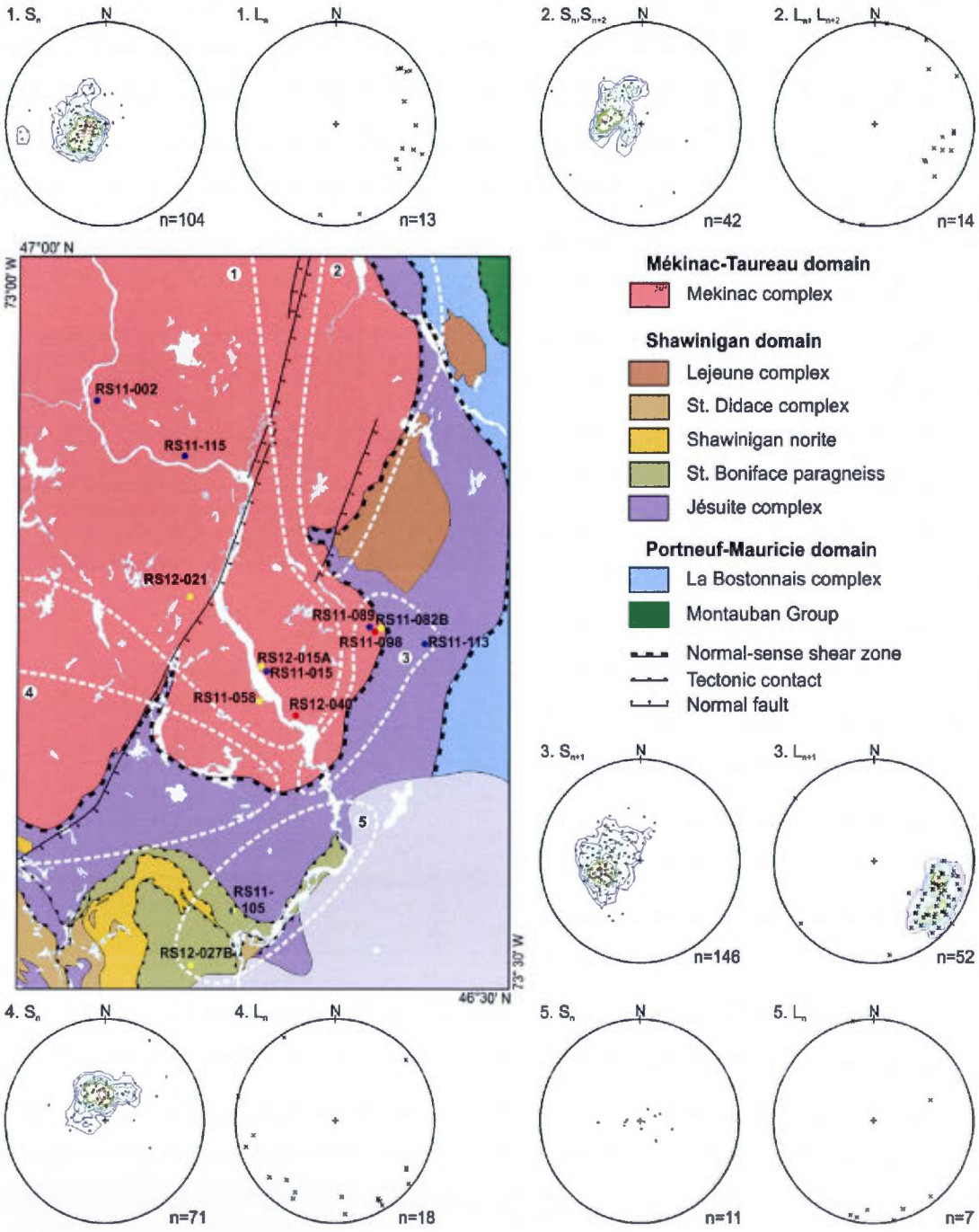

Fig. 2.2 Simplified geologic map of the study area with location of samples used for thermobarometry (yellow circles), $^{40}Ar/^{39}Ar$ thermochronology (blue circles) and U-Pb zircon geochronology (red circles). Structural data (poles to foliation (circles) and lineations (X)) are divided according to structural domains delimited by white dotted lines. Stereonets are lower hemisphere equal area projections. Contours were produced with Stereonet software v.1.5 using the 1% area method and 2 sigma contour intervals (2-20 sigma) for stereonets containing more than 40 data points. Geologic map from Nadeau et al. 2009.

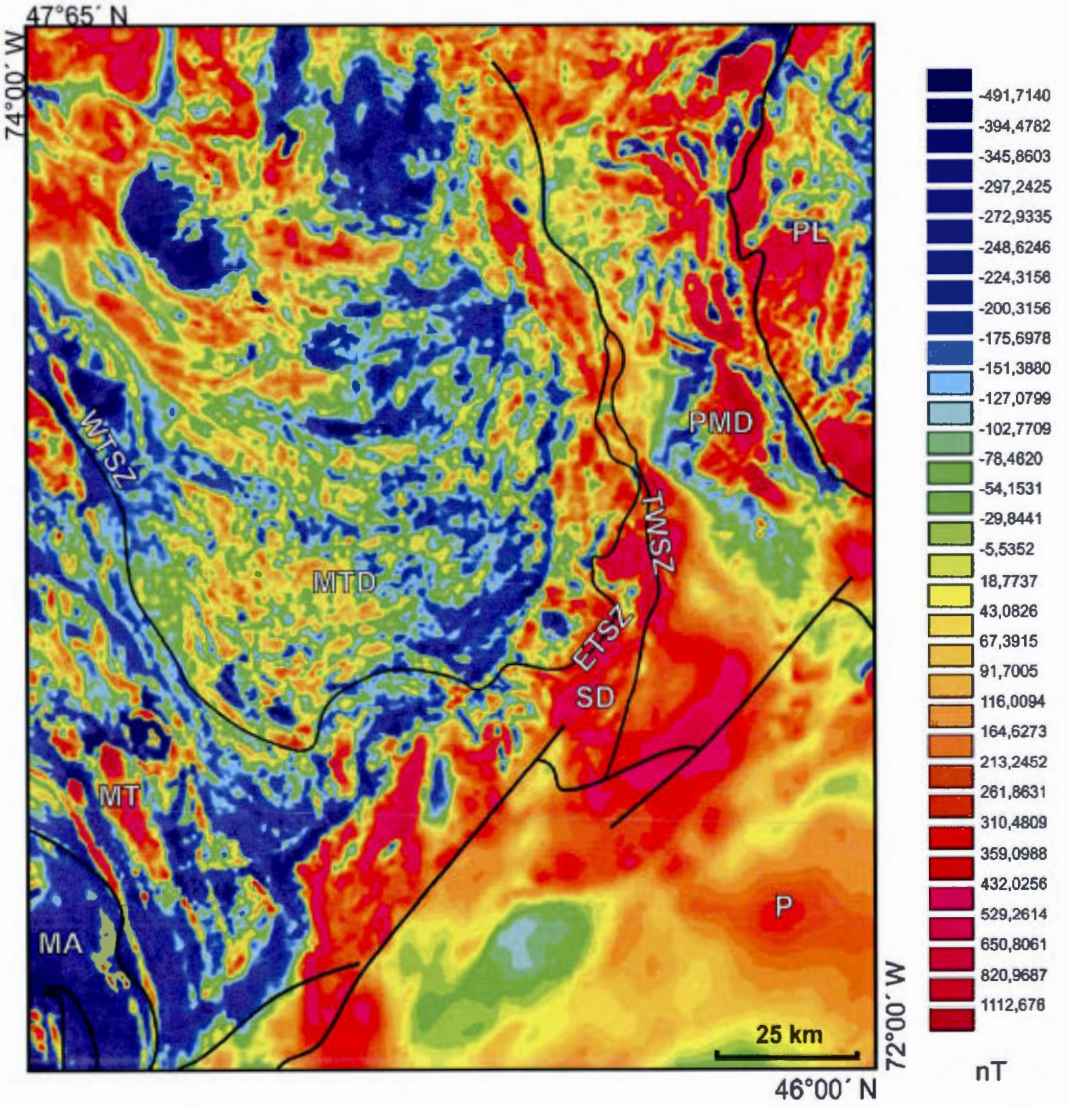

Fig. 2.3 Residual total field magnetic anomaly map of the Lanaudière-Mauricie area (same area as Fig. 1). The Mékinac-Taureau domain is easily recognized by its uniform, low to moderate magnetic amplitude. MT—Morin terrane, MTD—Mékinac–Taureau domain, SD—Shawinigan domain, PMD—Portneuf–Mauricie domain, PLD—Parc des Laurentides domain, MA—Anorthosite, P—Paleozoic cover, WTSZ— western Taureau shear zone, ETSZ— eastern Taureau shear zone, TWSZ—Tawachiche shear zone. Magnetic data are from the Geological Survey of Canada, domains boundaries are from Nadeau and Brouillette (1995).

2.3.1 Mékinac-Taureau domain

The Mékinac-Taureau domain is mostly composed of granulite-facies orthopyroxene-bearing granodioritic orthogneiss that forms part of the aMP Belt of Rivers (2008). Upper amphibolite-facies gneiss occurs in the Reservoir Taureau area of the Mékinac-Taureau domain (Nadeau and Brouillette, 1995). The orthogneiss of the eastern part of the Mékinac-Taureau domain has been dated at 1370 Ma by U-Pb geochronology on zircon (van Breemen and Nadeau, unpublished data in Corrigan and van Breemen, 1997). According to Corrigan and van Breemen (1997), the metamorphism occurred from 1120 to 1090 Ma and was due to crustal thickening during northwestward thrusting structurally above the present exposure of units. This period of crustal thickening is slightly older than the Ottawan phase and is generally not recognized as a period of contraction in the Grenville (e.g. Rivers et al. 1989; Rivers, 1997, 2008).

The Mékinac-Taureau domain orthogneiss is generally homogenous on the map scale, but varies between granodioritic, granitic, dioritic and gabbroic compositions in any one outcrop (Nadeau and Brouillette, 1995). Typical mineral assemblage of the orthogneiss consists of Pl + Qtz + Kfs (perthite) + Opx + Hbl + Bt ± Cpx ± Grt ± Zrn ± Ap in varying proportions (abbreviations after Kretz, 1983). Felsic and intermediate gneiss is pervasively migmatitic, whereas migmatitic mafic gneiss is only locally present. Based on our observations, the volume of leucosome increases structurally upward from only a few percents in the interior of the domain and reaches 20-40% close to upper structural levels. However, there are exceptions to this trend depending on the lithology. Leucosome contains the assemblage Qtz + Pl + Opx ± Kfs ± Bt ± Grt ± Cpx ± Hbl. They occur in two structural settings. Pre- to syn-deformation leucosome is observed as stromatic layers parallel to the foliation and as pockets of leucosome trapped in boudin necks of more competent mafic layers or in hinges of isoclinal folds. Post-deformation leucosome is observed as undeformed, coarse patches that cross-cut the foliation. This suggests that a first generation of leucosome was produced during the regional deformation and that a second generation was produced after that deformation event. It could be explained if two metamorphic events occurred, or if migmatisation

outlasted the deformation (e.g. Corrigan, 1995). The latter explanation is preferred since both types of leucosome contain the same mineralogy, indicating similar conditions of formation, and because they are locally intimately associated (i.e. stromatic leucosome merging into a cross-cutting pocket).

Rare, discontinuous layers of quartzite, calc-silicate gneiss, marble and metapelite, commonly concordant to the regional foliation, are found close to the eastern margin of the Mékinac-Taureau domain. Marble is characterized by the assemblage Cal/Dol + Di + Qtz + Ttn + Scp ± Phl ± Ap ± Zrn ± Spl. Metapelites are migmatitic and characterized by the assemblage Grt + Sil + Qtz + Pl + Kfs (perthite) + Bt ± Rt ± Ilm ± Zrn ± Mnz. Garnet is small to medium sized (1-10 mm) and subhedral, except in leucosome where it is bigger (10-30 mm) and euhedral, suggesting it was produced during melting and remained in equilibrium during the crystallization of the melt (Powell and Downes, 1990; White et al. 2004).

Field observations confirmed the general structural pattern outlined on Nadeau and Brouillette's (1994, 1995) compilation maps. A regional foliation (S_n), defined by preferred orientation of minerals, ribbon quartz, gneissic compositional banding and stromatic layers of leucosome, gently dips towards the margins of the domain, although local variations occur (Fig. 2.2). Rootless isoclinal folds transposed into the foliation are commonly outlined by mafic layers interpreted as deformed dykes (Corrigan, 1995). In the interior of the domain, marble layers record high qualitative strain, as evidenced by numerous sheath folds and contorted to rounded fragments of country rocks. They were interpreted as tectonic breccias by Nadeau and Brouillette (1995). Hanmer (1988) attributed similar structures to the relatively low viscosity of marbles at high temperature and pressure as compared to the surrounding gneiss. The stretching and mineral lineations (L_n) are generally poorly developed in the interior of the domain (Fig. 2.2). On the southern and southeastern boundary, a well-developed stretching lineation plunges gently to moderately (10-35°) to the east-southeast (L_{n+1}) (Fig. 2.2). A third population (L_{n+2}) plunging gently (0-20°) to the northeast is recognized on the eastern side along the Tawachiche shear zone (Fig. 2.2). However, there is no clear cross-cutting relationship between L_{n+1} and L_{n+2}, and this notation should not imply that one is older than

the other.

The Mékinac-Taureau domain is easily recognized on residual total field aeromagnetic anomaly maps by its uniform, low to moderate magnetic amplitude (Fig. 2.3; Geological Survey of Canada, 1987). According to Corrigan (1995), this low magnetic amplitude is due to the absence of highly magnetic, ~1080-1050 Ma anorthosite-mangerite-charnockite-granite (AMCG) plutons that are common in adjacent domains.

2.3.2 Morin Terrane

The Morin Terrane comprises granulite-facies gneiss and plutonic complexes belonging to the aMP Belt (Rivers, 2008). On the western side of the Morin terrane, gneisses have been subdivided into a basal sequence of orthogneiss, amphibolite and quartzofeldspathic gneiss and a supracrustal sequence of paragneiss, quartzite and marbles (Martignole, 1975). The crystallization of the orthogneiss is ~1330 Ma (U-Pb on zircon, Peck, 2012). According to Martignole (1975), the supracrustal sequence was deposited during the mid-Mesoproterozoic in a sedimentary platform setting and metamorphosed at the granulite-facies prior to the intrusion of the Morin and Lac Croche plutonic complexes (1065-1035 Ma; Barton and Doig, 1972; Doig, 1991; Friedman and Martignole, 1995). A second metamorphic event of similar grade followed the intrusion, but is otherwise temporarily unconstrained (Peck et al. 2005). In contrast to the granulite-facies west side, the eastern side of the Morin terrane, referred to as the Shawinigan domain, is characterized by the presence of upper amphibolite-facies rocks (Corrigan, 1995; Lévesque, 1995). The metamorphism is coeval with the metamorphism in the Mékinac-Taureau domain dated between 1120 and 1090 by Corrigan and van Breemen (1997).

The Shawinigan domain is composed of two major rock units in tectonic contact: felsic to intermediate orthogneiss of the Jésuite complex and the overlying St. Boniface paragneiss. Orthogneiss composition is mainly tonalitic (~1370 Ma, U-Pb on zircon, Corrigan and van Breemen, 1997), but granitic and rare gabbroic rocks are present locally. Stromatic migmatite is common, although not as pervasive as it is in the upper structural levels of the Mékinac-

Taureau domain. Typical mineral assemblage of the orthogneiss is composed of Pl + Qtz + Hbl + Bt ± Cpx ± Kfs (microcline with rare perthitic texture) ± Opx ± Ap ± Zrn in varying proportions. An important distinctive feature of this domain is the rare occurrence of orthopyroxene, which is commonly overgrown by hornblende, and the retrogression of clinopyroxene into hornblende.

The St. Boniface paragneiss comprises mainly metapelite with minor quartzite and marble. Metapelite is migmatitic and characterized by Grt + Sil + Qtz + Pl + Kfs (perthite and microcline) + Bt ± Rt ± Ilm ± Gr ± Tur ± Zrn ± Mnz. Garnet is subhedral and large (1-3 cm, and up to 10 cm in leucosome). Marble is characterized by Cal/Dol + Ol (Srp) + Di + Phl + Gr ± Zrn ± Qtz and generally lacks the brecciated aspect typical of tectonic marbles from the Mékinac-Taureau domain. Metasedimentary rocks were probably derived from Grenvillian sources and were deposited after 1180 Ma (U-Pb on zircon, Corrigan and van Breemen, 1997).

Important masses of AMCG, gabbro, porphyritic granite and monzonite intruded the Morin Terrane during two episodes of magmatism (Corrigan and van Breemen, 1997). The first episode includes the 1165-1135 Ma Morin anorthositic complex (Doig, 1991; Friedman and Martignole, 1995), the ~1140 Ma Lac Croche complex (Barton and Doig, 1972) and the 1153 Ma Lake Paul granite (Corrigan and van Breemen, 1997). The second pulse of magmatism occurred at 1080 to 1056 Ma and includes the Shawinigan norite, the Lejeune complex and the St. Didace complex (Corrigan and van Breemen, 1997; Nadeau and van Breemen, 2001).

The foliation in the Morin Terrane generally dips away from the contact with the Mékinac-Taureau domain. However, multiple folds described in Nadeau and Brouillette (1995) produce local variations to this trend. The regional structural pattern is also affected by pre-1135 Ma AMGC plutons that are wrapped by the foliation (Martignole, 1975; Nadeau and Brouillette, 1995). In the Shawinigan domain, the foliation (S_n) defined by compositional banding dips shallowly to moderately (0-45°) to the southeast (Fig. 2.2). The stretching and mineral lineations (L_n) plunge sub-horizontally to gently (0-15°) to the south and southeast (Fig. 2.2).

2.3.3 Portneuf-Mauricie domain

The Portneuf-Mauricie domain comprises the ~1450 Ma Montauban Group supracrustal rocks and the 1400-1370 Ma La Bostonnais calc-alkaline complex plutonic rocks (Nadeau and van Breemen, 1994; Nadeau and Brouillette, 1995; Corrigan and van Breemen, 1997). Rocks of the Portneuf-Mauricie domain are generally at a lower metamorphic grade than the other domains; with middle to upper amphibolite-facies recorded throughout most of the domain, except for the eastern strand where low- to medium-P granulite-facies is observed (Corrigan, 1995; Lévesque, 1995). Metamorphism of the Portneuf-Mauricie domain is associated with the ~1400 Ma pre-Grenvillian accretion of the Montauban Arc and was not overprinted by granulite facies metamorphism during the Grenvillian orogeny, as opposed to the adjacent Mékinac-Taureau and Shawinigan domains (Corrigan 1995; Corrigan and van Breemen, 1997). Therefore, Rivers (2012) included the Portneuf-Mauricie domain in the aLP Belt. The Montauban Group is composed of intermediate to granitic gneiss, amphibolite, metapelites and minor quartzite. Metasedimentary rocks, pillowed metabasalts and metavolcaniclastic rocks locally preserve relict primary textures (Nadeau et al. 1999). The Montauban Group is interpreted as a sequence of volcanic rocks and shallow marine sedimentary rocks deposited in an island-arc or back-arc setting (MacLean et al. 1982; Bernier and MacLean 1993) which was accreted to Laurentia at ~1400 Ma (Corrigan and van Breemen, 1997). The La Bostonnais complex is composed of gabbro, diorite, tonalite, monzonite and granodiorite which locally preserve primary mineral assemblages and igneous textures. Corrigan and van Breemen (1997) proposed that the La Bostonnais complex intruded the Montauban Group during and after its accretion to the Laurentian margin (Corrigan and van Breemen 1997). In contrast, Gauthier (1993) and Sappin et al. (2009) proposed that the oldest plutons were emplaced as the roots of a mature island arc prior to its collision with the Laurentian margin.

The structure of the Portneuf-Mauricie domain is dominated by a planar fabric dipping gently to moderately to the southeast or east. Mineral and stretching lineations are highly variable, but they can be divided into two sets (Nadeau and Brouillette, 1994, 1995). The first

set plunges to the southeast, occurs pervasively in the domain and has been attributed to regional northwest-directed thrusting (Nadeau and Brouillette, 1995). The second set plunges to the north-northeast and only occurs in discrete shear zones where it completely transposes the first lineation. It was developed during oblique-sinistral extensional ductile shearing after the peak of metamorphism (Nadeau and Brouillette, 1995).

2.4 Structural geology

2.4.1 Lithotectonic boundaries

The contact between the Mékinac-Taureau domain and the Morin Terrane on the western side of the dome is known as the Taureau shear zone (Fig. 2.1, Martignole and Friedman, 1998). This shear zone appears to be continuous with an unnamed tectonic discontinuity mapped on the eastern side of the dome (Nadeau and Brouillette, 1995), which is referred to as the eastern Taureau shear zone in this paper (Fig. 2.2). The western Taureau shear zone is presumed to be several hundred of meters wide and gently dips away from the Mékinac-Taureau domain. Associated subhorizontal stretching lineation trends towards the southeast and a dextral sense of shearing was proposed (Martignole and Friedman, 1998). Furthermore, the western Taureau shear zone is approximately coincident with the orthopyroxene isograd of Schrijver (1973) delimiting granulite-facies rocks of the Morin Terrane from upper amphibolite-facies rocks of the western part of the Mékinac-Taureau domain. Oblique thrusting of the Morin Terrane over the Mékinac-Taureau domain was therefore suggested to explain the superposition of higher grade over lower grade metamorphic rocks (Martignole and Friedman, 1998). This is also consistent with a study indicating northwestward tectonic transport in the Morin Terrane (Zhao et al. 1997). Martignole and Friedman (1998) constrained the minimum age of displacement on the Taureau shear zone by dating a late-kinematic dyke at 1074 ± 4 Ma by U-Pb on zircon. However, the eastern Taureau shear zone does not superpose granulite-facies rocks on top of amphibolite-facies rocks since the orthopyroxene isograd does not follow the lithotectonic contact, but rather strike north across the Mékinac-Taureau domain approximately six kilometers west of the Réservoir Taureau (Hocq and Dufour, 2002). The metamorphic contrast

between the domains is ambiguous, but previous work suggested higher grade in the Mékinac-Taureau domain (i.e. the footwall of the eastern Taureau shear zone) compared to the Shawinigan domain (i.e. the hanging wall of the shear zone) (Corrigan, 1995; Lévesque, 1995; Nadeau and Brouillette, 1995). If the suggested metamorphic contrast is true and if timing of metamorphism is the same for both the Mékinac-Taureau and Shawinigan domains, thrusting alone along the eastern Taureau shear zone could not explain the present configuration. Hence, oblique-thrusting along the western Taureau shear zone, as proposed by Martignole and Friedman (1998), cannot be applied directly to the eastern side (see below).

The contact between the Portneuf-Mauricie domain and the Shawinigan domain is marked by an anastomosing array of east-dipping shear zones, collectively known as the Tawachiche shear zone (Fig. 2.1) and was investigated by Lemieux (1992), Corrigan (1995) and Corrigan and van Breemen (1997). The total thickness of the area affected by these shear zones may be as wide as 25 km, but most of the shearing occurred directly at the contact between the two domains, along a strand that has an average map width of 1 km (Corrigan, 1995). The Tawachiche shear zone is almost co-planar with the north to north-east striking and gently dipping regional foliation of the Portneuf-Mauricie domain. The associated stretching lineation trends to the north-northeast with a shallow to moderate plunge (L_{n+2}). The shear zone accommodated top-down-to-the-north-northeast oblique extensional shear which caused a paleopressure offset of 200 to 300 MPa, equivalent to 7-10 km, between the footwall and hanging wall (Corrigan, 1995). Corrigan and van Breemen (1997) constrained the timing of movement along the Tawachiche shear zone between 1090 and 1035 Ma.

The St. Maurice fault (Fig. 2.1) is a northeast striking normal fault that cross-cut all ductile structures over a hundred kilometers (Nadeau and Brouillette, 1995) and extends within the Paleozoic cover to the southwest. Several minor faults with similar orientations also occur in the studied area. These faults are probably related to the opening of the Iapetus Ocean, which followed the Grenville orogen during late Neoproterozoic.

2.4.2 The eastern Taureau shear zone

As stated before, the eastern Taureau shear zone does not have the same structural characteristics that its western section, and therefore one of the main foci of this study is the assessment of its kinematic history. Field observations show a general trend from S-tectonites dominant in the interior of the Mékinac-Taureau domain towards S-L and locally L-tectonites developed on its eastern boundary. An opposite variation, that is a transition from S-L-tectonites to S-tectonites, is observed from the boundary structurally up in the Shawinigan domain. This clearly reveals the presence of the eastern Taureau shear zone, which separates the two domains. The main shear zone is several hundred meters thick and is heterogeneously strained: rock is generally well-foliated and lineated, and locally shows well-developed mylonitic textures that may contain a pre-shearing relict foliation. In the latter case, the relict foliation (S_n) is commonly crenulated and folded with axial planes parallel to the new foliation formed in the shear zone (S_{n+1}, Fig. 2.4D). The stretching lineation associated with this shear fabric (L_{n+1}) plunges gently (10-35°) towards the ESE (Fig. 2.2). Multiple shear-sense indicators such as σ-porphyroclast, δ-porphyroclasts and asymmetric folds (Hanmer and Passchier, 1991) point to a top-down-to-the-ESE tectonic displacement (Fig. 2.4A and C.). Highly deformed marble layers of variable thickness (5-200 cm) are observed within the shear zone (Fig. 2.4). The foliation cuts across the lithological contact at a low angle (<10°), but the internal foliation and stretching lineation are parallel to the external fabric. They are nowhere cross-cut by the abundant felsic pegmatites (deformed and undeformed) observed in the area, but rather contain variably deformed «clasts» of that lithological unit. Some pegmatites, undeformed away from the marble layers, are mylonitized in their vicinity, which suggest strain localization within these marble layers. The marble layers thus accommodated the lasts strain increments along the shear zone. The foliation of the host gneiss is locally clearly entrained at the margins of the marble layers and indicates a top-down-to-the-ESE sense of shear (Fig. 2.4B).

Kinematic indicators attesting for top-down-to-the-ESE sense of shear are also developed locally in a metapelite layer of the Mékinac-Taureau domain three kilometers structurally below the contact with the Shawinigan domain. In this sample, quartz ribbons are

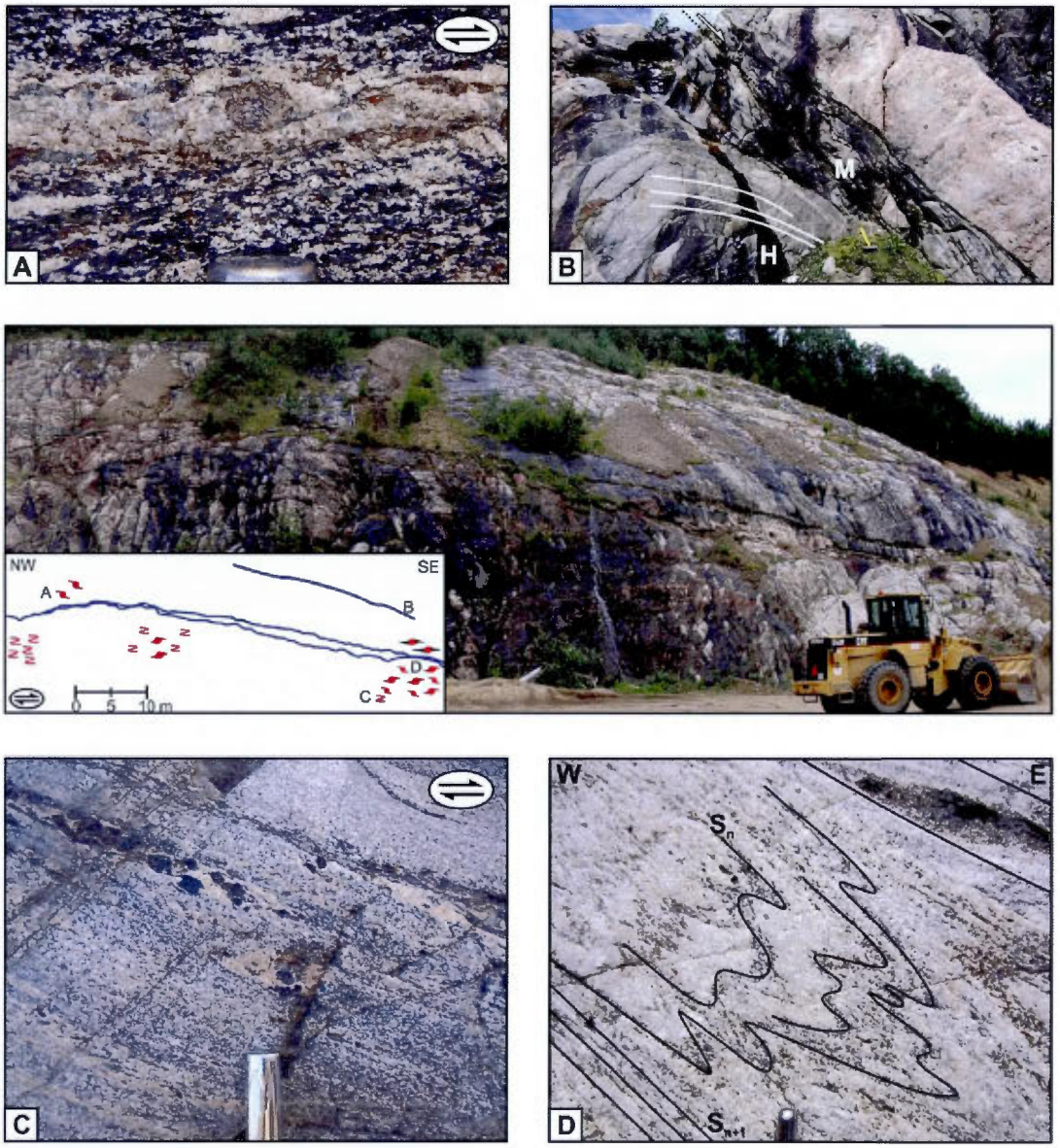

Fig. 2.4 Panoramic view of the St-Tite gravel pit, a key outcrop where the eastern Taureau shear zone is best exposed (central photograph) and where samples RS11-098, RS11-089 and RS11-082 were collected. The inset is a sketch of the principal structures of the outcrop. Blue lines represent strongly deformed marble layers. Prime locations for the observation of top-down-to-the-ESE kinematic indicators are shown in red (σ- and δ-porphyroclasts, asymmetric z-folds). Letters in the inset refer to the location of close-up photographs, which have the same orientation unless specified otherwise. Lineation (L_{n+1}) is plunging to the ESE (see structural subdomain 3 on Fig. 2), i.e. subparallel to the outcrop surface. **A.** δ-porphyroclast of orthopyroxene. **B.** foliation S_{n+1} of the host gneiss (H) entrained at the margins of an anastomosing marble layer (M). **C.** σ- porphyroclast of K-feldspar-rich leucosome pod. **D.** Lower strain area indicated by the preservation of an earlier, folded, foliation S_n that is not completely transposed into the S_{n+1} foliation.

syn-kinematically recrystallized to form an oblique grain-shape fabric (Snoke et al., 1998; Passchier and Trouw, 2005) (Fig. 2.5A). This contrasts with the orthogneiss and structurally lower metapelites in which quartz form fully annealed ribbons.

Finally, in the lower structural levels of the Shawinigan domain, there are multiple ductile-brittle extensional shear zones with a top-down-to-the-SE sense of shear (Fig. 2.5B). These shear zones probably accommodated only minor displacement since there are no

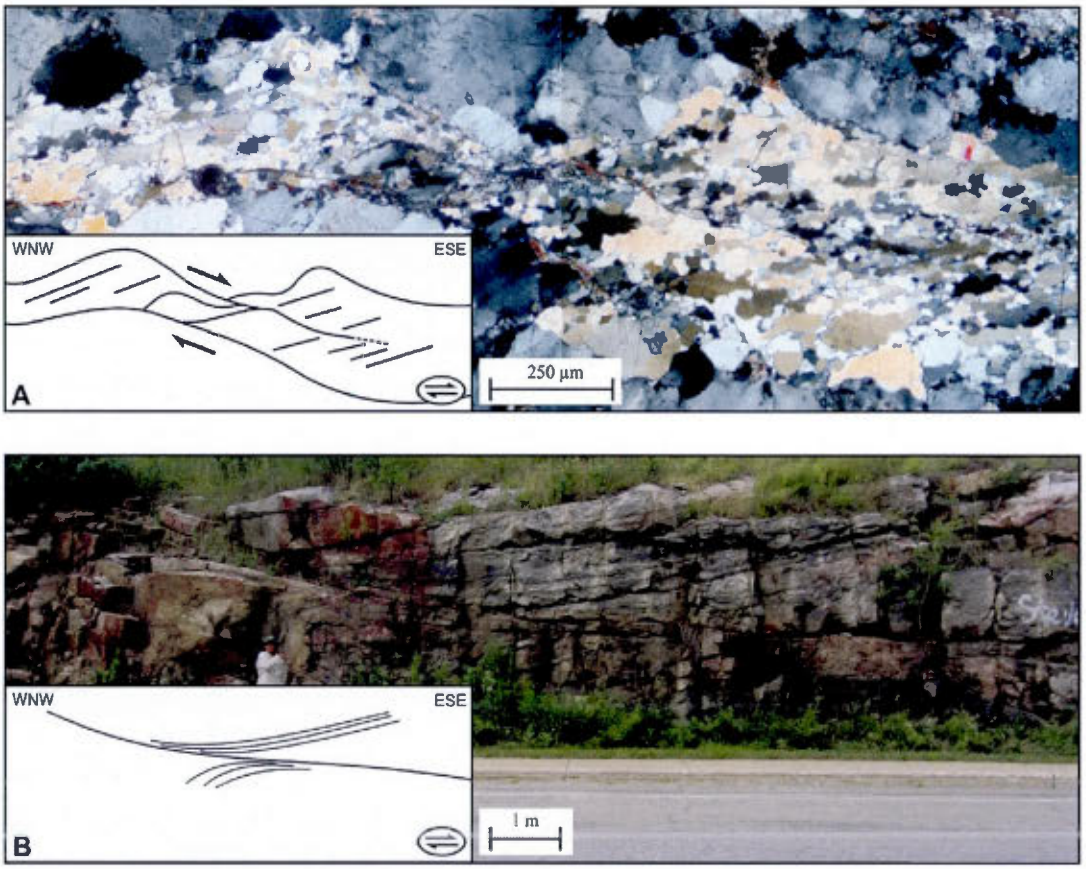

Fig. 2.5 A. Composite microphotograph in cross polarized light (XPL) of a paragneiss located in the Mékinac-Taureau domain ~3km below the eastern Taureau shear zone (sample RS11-058). Syn-kinematic recrystallization of quartz ribbons forming an oblique grain-shape fabric suggests top-down-to-the-ESE sense of shear. Fine grain material within the quartz layer is a mixture of Sil + Bt + Kfs + Pl + Rt. **B.** Extensional ductile-brittle structure in the Shawinigan domain showing top-down-to-the-SE sense of shear. View is not perfectly parallel to the stretching lineation along the shear plane, which plunges towards the SE. These structures are interpreted as structurally higher equivalents of the Taureau shear zone that were active during waning stages of extension.

metamorphic or lithological contrasts between the footwall and hanging wall. They may represent structurally higher equivalents of the Taureau shear zone that were active during the waning stages of normal shearing.

2.5 Thermobarometry

2.5.1 Qualitative interpretations

Granulite-facies metapelite from both the Mékinac-Taureau and the Shawinigan domains have a similar mineral assemblage composed of Qtz + Kfs + Pl + Grt + Sil + Bt ± Rt ± Ilm ± Zrn ± Mnz (Fig. 2.6A). The presence of K-feldspar and the absence of muscovite, orthopyroxene and kyanite in the peak assemblage of metapelite restrict the conditions above the second sillimanite isograd, below the opx-in isograd and within the sillimanite stability field. In felsic to intermediate orthogneiss, the occurrence of migmatitic melt indicates conditions above the wet-solidus of granitic rocks.

There are several differences between the orthogneiss units of the Mékinac-Taureau and the Shawinigan domains. Perthitic texture is pervasive the Mékinac-Taureau domain as opposed to the Shawinigan domain, where it occurs only locally. Also, the amount of leucosome material in the Mékinac-Taureau domain, especially at the proximity and within the Taureau shear zone (up to 40%), is much more important compared to the Shawinigan (<20%). Moreover, the occurrence of migmatitic mafic gneiss in the Mékinac-Taureau shear zone indicates P-T conditions above the wet solidus of gabbroic rocks, whereas unambiguous evidence of partial melting in mafic gneiss of the Shawinigan domain has not been observed. The most striking difference is the scarcity of orthopyroxene in Shawinigan domain orthogneiss and its common retrogression to hornblende. In the orthogneiss of the Mékinac-Taureau domain, orthopyroxene is abundant and unaltered, especially in the interior of the domain. Clinopyroxene is retrogressed to hornblende in the Shawinigan domain and only locally in the upper levels of the Mékinac-Taureau domain. This suggests that metamorphic retrogression affected the Shawinigan domain and, to a lesser extent, the Mékinac-Taureau domain.

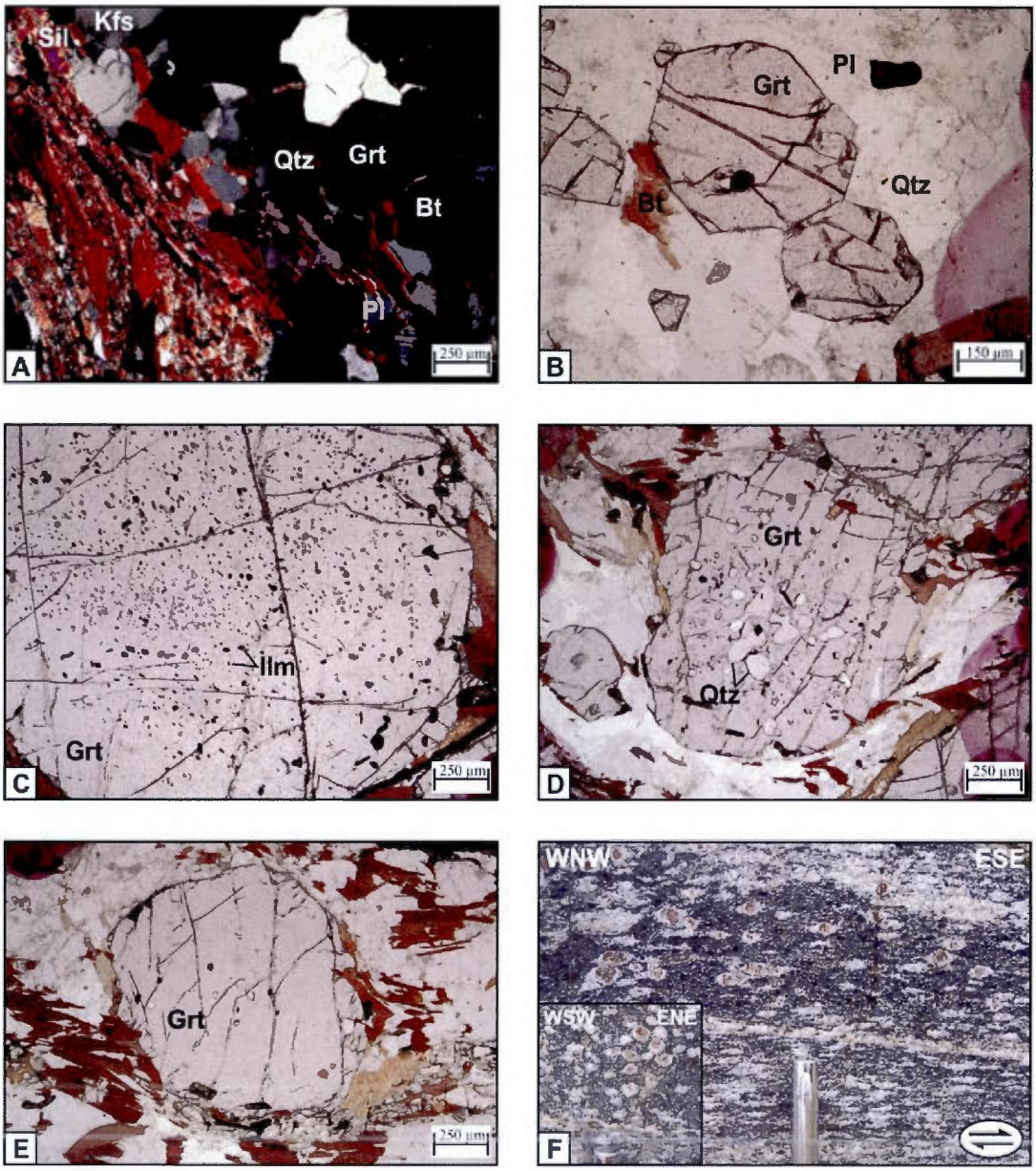

Fig. 2.6 Representative microphotographs of metapelite and amphibolite analyzed for thermobarometry. **A.** Typical metamorphic assemblage in metapelite RS11-105 of the Shawinigan domain containing Qtz + Kfs + Pl + Grt + Bt + Sil. This assemblage characterizes all metapelites from the Mauricie area. **B.** Perfectly euhedral garnet grains from the interior of the Mékinac-Taureau domain (sample RS11-021). **C.** Type 1 garnet containing abundant ilmenite inclusions (sample RS11-105). **D.** Type 2 garnet containing abundant quartz inclusions (sample RS11-105). **E.** Type 3 inclusion-poor garnet (sample RS11-105). **F.** View parallel to the lineation of an amphibolite with σ-shaped reaction rims of plagioclase and hornblende around garnet (sample RS11-082B). Inset is a view perpendicular to the lineation at the same scale. Sigmoid shape of reaction rims implies that the reaction was pre- to syn-kinematic.

The petrographical characteristics of these metamorphic rocks suggest higher metamorphic grade in the Mékinac-Taureau domain as compared to the Shawinigan domain and/or a different effect of metamorphic retrogression between these domains. As a clear metamorphic contrast between both domains cannot be demonstrated on the sole basis of observations, quantitative thermobarometry is required.

2.5.2 Analytical methods and strategy

Five metapelite samples containing metamorphic mineral assemblage (Qtz + Pl + Kfs + Grt + Sil + Bt) were selected along a transect of approximately ten kilometers of structural thickness to determine the overall metamorphic conditions characterizing the Mékinac-Taureau and Shawinigan domains. One sample comes from the interior of the Mékinac-Taureau domain (RS12-021), two samples from its external zone corresponding to the top 3 km structurally below the eastern Taureau shear zone (RS11-058 and RS12-015A) and two samples come from the Shawinigan domain south of the Mékinac-Taureau domain (RS12-027B and RS11-105) (see Fig. 2.2 for locations). A sixth sample made up of amphibolite (Hbl + Pl + Grt) located at the highest structural levels of the Mékinac-Taureau domain within the eastern Taureau shear zone was selected in order to evaluate the peak P-T and retrograde history of the rocks (RS11-082B).

Mineral compositions were determined with a JXA JEOL-8900L microprobe at McGill University. Acceleration voltage was 15 kV, beam current was 20 nA, beam size was 5µm and counting time was 20 seconds. Pressure and temperature (P-T) values were calculated with the computer software TWEEQU (Thermobarometry With Estimation of EQUilibrium state) developed by Berman (1991). The TWEEQU version 2.3 (Berman, 2007) was used for calculations on metapelites since it uses the most recent thermodynamic database (v2.32, Berman and Aranovich, in prep.) and solution models for garnet (Berman et al. 2007), biotite (Berman et al. 2007) and plagioclase (Furhman and Lindsley, 1988). TWEEQU version 1 was used for calculations on the amphibolite with the thermodynamic database 1.02 (Berman, 1988) and solution models for amphibole (Mäder et al. 1994), garnet (Berman, 1990) and plagioclase (Furhman and Lindsley, 1988). Since TWEEQU does not provide statistically valid

uncertainties, the results presented here are subject to ± 50°C and ± 100 MPa uncertainties as proposed by Essene (1989).

The following geothermometers and geobarometers were applied:

Metapelites

Ann + Prp = Alm + Phl (2.1)

An = Grs + Sil + Qtz (2.2)

Amphibolites

Tr + Alm = Prp + FeTr (2.3)

Ts + Qtz + Grs + Alm = An + Prp + FeTr (2.4)

Ts + Qtz + Grs + Alm = An + Tr + FeTr (2.5)

Grs + Prp + Qtz + Ts = Tr + An (2.6)

Metapelite

The proper evaluation of P-T conditions of high grade metapelite is a difficult task requiring many precautions (Spear and Florence, 1992). As several high temperature phenomena may modify the chemical composition of minerals, it is important to evaluate them to make sure that calculated P-T points are significant. At high temperature (>500-600°C), the growth zoning pattern of Fe, Mg, Ca and Mn in garnet is modified by intra-crystalline diffusion (e.g. Tracy et al. 1976; Yardley, 1977; Tracy 1982, Caddick, 2010), which depends on the maximum temperature reached, the size of the crystal and the duration of metamorphism. For example, complete homogenization of a garnet with a diameter of 1 mm at temperature reaching 800°C would require tens of m.y., but the growth zoning pattern would be modified significantly within a few m.y. (Caddick et al. 2010). Furthermore, Grt-Bt re-equilibration may occur during retrogression via exchange and net transfer reactions (Tracy, 1982; Spear, 1993; Spear and Parrish, 1996; Spear et al. 1999; Kohn and Spear, 2000). On the other hand, Fe-Mg diffusion in biotite in contact with garnet is effective at >525°C and at rates much faster than geological processes (Spear, 1993). Finally, the rate of Ca diffusion in plagioclase is much slower than the rate of most geological processes; therefore its composition will only be modified by dissolution and reprecipitation (Grove et al. 1984). Minerals analyzed for peak P-T determination were therefore carefully selected to prevent the inaccuracies introduced by these high temperature phenomena on the calculated P-T points

(e.g. Schaubs, 2002).

Petrographical observations (i.e. lack of muscovite and presence of sillimanite and K-feldspar in metapelite assemblage) suggest high peak temperature (>650°C). Garnet is thus expected to have partially to completely re-equilibrated during peak metamorphism and possibly undergone metamorphic retrogression afterwards. Hence, large (500µm to 4mm) garnets were selected because they are likely to preserve, in their core, a chemical plateau unaffected by retrogression reactions (Hozenberger, 2005). In the case where garnet crystals did not show perfectly flat zoning profile in the core, a plateau composition close to the rim was used in order to avoid the effect of relict growth zoning. Biotite in contact with garnet was avoided since its chemical composition re-equilibrates with garnet during metamorphic retrogression. Biotite isolated from garnet was preferred (e.g. trapped within a non-reacting phase such as quartz or feldspar). However, isolated biotite may have never been in equilibrium with a garnet core: a biotite crystal may have been trapped early in the prograde history, resulting in a lower apparent calculated temperature. To discard early biotite grains, Ti content is considered as a good indicator. Since Ti content in biotite increases with temperature and does not diffuse during either prograde or retrograde metamorphism (Henry et al., 2005 and references therein), Ti-poor biotite inclusions can be interpreted as early and not representative of metamorphic peak equilibrium. Isolated biotite crystals with Ti-content similar to the groundmass biotite were selected for peak P-T calculations. Due to slow Ca diffusion rate in plagioclase, its composition reflects the conditions of crystallization or reprecipitation. Plagioclase was therefore selected from the groundmass in the vicinity of garnets (Holdaway, 2001). Moreover, plagioclase rims were preferred over cores to avoid prograde plagioclase.

Amphibolite

The strategy followed with the amphibolite was different since the sample presents an incomplete metamorphic reaction interpreted as the result of decompression during retrogression. The amphibolite contains sigmoid-shaped reaction rims of plagioclase and minor hornblende surrounding garnet (Fig. 2.6F). The host unit also shows plagioclase-rich

patches similar in size to garnet crystals that are interpreted as garnet pseudomorphs formed where the reaction:

Tschermakite-Hbl + Grt + Qtz = Tremolitic-Hbl + Pl (Schaubs et al. 2002) (2.7)

was completed. This disequilibrium texture provides useful information about the retrograde history of the rock. Due to slower Fe-Mg diffusion rates between garnet and hornblende, the growth zoning pattern in garnet was not completely lost; the outer core was therefore used to determine the metamorphic peak conditions along with plagioclase and hornblende from the groundmass. To obtain retrograde P-T points, the rim of garnet was used along with plagioclase and hornblende from the reaction rims since they were produced during retrogression and therefore have a composition that was probably at equilibrium during the retrograde history of the amphibolite. The sigmoidal shape of the reaction rims suggests that they are pre- to syn-kinematic with respect to top-down-to-the-ESE movement. Retrograde conditions obtained with this sample therefore provides P-T constraints corresponding to shearing along the eastern Taureau shear zone.

2.5.3 Results

A summary of the chemical compositions and the calculated P-T results is presented in Table 2.1 whereas the complete chemical composition of analyzed minerals is provided in Appendix A. The following section outlines the major compositional variations observed in the minerals and presents the thermobarometric results obtained from the three different domains.

Interior of the Mékinac-Taureau domain (RS12-021)

Garnet zoning profiles are typically flat (Fig. 2.7A) and the chemical composition of garnet does not vary much between crystals. Biotite shows variation in chemical composition based on their relationship with garnet. Biotite in contact with garnet typically has low Fe/(Fe+Mg) values compared to isolated biotite. Plagioclase composition varies of less than 0.02 X_{An} and generally shows little increase in An content from core to rim but opposite

Table 2.1. Summary of chemical compositions from microprobe analyses and calculated P-T results

			Interior of the MTD[a]	External zone of the MTD[a]		Shawinigan domain			
			RS12-021	RS11-058	RS12-015A	RS12-027B	RS11-105 T.1[b]	RS11-105 T.2[b]	RS11-105 T.3[b]
Easting[c]			665301	671660	671945	667294	670199	670199	670199
Northing[c]			5180591	5174314	5175942	5153813	5158530	5158530	5158530
Grt	$Fe/(Fe+Mg)^d$	core	63-65	69-70	64-66	73	79-80	80-81	81
		rim	63-65	74-78	65-72	75-79	84-87	82-86	83-86
		Δmax[f]	0	<+8	<+6	<+6	<+7	<+5	<+5
	$X_{grs}{}^d$	core	8-9	5-6	1-2	6-7	3-4	3	3
		rim	7-8	5-6	2	5-6	3	3	3
		Δmax[f]	<1	0	<+1	<-1	<-1	0	0
	$X_{sps}{}^d$	core	1	2-3	<1	<1	2	2	2
		rim	1	2-3	<1	<1	2-3	2-4	3
		Δmax[f]	0	0	0	0	<+1	<+2	<+1
Bt	$Fe/(Fe+Mg)^d$	arm.[g]	36-39	40-44	36-40	47-48	53-56	53-56	53-56
		ct.[g]	31-33	36-37	26-34	40-47	51-54	51-54	51-54
	Ti (p.f.u., 6 O)[e]	arm.[g]	0.15-0.18	0.14-0.15	0.14-0.18	0.14-0.18	0.14-0.17	0.14-0.17	0.14-0.17
		ct.[g]	0.13-0.18	0.13-0.15	0.12-0.15	0.13-0.15	0.11-0.15	0.11-0.15	0.11-0.15
Pl	An		43.3-45.8	37.2-41.3	7.8-20.3	32.4-39.8	20.5-22.2	20.5-22.2	20.5-22.2
P[g]	MPa		1050-1120	780-790	N/A	740-790	720-860	620-650	640
T[g]	°C		820-850	780	740-780	780	730-750	700-710	700-710

Notes

a) MTD: Mékinac-Taureau domain

b) RS11-105 results are given for types 1-3 garnet (T.1; T.2; T.3, respectively)

c) UTM NAD 83, zone 18N

d) X_{alm}, X_{prp}, X_{grs}, X_{sps}, Fe/(Fe+Mg) and are given as %

e) Ti concentration is given as cation number per formula unit (p.f.u.) based on 6 oxygens formula.

f) Δmax represents the largest variation between the chemical composition of the core and the rim. "+" is an increase, "-" is a decrease.

g) arm.: armoured; ct.: contact with garnet; P : pressure; T: temperature.

Table 2.1. Continued

			Eastern Taureau shear zone
			RS11-082B
Easting[a]			680747
Northing[a]			5178829
Grt	Fe/(Fe+Mg)[b]	core	71-79
		inner rim	74-75
		outer rim	74-76
	X_{grs}[b]	core	18-30
		inner rim	27-32
		outer rim	18-20
	X_{sps}[b]	core	2-4
		inner rim	2-3
		outer rim	4-5
Hbl	Fe/(Fe+Mg)[b]	groundmass	43-45
		reaction rim	40-44
Pl	An	groundmass	40.2-50.7
		reaction rim	48.5-58.0
P[c]	MPa	peak[d]	1020-1090
		retro[d]	640-760
T[c]	°C	peak[d]	750-780
		retro[d]	640-680

Notes

a) UTM NAD 83, zone 18N

b) X_{alm}, X_{prp}, X_{grs}, X_{sps}, Fe/(Fe+Mg) and are given as %

c) T: temperature; P : pressure

d) peak: metamorphic peak; retro: retrograde metamorphism

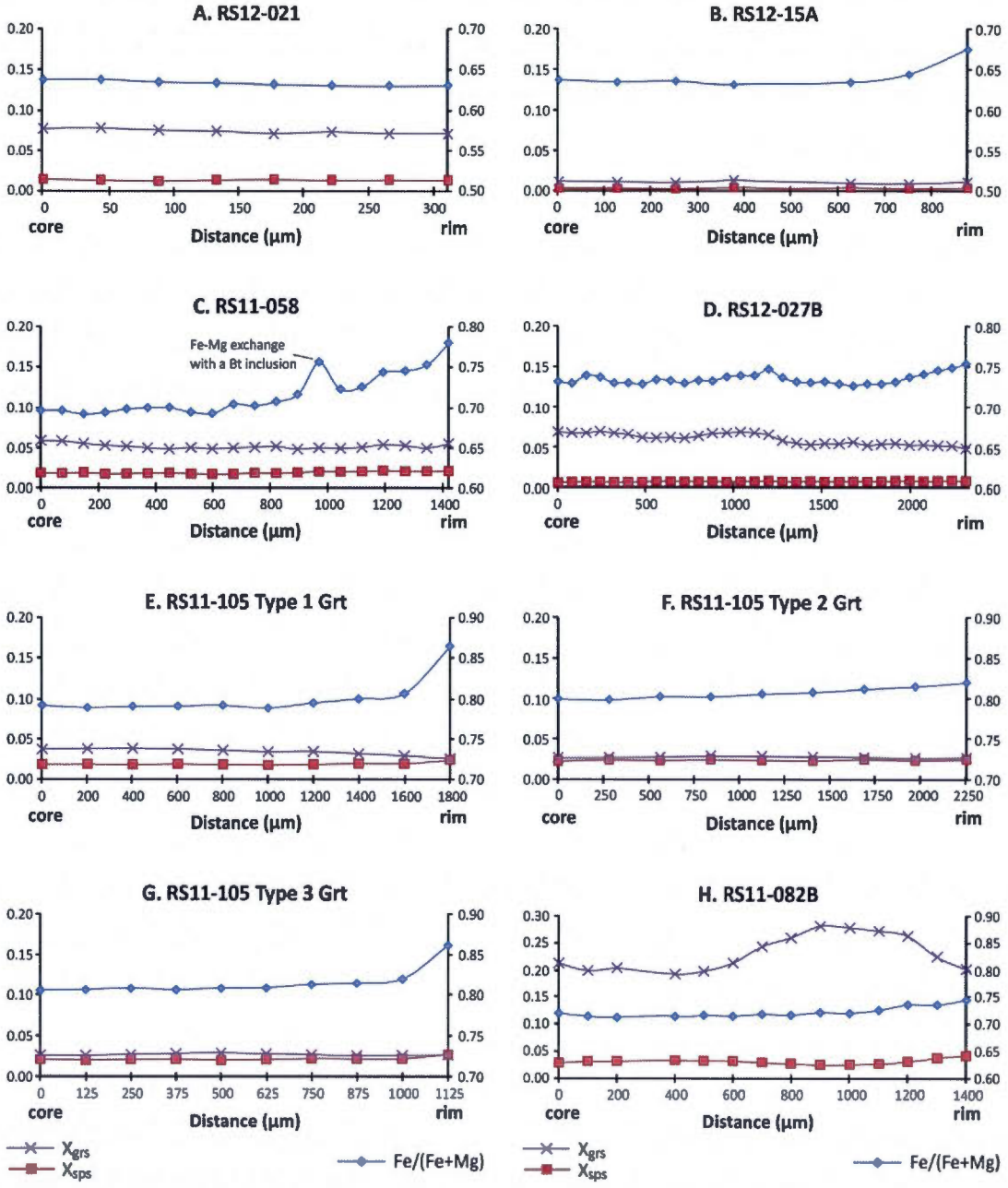

Fig. 2.7 Representative chemical composition profiles of garnet from core to rim. **A** Metapelite from the interior of the Mékinac-Taureau domain. **B-C.** Metapelite from the external zone of the Mékinac-Taureau domain. **D-G.** Metapelite from the Shawinigan domain. **H.** Amphibolite from the eastern Taureau shear zone. Notice the lack of zoning typical of retrograde net-transfer reaction of garnet in migmatitic metapelites, such as spike in X_{sps} at the rim (Spear et al. 1999). See text for additional interpretation of the zonation.

zonation has also been observed. Calculated pressures and temperatures range from 1050 to 1120 MPa and from 819 to 849 °C, respectively.

External zone of the Mékinac-Taureau domain (RS11-058 and RS12-015A)

Garnet zoning profiles of Fe/(Fe+Mg) are generally flat or increases slightly from the core towards the rim, (Δ <0.08) (Fig. 2.7B-C). Garnet zoning profiles of X_{sps} and X_{grs} are flat throughout. The chemical composition of garnet does not vary much between crystals within a single sample, except for smaller garnets (Δ <1mm) having abnormally high Fe/(Fe+Mg) in the core, interpreted as the result of diffusion throughout the grain. Biotite in contact with garnet typically has low Fe/(Fe+Mg) values compared to isolated biotite. Sample RS11-058 contains relatively homogeneous plagioclase (Δ <0.04 X_{An}), but sample RS12-15A contains rare plagioclase (only five analysis) of variable composition (Δ <0.13 X_{An}). In the latter sample, the large variation of composition and the small number of analyses prevented a confident selection of "good" plagioclase composition for geothermobarometric calculations. In sample RS11-058, calculated pressure ranges from 780 to 790 MPa and temperature was determined at 780 °C. Because of the lack of satisfying plagioclase analyses in sample RS12-015A, no pressure determinations were attempted. However, a temperature range of 740-780°C was obtained, assuming a conservative pressure range of 600-1100 MPa.

Shawinigan domain (RS12-27B and RS11-105)

Fe/(Fe+Mg) zoning profiles of all garnet from this domain are flat in the core and increases in the rim (<0.01, Fig. 2.7D-G). X_{grs} profiles are typically flat, but a decrease in X_{grs} (Δ <0.02) may be observed towards the rim of some garnets. In sample RS12-27B, X_{sps} is constant from core to rim, whereas systematic increases of Mn (<0.01 X_{sps}) are observed on garnet rims of sample RS11-105. Sample RS11-105 also contains three populations of garnet that have similar composition profiles but different absolute concentrations of Fe, Mg and Ca. Their morphology is also different: type 1 is characterized by abundant ilmenite inclusions in its core with an inclusion-poor rim (Fig. 2.6C); type 2 is characterized by abundant quartz inclusion in the core and inclusion-poor rim (Fig. 2.6D); whereas type 3 consists of inclusion-poor garnet (Fig. 2.6E).

Biotite in contact with garnet has systematically lower Fe/(Fe+Mg) compared to armoured biotite. In sample RS11-105, no systematic variation of the Fe/(Fe+Mg) value in biotite was observed depending on the position with respect to the garnet type. Plagioclase composition of sample RS12-027B varies of less than 0.08 X_{An} whereas sample RS11-105 contains homogeneous plagioclase (Δ <0.02 X_{An}). Ca-poor plagioclase (An_2 to An_{15}), interpreted as the result of exsolution or secondary precipitation, was observed as patches on K-feldspar and was not used for thermobarometric calculations.

Sample RS12-27B yielded pressures and temperature of 740-790 MPa and 780°C. In sample RS11-105, calculated pressures and temperatures for type 1 garnet range from 720 to 860 MPa and from 730 to 750°C, respectively, whereas both types 2 and 3 garnets registered lower P-T conditions of 620-650 MPa and 700-710°C.

Eastern Taureau shear zone (RS11-082B)

Garnet zoning profiles are more complex in this sample compared to metapelites, although garnets have similar variations profiles within the sample (Fig. 2.7H). Fe/(Fe+Mg) is either flat or progressively decreases from core to inner rim (Δ <0.05) and increases at the outer rim (Δ <0.02). X_{grs} progressively increases from core to inner rim (Δ <0.09) and decreases in the outer rim (Δ <0.13). X_{sps} profiles are either flat or decreasing from the core to the inner rim (Δ <0.04) and increase in the outer rim (Δ <0.02).

Two populations of hornblende are recognized. The first one occurs in the groundmass and is characterized by higher Fe/(Fe+Mg) values (0.43-0.45) compared to the second population found in the coronas surrounding the garnet (0.40-0.44). Plagioclase from the groundmass can also be clearly distinguished from plagioclase in the coronas based on its chemical composition. Groundmass plagioclase composition ranges from An_{40} to An_{51}, with most analyses around An_{45} whereas plagioclase in the coronas ranges from An_{49} to An_{58}, and most analyses are around An_{53}.

The chemical composition of the of high-grossular garnet inner rims were used along with plagioclase and hornblende compositions from the groundmass to calculate

metamorphic peak conditions of 750-780°C and 1020-1090 MPa. The chemical composition of low-grossular garnet rims with plagioclase and hornblende from the coronas was used to calculate retrograde conditions of 640-680 °C and ~640-755 MPa.

2.5.4 Interpretation of thermobarometry results

The chemical composition of analyzed garnet and biotite reveals important information about the metamorphic history of the metapelites from the Mauricie area. First, completely flat Fe/(Fe+Mg), X_{grs} and X_{sps} zoning profiles of most garnets from the interior of the Mékinac-Taureau domain suggest complete intra-crystalline diffusion of Fe, Mg, Ca and Mn in garnet during peak metamorphism. Since biotite in contact with garnet has a lower Fe/(Fe+Mg) value compared to armoured biotite, the exchange reaction (2.1) probably occurred during retrogression, although the expected increase in Fe/(Fe+Mg) on the rim of garnet is not observed. This is most likely due to slower Fe and Mg diffusion in garnet and to the location of transects in areas where contact with biotite is limited. Furthermore, garnet in sample RS11-021 is euhedral (Fig. 2.6B) and does not show a variation in X_{sps}, which suggest that it did not start to break down during retrogression via net transfer reactions:

$$Grt + Kfs + H_2O = Sil + Bt + Qtz \text{ (Spear, 1993)} \quad (2.8)$$
$$Grt + Kfs + H_2O = Bt + Sil + Pl \text{ (Spear and Parrish, 1996)} \quad (2.9)$$
$$Grt + Kfs + melt = Bt + Sil \text{ (Spear et al. 1999)} \quad (2.10)$$

Pressure and temperature calculated with compositional plateaus of garnet, armoured biotite and matrix plagioclase are therefore interpreted as the metamorphic peak conditions of the Mékinac-Taureau domain at ~1075 MPa and ~825°C. Furthermore, mineral chemical compositions used for calculations were not affected during retrogression. The temperature measured in this study is in agreement with previous results of ≥800°C by (Herd et al. 1986; Corrigan, 1995). However, the pressure estimate of 1075 MPa is slightly above the previous results of 800-900 MPa (Herd et al. 1986; Corrigan, 1995). P-T conditions of ~825°C and ~1075 MPa would lie in the kyanite stability field (Fig. 2.8), which is not supported by the petrographical observations since sillimanite is the only Al_2SiO_5 polymorph that has been observed. However, such a P-T value falls close to the kyanite-sillimanite phase transition and

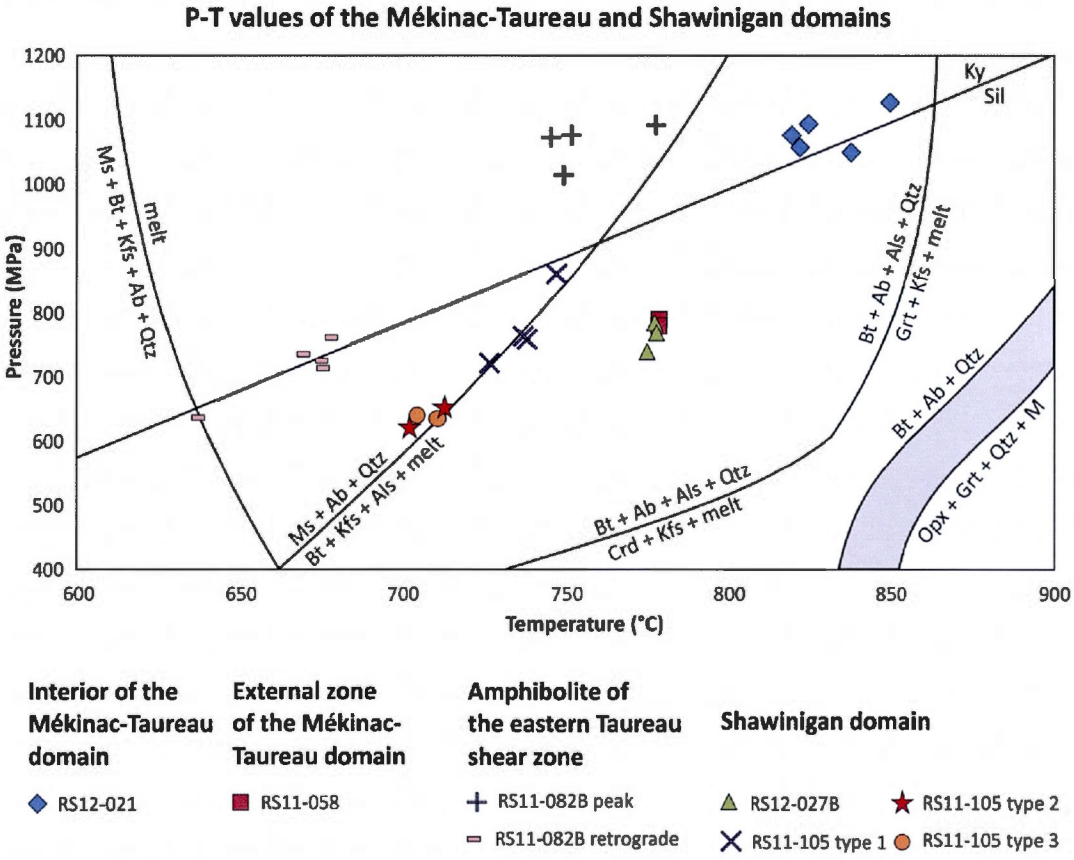

Fig. 2.8 Pressure and temperature obtained from the Mékinac-Taureau and the Shawinigan domain. Samples are located on figure 2.2. All rocks are metapelites except for sample RS11-082B, an amphibolite. The amphibolite was used to calculate peak and retrograde conditions, but temperature is possibly underestimated by ~75°C (see text for details). Uncertainties are ± 50 °C and ± 100 MPa on temperature and pressure, respectively. Results suggest high grade (~825°C; ~1075 MPa) metamorphism in the Mékinac-Taureau domain overprinted by retrograde metamorphism (675-775°C; 700-800 MPa) in the upper structural levels, whereas the Shawinigan domain was metamorphosed at conditions varying from 775 to 700°C and from 850 to 625 MPa. See text for further explications. Ky-Sil transition is from Pattison (1992). Other reaction curves are from Vielzeuf and Schmidt (2001) and references therein.

its uncertainty ellipse overlaps with the sillimanite field. The accurate P-T value may thus lie in the sillimanite side of the uncertainty ellipse.

In the external zone of the Mékinac-Taureau domain, garnet cores in metapelite have essentially flat zoning profiles in Fe/(Fe+Mg), X_{grs} and X_{sps}, suggesting complete intra-crystalline diffusion of Fe, Mg, Ca and Mn in garnet during peak metamorphism. However, garnet crystals show a slight increase in Fe/(Fe+Mg) toward their rims (Δ <0.08). This is the result of limited diffusion during retrogression by the exchange reaction (2.1). The systematic decrease in Fe/(Fe+Mg) value of biotite in contact with garnet, as compared with armoured biotite, supports such an interpretation. The lack of X_{sps} increase at the rim suggests that net transfer reactions (2.8, 2.9, 2.10) did not operate. Pressure of 790 MPa and temperature of ~775°C calculated with compositional plateaus from garnet core, armoured biotite and matrix plagioclase are therefore interpreted as the prevailing conditions during high grade Grt-Bt re-equilibration in the external zone of the Mékinac-Taureau domain. Furthermore, Grt and Bt were only affected by limited exchange reaction (2.1) during retrogression and chemical compositions used for calculations were selected to avoid the effects of this reaction. A metamorphic temperature estimate of ~770°C in the southeastern margin of the Mékinac-Taureau domain has been previously provided by Lévesque (1995), which is consistent with data presented above. In any case, these results are much lower than metamorphic peak conditions obtained for the interior of the Mékinac-Taureau domain.

The amphibolite RS11-082B collected within the Mékinac-Taureau domain at the eastern Taureau shear zone indicates that higher pressure of ~1075 MPa may have prevailed during the metamorphic peak. Due to lower Fe and Mg diffusion rates between garnet and hornblende as compared to garnet and biotite (Spear, 1993), this amphibolite sample yields more valuable information about the metamorphic history of the region than metapelite samples. As shown on figure 2.8, the pressure peak and retrograde pressure values recorded by this amphibolite are equivalent to those yielded by the metapelites from the interior and the margin of the Mékinac-Taureau domain. The calculated P-T path also has a similar slope compared to metapelites, even though temperatures are ~75°C lower. Even though P-T values

difference is within the uncertainty of measurements (± 50°C and ± 100 MPa) and cannot be considered statistically significant, it is possible that temperature calculations with the Grt-Hbl-Pl thermobarometer yield underestimated temperatures since it uses TWEEQU v.1 with older thermodynamic database and solution models for the amphibolite. TWEEQU v.1 uses solution model of amphibole taken from Mäder et al. (1994) and, for a Grt-Hbl-Bt-Pl-Qtz natural assemblage, these authors obtained systematically lower temperatures (with variations up to 120°C) with the Grt-Hbl thermometer as compared to the Grt-Bt thermometer. The amphibolite and metapelite results therefore suggest that the margin of the Mékinac-Taureau domain underwent metamorphic peak conditions similar to those measured in the interior of that domain (i.e. ~825°C, ~1075 MPa), followed by a metamorphic retrogression that partially to totally re-equilibrated the chemical compositions of metamorphic minerals under P-T conditions of 675-775°C and 700-800 MPa. Moreover, the reaction rims around garnet in the amphibolite were deformed during top-down-to-the-ESE shearing along the eastern Taureau shear zone and must have formed prior to or during that shearing. This implies that the eastern Taureau shear zone was formed under P-T conditions ≤700-800 MPa and ≤675-775°C, respectively, which is in agreement with the ~700°C temperature of crystallization obtained with the Ti-in-zircon thermometer applied on a syn-kinematic pegmatite from that same shear zone (see section 2.6 below).

In the Shawinigan domain, the garnet cores in metapelite have essentially flat zoning profiles Fe/(Fe+Mg), X_{grs} and X_{sps}, suggesting complete intra-crystalline diffusion of Fe, Mg, Ca and Mn in garnet during peak metamorphism. However, garnet crystals show a slight increase Fe/(Fe+Mg) toward their rims (Δ <0.07). Sample RS11-105 contains garnet that has a small X_{sps} increase at the rim (Δ <0.02), which probably resulted from net transfer reactions (2.8, 2.9, 2.10). Such reactions theoretically increase the Fe/(Fe+Mg) value of biotite in contact with garnet, but in our sample, Fe/(Fe+Mg) values are lower in biotite in contact with garnet as compared to armoured biotite. This suggests that the impact of net transfer reactions (2.8, 2.9 and 2.10) was overwhelmed by the impact of exchange reaction (2.1), which decreases the Fe/(Fe+Mg) value of biotite. Although metamorphic retrogression affected the composition of the rim of garnet, the large compositional plateau in the core indicates a

complete Grt-Bt re-equilibration at high temperature. P-T values yielded by this sample are dispersed along an array (Fig. 2.8) with type 2-3 garnets lying on the lower grade side, suggesting that two episodes of garnet growth occurred. Type 2-3 garnets cannot be considered as prograde since chemical plateaus in type 1 garnet imply complete intra-crystalline diffusion at higher grade than conditions recorded by types 2-3. Since type 2 garnets are equivalent in size to type 1 and that type 3 garnets are approximately half the size of type 1, intra-crystalline diffusion would also have affected the chemical compositions of type 2-3 garnets at high temperature if these were prograde. An alternative hypothesis would be that type 2-3 garnets grew during decompression and cooling, but this would require an unexplained thermal spike during the retrograde path. Molar isopleths of garnet in metapelites (e.g. Storm and Spear, 2005) have steep slopes on P-T diagrams for the considered P-T conditions (i.e. 625-650 MPa and 700°C). Therefore, temperature must increase to produce new garnet. Pressure and temperature calculated with compositional plateaus from garnet core of sample RS12-027B and type 1 garnet of sample RS11-115 along with and armoured biotite and matrix plagioclase are interpreted as the metamorphic peak conditions of the Shawinigan domain at ~725-850 MPa and ~725-775°C. A second episode of garnet growth under lower conditions of ~625-650 MPa and ~700°C is proposed from P-T points calculated with type 2-3 garnets of sample RS11-115. Such metamorphic conditions are consistent, within error, with data from Lévesque (1995) (725-800°C at 720-880MPa).

Great precautions in the selection of minerals to analyze and careful interpretation of the results are necessary — and were taken — to provide significant P-T values for high grade rocks. Peak metamorphism in the Mékinac-Taureau domain attained P-T conditions of ~1075 MPa and ~825°C, whereas retrograde conditions varying from 800 to 700 MPa and from 775 to 675°C were recorded in its upper structural levels. The Shawinigan domain records P-T conditions varying from 850 to 625 MPa and from 775 to 700°C. The decreasing P-T trend from the Mékinac-Taureau domain to the Shawinigan domain described in this study is therefore significant despite the difficulty to obtain reliable thermobarometric data in high-grade domains.

2.6 U-Pb geochronology

2.6.1 Pegmatite samples description and setting

Sample RS11-098

In order to constrain the timing of deformation along the eastern Taureau shear zone, a syn-kinematic pegmatite intrusion (RS11-098) was sampled at the St-Tite gravel pit (Fig. 2.9A). This pegmatite has a granitic composition (Qtz + Kfs + Pl + Bt + Chl (late) + Zrn + Mnz) and forms a 3 meters-large «pod» surrounded by abundant dykelets, extending away from it. The pegmatite cross-cuts the S_{n+1} foliation in the host gneiss (S_{n+1}≈330/32), but locally shows a weakly-developed internal foliation parallel to S_{n+1}. Above the main mass of pegmatite, a series of foliated dykelets are clearly transposed parallel to S_{n+1} whereas the foliation in the

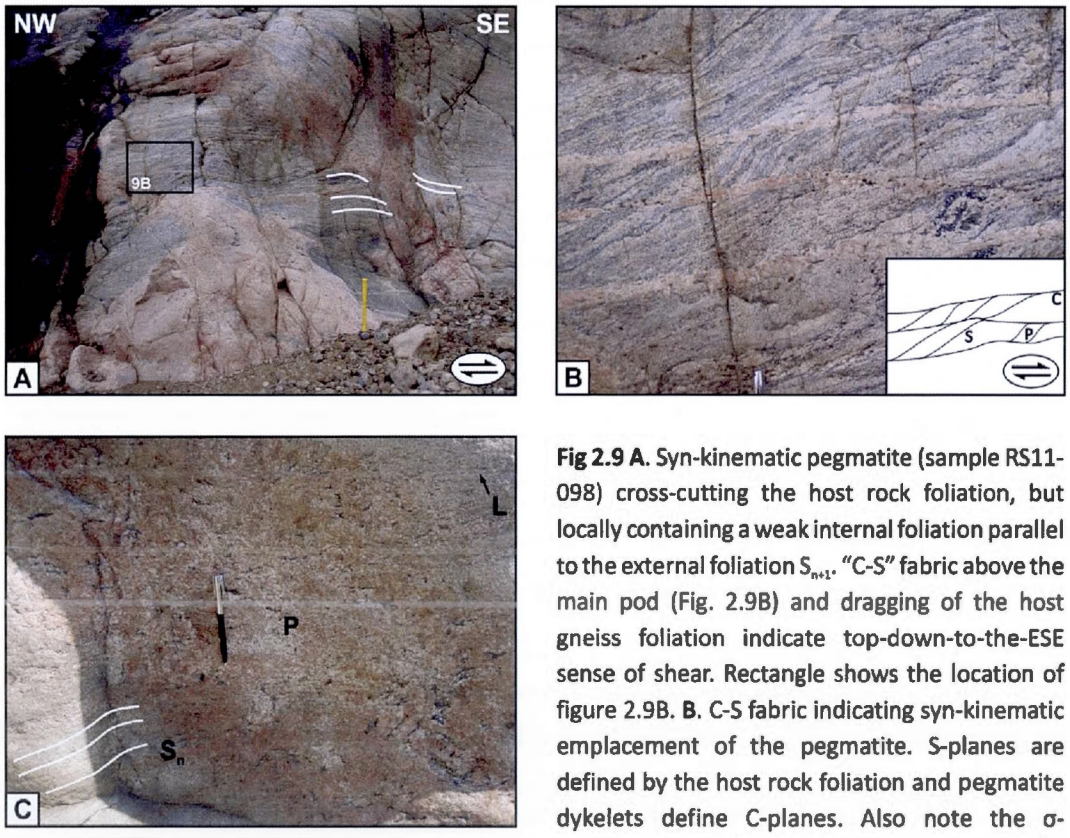

Fig 2.9 A. Syn-kinematic pegmatite (sample RS11-098) cross-cutting the host rock foliation, but locally containing a weak internal foliation parallel to the external foliation S_{n+1}. "C-S" fabric above the main pod (Fig. 2.9B) and dragging of the host gneiss foliation indicate top-down-to-the-ESE sense of shear. Rectangle shows the location of figure 2.9B. **B.** C-S fabric indicating syn-kinematic emplacement of the pegmatite. S-planes are defined by the host rock foliation and pegmatite dykelets define C-planes. Also note the σ-porphyroclast (P) of clinopyroxene partially replaced by hornblende, indicating retrogression prior to or during shearing. **C.** Pegmatite interpreted as the last crystallization product of partial melting following deformation, as seen on outcrop RS12-040. Pegmatite (P) cross-cuts the regional foliation (S_n) and leucosome layers (L) are diffusely merging in it.

hosting gneiss forms S-shaped planes. Planar fabrics defined by both the pegmatite dykelets and the host rock foliation are interpreted as similar to a C-S structure indicating top-down-to-the-southeast shearing (Fig. 2.9B). The transposition of S planes during shearing was probably interrupted by the emplacement of the dykelets, which then accommodated further strain. To the right end of the pegmatite «pod», a 20 cm-thick dyke dips ESE and cuts across S_{n+1} at an angle of ~40°; an orientation that is essentially perpendicular to that of direction of minimum shortening under a top-down-to-the-ESE shearing deformation. This dyke was thus emplaced in a fracture conjugate to the shear plane (e.g. Davidson et al (1994). At the margins of that dyke, S_{n+1} is dragged downward on the NW side and upward on the SE side, which is also consistent with top-down-to-the-southeast shearing during the emplacement of the pegmatite (Fig. 2.9A). We therefore consider that the isotopic dating of pegmatite crystallization would provide age constraint for the normal-sense shearing deformation observed on the eastern Taureau shear zone.

Sample RS12-040

Another granitic pegmatite (RS12-040) was sampled at an outcrop located approximately 2 km structurally below the eastern Taureau shear zone. This outcrop is composed of strongly migmatised and folded, felsic to mafic orthogneiss. Leucosome material contains orthopyroxene and is commonly trapped within the hinges of recumbent folds, indicating that partial melting is contemporaneous to peak metamorphism and deformation. Moreover, some pockets of leucosome locally cut across the foliation, suggesting that partial melting outlasted deformation. This outcrop does not show evidence of shearing typical of the eastern Taureau shear zone and therefore, deformation there is attributed to the older event associated with the development of foliation S_n. Our field observations (i.e. shear-sense indicators such as σ- and δ-porphyroclasts dispersed in the Shawinigan and Mékinac-Taureau domains away from the Taureau shear zone), support Corrigan's (1995) tectonic interpretation that regional deformation is the result of crustal thickening following northwestward-directed thrusting. This deformational event is consequently older than normal shearing along the eastern Taureau shear zone, an interpretation that is supported by our geochronological data

(see below). The sampled pegmatite is made up of Qtz + Kfs (perthitic) + Pl + Bt + Chl (late) + Zr + Mnz and is associated with opx-bearing leucosome (i.e. that leucosome commonly merges into the pegmatite without clear cross-cutting relationships, Fig. 2.9C). It is interpreted as the last crystallization product of partial melting following deformation and its dating should therefore provide a minimum age for the deformational episode related to crustal thickening and associated peak metamorphism.

2.6.2 Analytical methods

Zircon grains were separated from rocks using standard techniques. Data were collected in three experiments: 11RS-098 in June 2012 (experiment 1), 12RS-040 in August 2012 (experiment 2), and 11RS-098 in April 2013 (experiment 3). Zircon grains in experiments 1 and 3 were annealed at 900°C for 60 hours in a muffle furnace. Zircon was mounted in epoxy, polished until the centers of the grains were exposed, and imaged with cathodoluminescence (CL). Zircon was analyzed by Laser Ablation Inductively Coupled Plasma Mass Spectrometry (LA-ICPMS) using a ThermoElectron X-Series II quadrupole ICPMS and New Wave Research UP-213 Nd:YAG UV (213 nm) laser ablation system at Boise State University (Idaho, USA). In-house analytical protocols, standard materials, and data reduction software were used for acquisition and calibration of U-Pb dates and a series of selected high field strength (HFSE) and rare earth elements (REE). Zircon was ablated with a laser spot of 25 µm wide (experiment 1 and 2) or 30 µm wide (experiment 3) using fluence and pulse rates of 5 J/cm^2 and 10 Hz, respectively, during a 45 second analysis (15 sec gas blank, 30 sec ablation) that excavated a pit ~25 µm deep. Ablated material was carried by a 1.2 L/min He gas stream to the nebulizer flow of the plasma. For experiments 1 and 2, dwell times were 5 ms for Si and Zr, 200 ms for ^{49}Ti and ^{207}Pb, 40 ms for ^{202}Hg, ^{204}Pb, ^{206}Pb, ^{208}Pb, ^{238}U, ^{232}Th and 10 ms for all other HFSE and REE. For experiment 3, dwell times were the same except 200 ms for ^{49}Ti and ^{207}Pb, and 80 ms for ^{206}Pb and ^{238}U. Background count rates for each element were obtained prior to each spot analysis and subtracted from the raw count rate for each element. Ablations pits that appear to have intersected glass or mineral inclusions were identified by time-resolved data that show large fluctuations in Ti or P, and were rejected. Similarly, pits that appear contaminated by

common Pb were rejected based on an intensity of mass 204 above baseline. For concentration calculations, background-subtracted count rates for each element were internally normalized to ^{29}Si and calibrated with respect to NIST SRM-610 and -612 glasses as the primary standards.

For U-Pb and $^{207}Pb/^{206}Pb$ age calculations, instrumental fractionation of the background-subtracted ratios was corrected and dates were calibrated with respect to interspersed measurements of the Plešovice zircon standard (337.13 ± 0.37 Ma, Sláma et al., 2008). Two analyses of Plešovice were done for every 10 analyses of unknown zircon; a polynomial fit to the standard analyses yields each sample-specific fractionation factor. Signals at mass 204 were indistinguishable from zero following subtraction of mercury backgrounds measured during the gas blank (<1000 cps ^{202}Hg), and thus dates are reported without common Pb correction. Radiogenic isotope ratio and age error propagation for all analyses includes uncertainty contributions from counting statistics and background subtraction.

For groups of analyses that are collectively interpreted from a weighted mean date (i.e., igneous zircon analyses), a weighted mean date is first calculated with Isoplot 3.0 (Ludwig, 2003) using errors on individual dates that do not include a standard calibration uncertainty, and then a standard calibration uncertainty is propagated into the error on the weighted mean date. This uncertainty is the standard deviation of the time-varying U/Pb fractionation factor and the standard error of the mean of the time-invariant, smaller $^{207}Pb/^{206}Pb$ fractionation factor. The averages of the standard calibration uncertainties from the experiments are used. Standard calibration uncertainties for $^{207}Pb/^{206}Pb$ are 0.4, 0.9 and 0.8% (2σ) for experiments 1-3, respectively. Standard calibration uncertainties for $^{206}Pb/^{238}U$ dates are 2.7, 3.4 and 2.5% (2σ) for experiments 1-3, respectively. Age interpretations are based on weighted mean $^{207}Pb/^{206}Pb$ dates, which are more precise than U/Pb dates upon propagation of the standard calibration uncertainties. Dates that are >15% discordant are interpreted as being from domains that suffered Pb loss and are not considered. A few dates with <15% discordance are not included in the weighted mean calculations because they are not equivalent with the other dates, most likely due to small amounts of Pb loss ($^{206}Pb/^{238}U$ dates) or common Pb

($^{207}Pb/^{206}Pb$ dates). Errors on the $^{207}Pb/^{206}Pb$ and $^{206}Pb/^{238}U$ dates from individual analyses are given at 2σ, as are the errors on the weighted mean dates.

A zircon secondary reference material was treated as unknowns to assess accuracy, interspersed as groups of two analyses for every 20 unknown analyses. Weighted mean dates are calculated using Isoplot 3.0 (Ludwig, 2003) from errors on individual dates that do not include the standard calibration uncertainties. However, errors on weighted mean dates include the standard calibration uncertainties within each experiment and are given at 2σ. FC1 zircon (1098 Ma from unpublished chemical abrasion thermal ionization mass spectrometry (CA-TIMS) data, Boise State University) yielded weighted mean $^{207}Pb/^{206}Pb$ dates of 1093 ± 15 Ma (mean square weighted deviation (MSWD)=1.0, n=10), 1116 ± 18 Ma (MSWD=1.3, n=9) and 1089 ± 18 Ma (MSWD=1.2, n=7) for experiments 1-3, respectively. Weighted mean $^{206}Pb/^{238}U$ dates are 1120 ± 30 Ma (MSWD=0.4, n=10) 1130 ± 38 Ma (MSWD=0.4, n=9), and 1104 ± 28 Ma (MSWD=0.9, n=8) for experiments 1-3, respectively. These results show that accurate $^{207}Pb/^{206}Pb$ and $^{206}Pb/^{238}U$ dates were obtained.

2.6.3 Results

Pegmatite sample RS11-098

Zircon was classified into four compositional groups according to trace element concentrations. Some differences are also apparent in their morphology and zoning patterns in cathodoluminescence (CL) images (Fig. 2.10A). Trace element contents are presented below in the following format: (min-max values; average value). Complete chemical composition data and concordia diagrams are presented in Appendix B, whereas a summary of corrected isotope ratios, ages and temperature of crystallization is presented in Table 2.2.

Group 1 zircon is composed of homogeneous to oscillatory-zoned, CL dark, subequant grains (Fig 2.10A), characterized by high U and Th contents (210-420; 306 and 110-330; 201 ppm; Fig 2.11A) and low Th/U ratios (0.5-0.8; 0.7). It has medium Y (480-1300; 829 ppm), Nb (4-8; 5 ppm), Hf (9940-11530; 10783 ppm), middle rare earth elements (MREE : Sm-Gd) and heavy rare earth elements (HREE : Tb-Lu) contents.

Table 2.2. Summary of U-Pb results

Sample	Easting[a]	Northing[a]	Group	Ages (Ma)										Temperature (°C)
				$^{207}Pb^*/^{206}Pb^*$	±2σ (Ma)	MSWD[b]	PF[b]	n[b]	$^{206}Pb^*/^{238}U^*$	±2σ (Ma)	MSWD[b]	PF[b]	n[b]	Ti-in-zircon ±30 °C
RS11-098	680719	5178838	Group 1 average	1064	12	1,3	0,16	22	1058	27	1,1	0,32	21	691
			Group 2 average	1059	13	1,1	0,34	28	1042	26	0,9	0,55	25	703
			Group 3 average	1065	16	1,5	0,03	32	1047	26	1,0	0,41	34	707
			Group 4 min	1052	53				1032	58				716
			Group 4 max	1459	50				1421	60				794
RS12-040	674542	5172883		1084	18	1,3	0,11	34	1055	34	1,3	0,11	39	755

Notes

a) UTM NAD 83, zone 18N

b) MSWD: mean square weighted deviation; PF: probability of fit; n: number of analyses

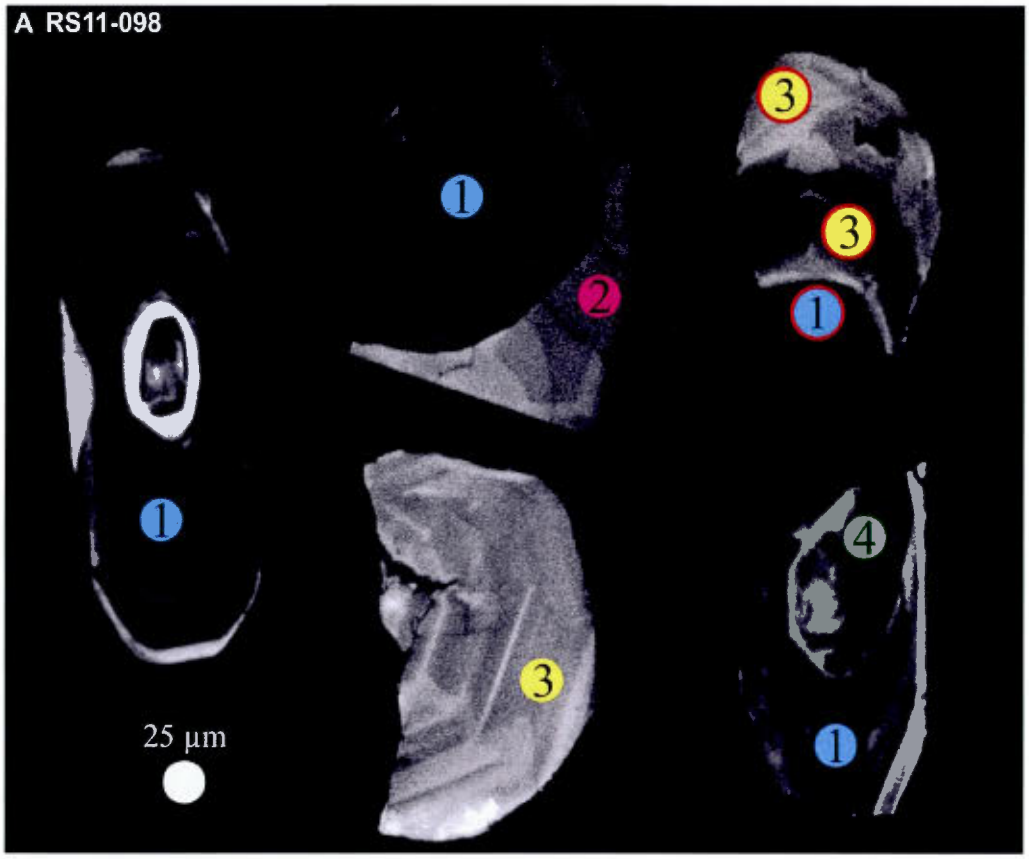

Fig 2.10 A. Cathodoluminescence images of representative zircon from sample RS11-098. Group 1 zircon is commonly overgrown by Group 2 and rarely by Group 3 zircon, but no physical relationship is observed between Groups 2 and 3. Group 1 zircon is interpreted as primary igneous zircon, Groups 2 and 3 as metamorphic zircon, and Group 4 as inherited zircon. Circles are spots analyzed for geochronology. Their diameters are 25 µm large except for spots outlined in red, which are 30 µm. **B**. Cathodoluminescence images of representative zircon crystals from sample RS12-040. Prismatic shape and oscillatory zoning of zircon from this sample are typical of igneous crystallization. Analyzed spots are 25 µm large.

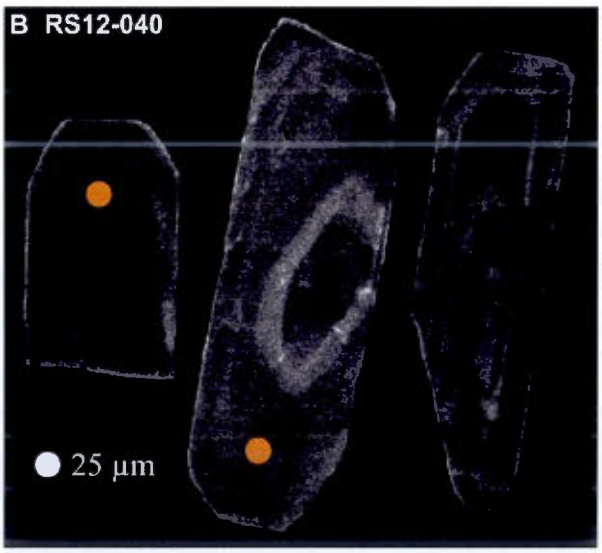

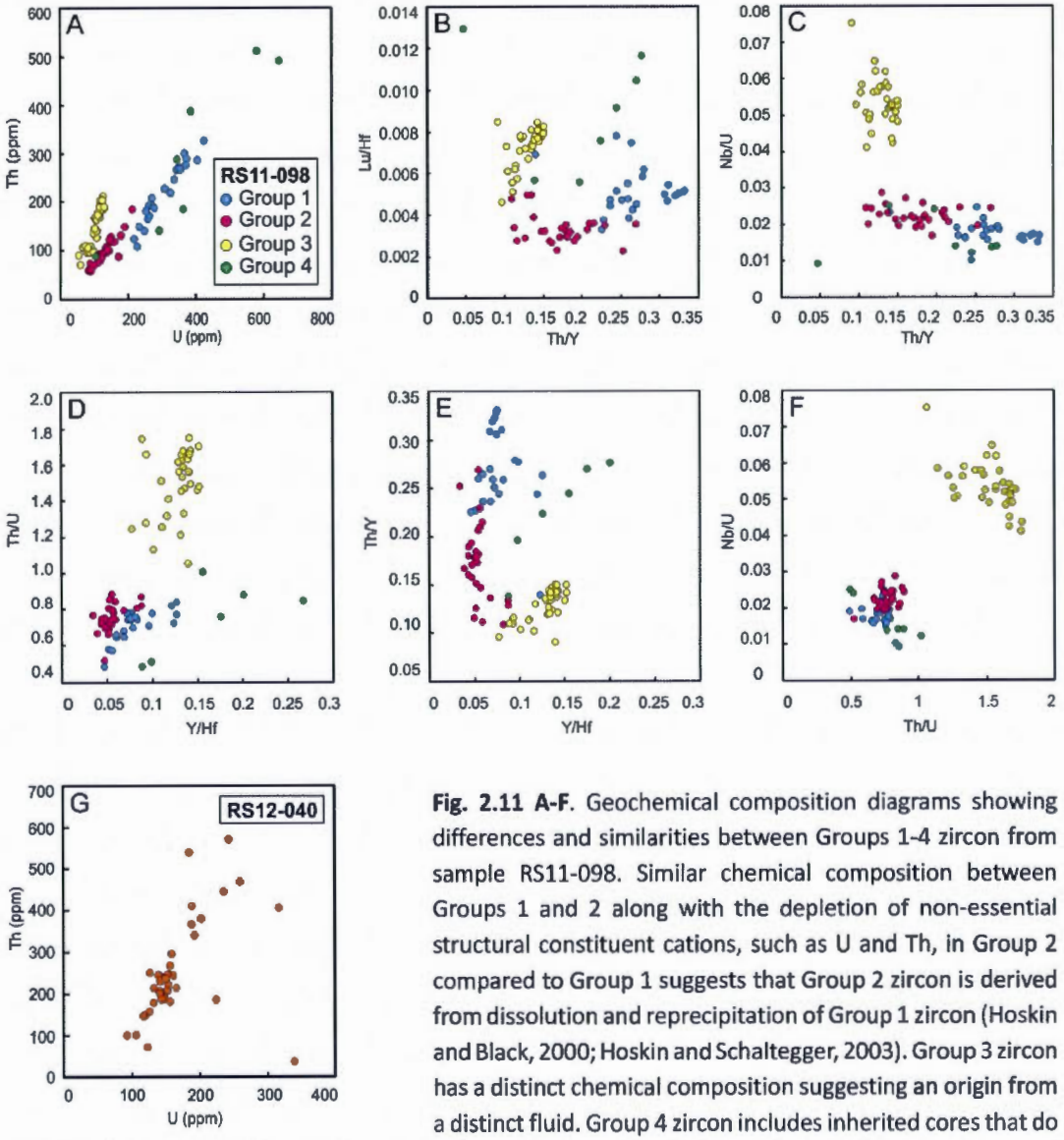

Fig. 2.11 A-F. Geochemical composition diagrams showing differences and similarities between Groups 1-4 zircon from sample RS11-098. Similar chemical composition between Groups 1 and 2 along with the depletion of non-essential structural constituent cations, such as U and Th, in Group 2 compared to Group 1 suggests that Group 2 zircon is derived from dissolution and reprecipitation of Group 1 zircon (Hoskin and Black, 2000; Hoskin and Schaltegger, 2003). Group 3 zircon has a distinct chemical composition suggesting an origin from a distinct fluid. Group 4 zircon includes inherited cores that do not match the composition and/or age of Group 1-3 zircon. See text for details. **G**. U vs. Th diagram of zircon from sample RS12-040. No zircon groups were determined on the basis of the chemical composition.

Group 2 zircon is composed of CL paler grains that are frequently sector or patchy zoned. It commonly forms individual grains and/or secondary rims of overgrowth on Group 1 (Fig 2.10A). It is characterized by low to medium U content (80-210; 133 ppm; Fig 2.11A), low Th content (60-190; 101 ppm; Fig 2.11A) and low Th/U value similar to group 1 (0.5-0.9; 0.8). It has relatively low Y (360-970; 591 ppm), Nb (2-5; 3 ppm), MREE, HREE contents and relatively high Hf content (9200-13410; 10968 ppm).

Group 3 zircon is composed of CL pale oscillatory and patchy zoned zircon. It usually forms individual grains, but one occurrence shows Group 3 zircon rim overgrowing a Group 1 zircon core (Fig 2.10A). Group 3 is characterized by low U content, (50-130; 103 ppm; Fig 2.11A), medium Th content (70-210; 157 ppm; Fig 2.11A) and relatively high Th/U value (1.1-1.8; 1.5). It has relatively high Y (750-1450; 1198 ppm), Nb (2-7; 6 ppm), MREE and HREE contents and relatively low Hf content (7820-10930; 9407 ppm).

Group 4 zircons are composed of homogeneous to patchy zoned CL dark cores (Fig 2.10A). It has low to very high U and Th content (100-650; 387 and 90-510; 300; Fig 2.11A) and medium Th/U values (0.5-1.0; 0.8). It has relatively high Y (940-1920; 1491 ppm) and Nb (1-9; 6 ppm) contents, very high MREE (Sm-Gd) and HREE (Tb-Lu) contents and relatively low Hf content (7210-11780; 9855 ppm).

Differences and similarities in the chemical composition of Groups 1-4 are well illustrated by a series of selected compositional variation diagrams (Fig. 2.11). The distinction between zircon groups is particularly obvious in the Th vs. U diagram (Fig. 2.11A), in which each group shows a distinctive compositional trend that reflects variations in the Th/U value. Other diagrams such as Lu/Hf vs. Th/Y, Nb/U vs. Th/Y, Th/U vs. Y/Hf and Th/Y vs. Y/Hf (Fig. 2.11B-E) also show clear differences between the four groups. Groups 1 and 2 typically have overlapping chemical composition, whereas Group 3 is clearly distinguishable, as shown by the Nb/U vs. Th/U diagram (Fig. 2.11F). Group 4 comprises zircon cores of various chemical compositions that generally lie off the chemical composition field of Group 1-3 in some diagrams.

The temperature of crystallization of the analyzed zircons was calculated based on the Ti-in-zircon thermometer, developed by Watson et al. (2006), using the more recent calibration of Ferry and Watson (2007). The average temperature of crystallization of Group 1 is 691°C; Group 2 is 703°C and Group 3 is 707°C. Group 4 zircon crystallized at temperature varying from 716 to 794°C. The uncertainty of ± 30°C on the temperatures will be explained and discussed in section 2.6.4 below.

Weighted mean $^{207}Pb/^{206}Pb$ and $^{206}Pb/^{238}U$ ages obtained from Group 1-3 are equivalent whereas they are older in Group 4. Group 1 yielded a $^{207}Pb/^{206}Pb$ age of 1064 ± 12 Ma (MSWD=1.3, probability of fit (PF) = 0.16, n=22) and a $^{206}Pb/^{238}U$ age of 1058 ± 27 Ma (MSWD=1.1, PF=0.32, n=21). Group 2 yielded a $^{207}Pb/^{206}Pb$ age of 1059 ± 13 Ma (MSWD=1.1, PF=0.34, n=28) and a $^{206}Pb/^{238}U$ age of 1042 ± 26 Ma (MSWD=0.9, PF=0.55, n=25). Group 3 yielded a $^{207}Pb/^{206}Pb$ age of 1065 ± 16 Ma (MSWD=1.5, PF=0.03, n=32) and a $^{206}Pb/^{238}U$ age of 1047 ± 26 Ma (MSWD=1.0, PF=0.41, n=34). Group 4 yielded $^{207}Pb/^{206}Pb$ ages of 1459 ± 50 to 1052 ± 53 Ma and $^{206}Pb/^{238}U$ ages of 1421 ± 60 to 1032 ± 58 Ma.

Pegmatite sample RS12-040

Although variable, the chemical composition of zircons from sample RS12-040 does not define distinct groups. The morphology of these zircons, their zoning patterns in CL images and ages are homogeneous and all these analyses are consequently treated as a unique group. In this sample, dark xenocrystic cores were easily distinguished and avoided during analysis. Their trace element contents are presented in the following format: (min-max values; average value) and the complete chemical composition data is presented in Appendix B. A summary of corrected isotope ratios, ages and temperature of crystallization is presented in Table 2.2.

Theses zircon grains are generally prismatic and have an aspect ratio varying from 1:1 to 1:5. They are commonly oscillatory zoned and dark in CL (Fig. 2.10B). They are also characterized by medium to high U and Th content (90-340; 166 and 40-570; 252) (Fig. 2.11G) and high Th/U value (0.1-2.9; 1.52). They have high Y and Nb content (540-2790; 1148 and 3-8; 6), variable Hf content (8230-15060; 10362), medium MREE and relatively high HREE (Tb-

Lu) contents. Their temperature of crystallization has been estimated at 755 ± 30°C.

Weighted mean $^{207}Pb/^{206}Pb$ and $^{206}Pb/^{238}U$ ages from sample RS12-040 are equivalent. It yielded a $^{207}Pb/^{206}Pb$ age of 1084 ± 18Ma (MSWD=1.3, PF = 0.11, n=34) and a $^{206}Pb/^{238}U$ age of 1055 ± 34 Ma (MSWD=1.3, PF=0.11, n=39).

2.6.4 Interpretation of zircon U-Pb ages

Relatively large errors on U-Pb ages yielded by the LA-ICP-MS method preclude a clear distinction between Groups 1-3 zircons of the pegmatite sample RS11-098. More precise TIMS dating is needed to precisely determine age differences, if any. However, petrographical relationships suggest that Group 1 zircons are the oldest since they are commonly overgrown by Group 2 and rarely by Group 3 (Fig. 2.10A). Given their homogeneous chemical composition and the lack of sector zoning or zonation perturbation, Group 1 zircons are interpreted as primary igneous zircons that formed during the crystallization of the pegmatite. The great compositional similarity between Groups 1 and 2 zircons suggests that Group 2 formed by recrystallization and/or dissolution and re-precipitation of Group 1. Such an interpretation is supported by the constant depletion in non-essential structural constituent cations such as U, Th, Y, Nb and REE, which are commonly removed in fluid-altered zircon, of Group 2 as compared to Group 1 (Hoskin and Black, 2000; Hoskin and Schaltegger, 2003). Furthermore, the small enrichment in Hf content of Group 2 zircons compared to Group 1 is also characteristic of recrystallization of a pre-existing zircon population (Pan, 1997). Finally, the patchy and sector zonation common in Group 2 is considered as typical of metamorphic zircon or igneous zircon perturbed by late-magmatic processes (Corfu et al. 2003).

Group 3 zircons have a distinct chemical composition, suggesting that it possibly originated from a distinct fluid phase. Overgrowing of Group 1 zircon grains indicates, however, that Group 3 zircons are younger, but no physical relationship were observed between Groups 2 and 3 (Fig. 2.10A). Group 3 zircons comprise mostly patchy zoned crystals that probably grew in solid state, but minor oscillatory zoned zircon grains suggest that some may have grown in the presence of a fluid phase. Group 3 zircons are therefore interpreted as

being metamorphic, but derived from a different source than those of Group 2. It is possible that Group 3 zircons only formed in discrete domains related to fluid infiltration following the crystallization of the pegmatite. This would explain the lack of Group 3 zircon overgrowing Groups 1-2. However, further in-situ work on new samples is needed to test this hypothesis since the crushing process would have destroyed evidence of such domains, if any.

Group 4 is composed of zircon cores of various chemical compositions that do not fit with Group 1-3 chemical composition. Group 4 also typically yields older U-Pb dates and is therefore interpreted as being xenocrystic (inherited).

In order to properly evaluate the implications of the inferred temperatures of crystallization of the different groups of zircons, it is essential to clearly understand the parameters involved in the uncertainty. The calibration error on the equation of the thermometer at 750°C is ±11°C according to Ferry and Watson (2007), but many variables are estimated and introduce a significantly larger error. First, there is a ± 10% error on the Ti content measurements that introduces an error on the temperature calculation varying from ± 4 to ± 7°C depending on zircon groups. Second, the TiO_2 activity ($aTiO_2$) of the source rock during zircon crystallization is not well constrained and have to be estimated. The absence of rutile in the assemblage implies $aTiO_2$ below 1, whereas $aTiO_2$ above 0.5 is expected in natural melts able to precipitate zircon (Watson and Harrison, 2005). Furthermore, silicic melts generally have $aTiO_2$ above 0.6 (Hayden and Watson, 2007). The activity of TiO_2 in the pegmatite should therefore lie between 0.6 and 1, so an average value of 0.8 was used with and a ± 25°C uncertainty was added to the total error. Finally, the effect of pressure on the Ti-in-zircon thermometer must be taken into account even though the original paper of Watson et al. (2006) proposes a relative insensitivity of the thermometer to change in pressure. The Ti-in-zircon thermometer is calibrated at pressures of 1 GPa, but recent developments in its calibration showed that lower pressure leads to an overestimation of the temperature of crystallization and vice-versa. Ferry and Watson (2007) suggest an approximate dependence of ±50°C/GPa, whereas Ferriss et al. (2008) proposed a dependence of ±100°C/GPa for pressures below 2GPa. Based on thermobarometric results described in section 2.5, the

pegmatite was emplaced at pressure decreasing from 800 to 600 MPa. Assuming a pressure of 700 ± 100 MPa for all groups, temperatures calculated directly from the equation of Ferry and Watson (2007) should be reduced by 30°C and an uncertainty of ± 10°C should be added to the total error (according to Ferriss et al. (2008) pressure dependence calculation). The temperature of crystallization presented here for Groups 1-3 do account for the lower pressure effect. Temperature of crystallization of Group 4 zircon was not adjusted since there is no way to estimate the pressure at the time of crystallization of these inherited zircons. The calibration error on the equation of the thermometer, the error on Ti measurements and the errors due to the estimation of $aTiO_2$ and pressure of formation result, when added in quadrature, in a total error of ± 30°C on the temperature of crystallization of zircons.

Temperatures of crystallization of Groups 1-3 (691°C, 703°C and 707°C, respectively) are therefore equivalent within the ± 30°C uncertainty. Since the pegmatite was emplaced during the exhumation of the hosting units, it would be expected to see a temperature decrease from the oldest to the youngest group of zircons. However, such a decrease is not detected. A 14°C increase is even observed from group 1 to group 3. A pressure decrease between Group 1 and Group 3 crystallization would elegantly explain this apparent increase in temperature, but the large uncertainties on many other parameters (especially $aTiO_2$) impede confident interpretation of temperature variations between zircon groups from sample RS11-098. However, temperatures calculated for the crystallization of Groups 1-3 zircons (691-707 ± 30°C) are equivalent, within error, to temperatures of retrograde metamorphism registered by the amphibolite and the metapelites of the upper structural levels of the Mékinac-Taureau domain (675-780 ± 50°C; section 2.5.3). Temperatures of zircon crystallization thus support the emplacement of the pegmatite during retrogression and exhumation of this domain. The crystallization of this syn-kinematic pegmatite at 1064 ± 12 Ma (Group 1, $^{207}Pb/^{206}Pb$) therefore provides a time constrain on the top-down-to-the-ESE shearing along the eastern Taureau shear zone.

Zircons from sample RS12-040 are interpreted as igneous zircon grains because their prismatic shape and oscillatory zoning are characteristic of this type of zircon (Corfu et al.

2003). Their high content in trace elements (e.g. U, Th, Y, Nb, HREE) is also typical of igneous zircon. These zircon grains are therefore the result of the crystallization of the pegmatite, and their age is representative of the age of crystallization. To calculate the temperature of crystallization of these zircons, $aTiO_2$ was estimated at 0.8 with an associated uncertainty of ± 25°C, following our reasoning for sample RS11-098 (see above). Considering that the pressure during peak metamorphism was around 1000-1100 MPa and because zircon probably crystallized shortly after that peak, no adjustment was applied and the temperature was calculated at 1GPa. However, an uncertainty of ± 10°C is added to take a ± 100 MPa uncertainty on the crystallization pressure (assuming a pressure dependence of 100°C/GPa, Ferriss et al. 2008). The temperature of crystallization of pegmatite RS12-040 (755 ± 30°C) is then higher as compared to pegmatite RS11-098 (691 ± 30°C). This is consistent with the emplacement of pegmatite RS12-040 shortly after peak metamorphism at ~825°C ± 50°C and before the emplacement of pegmatite RS11-098 during cooling and extension along the eastern Taureau shear zone. The age of crystallization of the pegmatite RS12-040 (1084 ± 18 Ma, $^{207}Pb/^{206}Pb$) implies a minimum age constraint for deformation and metamorphism related to thrusting and crustal thickening in the Mékinac-Taureau domain. That result is moreover consistent with data of Corrigan and van Breemen (1997) who suggested a lower age limit of 1087 ± 2 Ma for the thrusting in the adjacent Shawinigan domain.

2.7 $^{40}Ar/^{39}Ar$ thermochronology

2.7.1 Analytical methods

Single grains of biotite and amphibole used for the experiments were handpicked under a binocular microscope from the 0.25–1.00 mm fractions of crushed rock samples. The samples were wrapped in Al foil to form small packets (11 × 11 mm) that were stacked up to form a pile within which packets of fluence monitors were inserted every 10 samples. Irradiation was performed at the HFR Petten reactor (Petten, the Netherlands) in the Cd-shielded Rodeo P3 facility and lasted 72h. The irradiation standard was amphibole Hb3gr [(Turner et al., 1971; Roddick, 1983; Jourdan et al., 2006; Jourdan and Renne, 2007); 1081.0 ± 1.2 Ma according to Renne et al., 2010, 2011].

Step-heating analyses of single grains were performed with a CO_2 laser probe. The experimental procedure is described in Ruffet et al. (1991, 1995). The five argon isotopes and the background baselines were measured in eleven cycles, in peak-jumping mode. Blanks were performed routinely each first or third/fourth run, and subtracted from the subsequent sample gas fractions. All isotopic measurements are corrected for K, Ca and Cl isotopic interferences, mass discrimination and atmospheric argon contamination. Apparent age errors are plotted at the 1σ level and do not include the errors on the $^{40}Ar^*/^{39}Ar_K$ value and age of the monitor and decay constant. The errors on the $^{40}Ar^*/^{39}Ar_K$ value and age of the monitor and decay constant are included in the final calculation of the (pseudo-)plateau age error margins or for apparent ages individually cited. Analyses were performed on a Map215® mass spectrometer.

It is commonly considered that a plateau is obtained when calculated $^{40}Ar^*/^{39}Ar_K$ ratios of at least three consecutive steps, comprising a minimum of 70% of the ^{39}Ar released, agree within 1 or 2σ error bars with the weighted mean calculated $^{40}Ar^*/^{39}Ar_K$ value of the plateau segment. Pseudo-plateau ages can be defined with less than 70% of the ^{39}Ar released. All ages are displayed at the 1σ level. Analytical data, parameters used for calculations (isotopic ratios measured on K, Ca and Cl pure salts; mass discrimination; atmospheric argon ratios; J parameter; decay constants, etc.) and reference sources are available in Appendix C.

2.7.2 Isotopic closure temperature

Isotopic mineral ages are interpreted to record cooling below a critical temperature, known as the closure temperature (T_C). Closure temperatures for amphibole are difficult to estimate. In addition to the effect of cooling rate and the size of diffusion domains, amphibole diffusivity is also influenced by ionic porosity (Dahl, 1996; Fortier and Giletti, 1989). On the basis of natural hornblende compositions measured by various authors (i.e. Leake, 1978; Robinson et al., 1982), Dahl (1996) suggested a T_c range of 480–560 °C, calculated for an effective diffusion radius of 80 μm and a cooling rate of 10 °C/Ma. For higher cooling rates (e.g. ~200 °C/Ma), this T_c range could increase to ~520–600 °C. Harrison (1981) estimated from measured 40Ar* loss following isothermal-hydrothermal treatments the activation

energy and frequency factor of hornblende. With an effective diffusion radius of 80 μm, these diffusion parameters predict closure temperatures between 500 °C and 580 °C for cooling rates in the range of 10 to 500 °C/Ma. This closure temperature has been slightly re-estimated at 550–650 °C by Villa (1998) using Dahl's (1996) experiments that suggest that, depending on its lattice characteristics, hornblende may form a closed system for Ar diffusion at temperatures as high as 580 °C under cooling rates of 0.7 K/Ma (Villa et al., 1996). In this study, we will consequently use a T_c range value of 550–600 °C for amphiboles. The suggested closure temperature for biotite may be as high as 450 °C (e.g. Villa and Puxeddu, 1994l; Allaz, 2008; Allaz et al. 2011), 150 °C higher than the commonly accepted temperature of 300 °C (ex: Dodson, 1973; Harrison et al. 1985).

2.7.3 Results

Six samples containing coarse amphibole and/or biotite were collected in the Mékinac-Taureau and the Shawinigan domain to investigate the cooling history of the area with $^{40}Ar/^{39}Ar$ thermochronology (See Fig. 2.2 for locations). With one exception, all samples yield undisturbed plateau ages for amphibole and biotite (Fig. 2.12, Table 2.3). Samples RS11-002 and RS11-115 come from two amphibole- and biotite-rich mafic layers transposed within the hosting orthogneiss foliation (S_n) in the interior of the Mékinac-Taureau domain. Samples RS11-002 and RS11-115 are respectively located ~11 and ~9 km structurally below the eastern Taureau shear zone They yield amphibole plateau ages of 998.6 ± 3.7 Ma and 1010.0 ± 3.7 Ma, respectively (Fig. 2.12A and 2.12B). Biotite plateau ages of 923.2 ± 3.5 Ma and 969.8 ± 3.6 Ma, respectively, were also obtained from these samples (Fig. 2.12a and 2.12b). Sample RS11-015 come from a metapelite layer located ~3 km below the Taureau shear zone and contains biotite but not amphibole. The biotite spectrum defines a plateau at 926.1 ± 3.5 Ma (Fig. 2.12C). Sample RS11-089 is a biotite-free amphibolite layer located within the eastern Taureau shear zone, on the Mékinac-Taureau domain side, that yielded an amphibole plateau age of 1031.6 ± 3.8 Ma (Fig. 2.12D). Finally, two samples were collected in the Shawinigan domain: RS11-113 is a biotite and amphibole bearing intermediate orthogneiss whereas RS11-105 is an amphibole-free metapelite. These samples are respectively located ~1 km and ~4 km

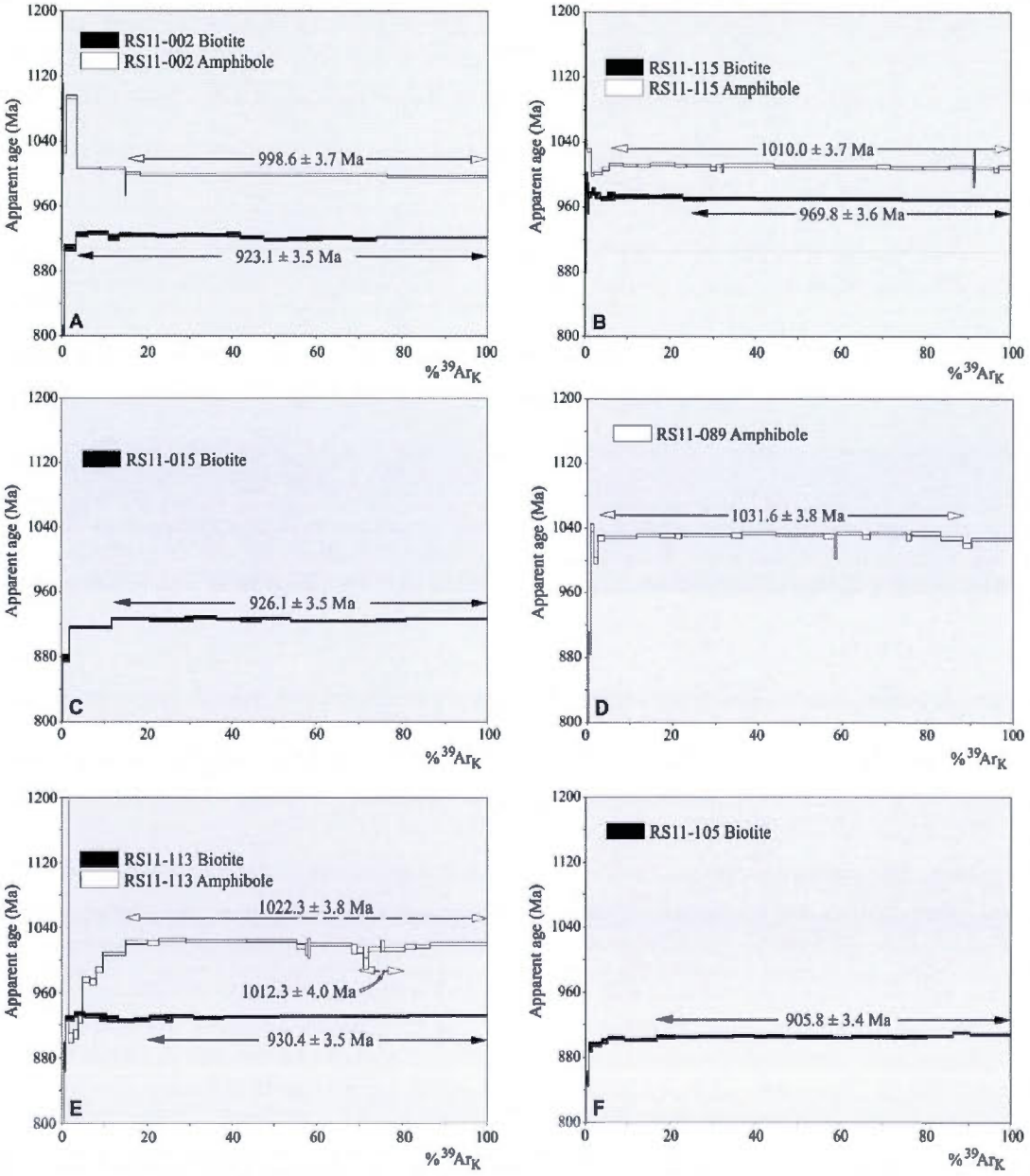

Fig. 2.12 $^{39}Ar/^{40}Ar$ age spectra for **A.** amphibole and biotite of sample RS11-002; **B.** amphibole and biotite of sample RS11-115; **C.** biotite of sample RS11-015; **D.** amphibole of sample RS11-089; **E.** amphibole and biotite of sample RS11-113; **F.** biotite of sample RS11-105. The age error bars for each temperature steps are at the 1σ level. Plateau and pseudo-plateau ages (1σ uncertainties) are given when applicable. See text for interpretations. Samples are located on figure 2.2.

Table 2.3. Summary of $^{40}Ar/^{39}Ar$ results

Sample	Easting[a]	Northing[a]	Mineral dated	Age[b] (Ma)	± 1σ (Ma)	$\%^{39}Ar_K$ defining plateau
Core of the Mékinac-Taureau domain (12 and 8 km below the ETSZ)						
RS11-002	657793	5196510	Hbl	998,6	3,7	85,8
RS11-002	657793	5196510	Bt	923,2	3,5	96,5
RS11-115	666117	5191538	Hbl	1010,0	3,7	93,4
RS11-115	666117	5191538	Bt	969,8	3,6	74,8
External zone of the Mékinac-Taureau domain (3 km below the ETSZ)						
RS11-015	671176	5177599	Bt	926,1	3,5	88,2
Eastern Taureau shear zone (within the ETSZ)						
RS11-089	680697	5178880	Hbl	1031,6	3,8	86,4
Shawinigan domain (2 and 4 km above the ETSZ)						
RS11-113	685301	5177182	Hbl	1022,3	3,8	49,2
RS11-113	685301	5177182	Hbl (pert.[c])	1012,3	4,0	13,6
RS11-113	685301	5177182	Bt	930,4	3,5	79,3
RS11-105	670199	5158530	Bt	905,8	3,4	83,1

Notes
a) UTM NAD 83, zone 18N
b) all dates are plateau ages except for RS11-113 Hbl
c) pert. : thermal perturbation pseudo-plateau.

structurally above the eastern Taureau shear zone. Sample RS11-113 yields an older 1022.3 ± 3.8 Ma amphibole pseudo-plateau with a younger perturbation at 1012.3 ± 4.0 Ma (Fig. 2.12E). Its biotite spectrum defines a plateau at 930.4 ± 3.5 Ma (Fig. 2.12E). Sample RS11-105 yielded a biotite cooling age of 905.8 ± 3.4 Ma (Fig. 2.12F).

2.7.4 Interpretation of ^{40}Ar-^{39}Ar ages

^{40}Ar-^{39}Ar ages provide timing constraints on cooling of the area through the closure temperature of amphibole (550-600 °C) and biotite (450 °C). The youngest amphibole ages (998.6 ± 3.6 Ma and 1010.0 ± 3.7 Ma) were obtained in the interior of the Mékinac-Taureau domain, whereas the oldest (~1031.6 ± 3.8 Ma) is yielded by the amphibolite located within

the eastern Taureau shear zone. A sample from the Shawinigan domain yields an intermediate age of 1022.3 ± 3.8 Ma. Unsurprisingly, all amphibole ages are younger than ~1060 Ma, the age of maximum shearing along the eastern Taureau shear zone when rocks were at ~700 °C (see section 2.6). An interesting younging trend is identified from the eastern Taureau shear zone towards the interior of the Mékinac-Taureau domain. Corrigan (1995) obtained a similar younging trend, from the Tawachiche shear zone towards the Mékinac-Taureau domain, that he explained by the progressive cooling of the footwall downwards from the detachment surface (e.g. England and Jackson 1987; Ruppel et al. 1988; Hodges et al. 1993). In this study, we have shown the importance of the eastern Taureau shear zone for the exhumation of the Mékinac-Taureau domain and consequently propose that cooling may have propagated from this shear zone towards the interior of the Mékinac-Taureau domain, as suggested by the younging trend of amphibole cooling ages in that direction. It would be expected to have even older age in the hanging wall of the shear zone (i.e. the Shawinigan domain), but sample RS11-113 yield an intermediate age of 1022.3 ± 3.8. However, the thermal perturbation at 1012.3 ± 4.0 of the amphibole spectrum of this sample limits the confidence we have on this date and the interpretations we can make from this sample.

Biotite cooling ages vary from ~905 to ~970 Ma and do not show a pattern that is similar to amphibole cooling ages. For samples containing both amphibole and biotite, the time gap between cooling through the T_c of amphibole and the T_c of biotite varies from 40 to 90 m.y. This correspond to a cooling rate of 1.36 to 3.10 °C/m.y. for the interval ~1020-920 Ma, assuming a closure temperature of ~575°C and 450°C for amphibole and biotite, respectively. This is comparable to the cooling rate of 1.1 to 2.5 °C/m.y. calculated by Corrigan (1995) for the interval 1040-990 Ma.

2.8 Discussion

2.8.1 Metamorphic history and timing constraints

A summary of metamorphic constraints for the Mauricie area is presented in figure 2.13. Our results suggest that the interior of the Mékinac-Taureau domain records

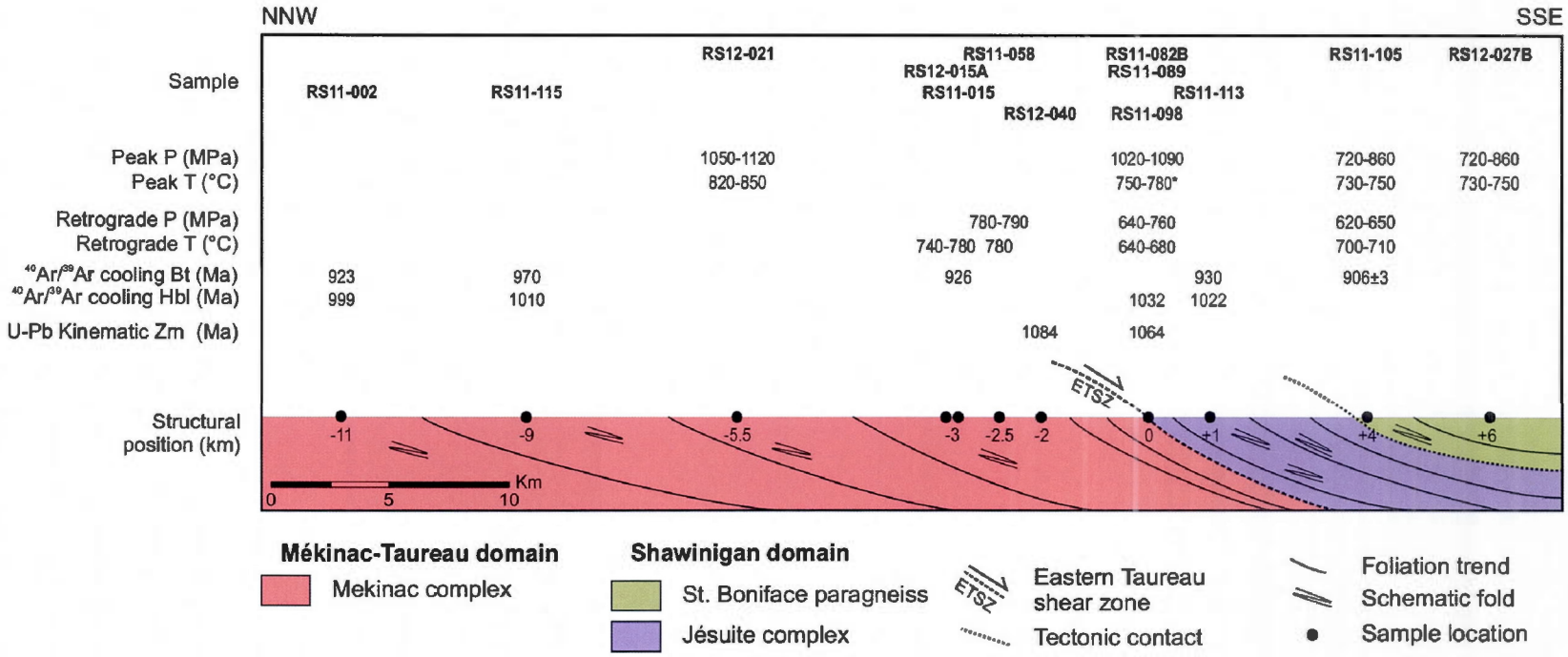

Fig.2.13. Compilation of thermobarometric, thermochronologic and geochronologic results placed on a schematic cross-section of the southeastern Mékinac-Taureau and Shawinigan domains. Samples are located on figure 2.2 and their structural positions (in Km) is projected perpendicular to the eastern Taureau shear zone. *Temperature of RS11-082B may be underestimated by ~75°C. $^{40}Ar/^{39}Ar$ cooling ages are defined by plateau ages, except for sample RS11-113 (Hbl) that is defined by a pseudo-plateau. U-Pb ages ($^{207}Pb/^{206}PB$ on zircon) provide a minimum age for regional deformation and peak metamorphism (RS12-040) and a age of significant shearing along the eastern Taureau shear zone (RS11-098). See text for further details and interpretation.

metamorphic peak conditions of ~1075 MPa and ~825°C. However, less than 3 km structurally below the eastern Taureau shear zone, the Mékinac-Taureau rocks have been retrogressed under P-T conditions varying from 800 to 700 MPa and from 775 to 675°C, although they clearly underwent peak conditions similar to those that prevailed in the interior of the domain. Furthermore, metapelite from the Shawinigan domain records P-T conditions varying from 850 to 625 MPa and from 775 to 700°C, values that are equivalent or slightly lower than P-T values from the retrogressed metapelite and amphibolite samples from the external zone of the Mékinac-Taureau domain. Evidence of higher grade metamorphism (e.g. >800°C, 1000 MPa) in the Shawinigan domain is lacking, in agreement with petrographical observations suggesting lower grade and higher degree of retrogression within this domain as compared to the Mékinac-Taureau domain. We emphasize here that metapelitic garnet from the external zone of the Mékinac-Taureau domain has flat chemical composition profiles implying complete homogenization by intra-crystalline diffusion during a lower granulite-facies retrograde metamorphic event and that, due to lower diffusion rates, relict of higher grade metamorphism was only detected in the amphibolite sample. Complete homogenization of garnet chemical profile implies that P-T conditions prevailing during metamorphic retrogression occurred for several tens of m.y. (see Caddick, 2010).

As a consequence, it is difficult to confidently determine the presence of a significant metamorphic contrast between both sides of the eastern Taureau shear zone. It can be argued that the relatively small decrease in metamorphism from the Mékinac-Taureau to the Shawinigan domain implies only limited vertical displacement along the eastern Taureau shear zone, but the occurrence of pre- to syn-kinematic disequilibrium textures imply a re-equilibration of the units before or during the shearing. Temperature of crystallization of zircon from the syn-kinematic pegmatite RS11-098 (~700°C) further supports lower temperature conditions during extension along the eastern Taureau shear zone as compared to peak metamorphism. Re-equilibration during shearing would certainly obscure the true metamorphic contrast, if any. Unless pre-kinematic metamorphic peak conditions are precisely determined for both domains, quantitative assessment of the amount of vertical displacement along the eastern Taureau shear zone remains impossible. In addition, a

pervasive metamorphic retrogression in rocks of the Shawinigan domain would likely make this task quite difficult. Furthermore, the timing of the pre-shearing metamorphic peak conditions must be proven to be the same in both domains in order to assess any significant interpretation of the metamorphic contrast. Present dataset implies, at least, that the Mékinac-Taureau domain was exhumed by ~350-400 MPa shortly before or during the normal-sense shearing event that occurred along the eastern Taureau shear zone.

U-Pb geochronology on two pegmatites provided time constraints on the tectono-metamorphic history of the Mauricie area (Fig. 2.13). Pegmatite RS12-040 was emplaced after the metamorphic peak (1075 MPa and ~825°C) and yielded a $^{207}Pb/^{206}Pb$ age of 1084 ± 18 Ma, interpreted as the a minimal age for the metamorphic peak and regional deformation related to NW-directed thrusting in the Mékinac-Taureau domain. Metamorphic conditions decreased to 700-800 MPa and 675-775°C before and/or during the emplacement of the second pegmatite, RS11-098, that yielded a $^{207}Pb/^{206}Pb$ age of 1064 ± 12 Ma. This latter pegmatite also provides an age constraint on the timing of significant extension localized along the eastern Taureau shear zone. Between ~1090 and ~1060 Ma, pressure conditions thus decreased by 350 to 400 MPa, which is equivalent to ~12-13 km of exhumation if one assumes a lithostatic gradient of 30MPa/km (Winter, 2001).

Finally, $^{40}Ar/^{39}Ar$ thermochronology data on amphibole and biotite provided time constraints on the cooling of the area. Based on amphibole and biotite $^{40}Ar/^{39}Ar$ ages, respectively, the Mauricie area cooled below 550-600°C at ~1000-1030 Ma and below 450°C at ~900-970 Ma. Amphibole cooling ages define a younging trend from the eastern Taureau shear zone towards the interior of the Mékinac-Taureau domain (Fig 2.13).

2.8.2 Mechanisms of exhumation

Exhumation of mid-crustal rocks in the hinterland of orogens may be the result of different mechanisms such as (1) syn-convergence channel flow (e.g. Beaumont et al. 2001, 2006, Godin et al. 2006), (2) buoyancy-driven rise of migmatitic diapirs (e.g. Calvert et al. 1999; Teyssier and Whitney, 2002) or (3) post-convergence gravitational collapse and

metamorphic core complex (MCC) development (e.g. Brun et al. 1994; Rey et al. 2009; Tirel, 2004). Here, we will compare the tectono-metamorphic characteristics of the Mauricie region with distinguishing features expected from these various tectonic mechanisms.

The regional deformation pattern in the Mauricie area is characterized by a dome-shaped foliation parallel to the lithotectonic boundaries and dipping away from the interior of the Mékinac-Taureau domain (Fig. 2.2). This regional pattern is considered as the result of thrust-related deformation prior to 1084 Ma in the Mékinac-Taureau domain (this study) and prior to 1087 Ma in the Shawinigan domain (Corrigan and van Breemen, 1997). Regional deformation is associated with high-grade metamorphism and partial melting in both domains, migmatites being particularly extensive in the upper structural levels of the Mékinac-Taureau domain. Strain increases in the vicinity of lithotectonic boundaries, i.e. the eastern Taureau and the Tawachiche shear zones. As argued above, the eastern Taureau shear zone played a significant role in the exhumation of the Mékinac-Taureau domain at 1064 ± 12 Ma. However, the Tawachiche shear zone must also be considered when assessing the exhumation history of the Mauricie area. Corrigan and van Breemen (1997) dated syn- and late-extension pegmatites, constraining NNE-directed extension along the Tawachiche shear zone, between 1065 ± 1 and 1036 +4/-2 Ma. Combined with data from our study, this therefore suggests that ESE-directed extension along the eastern Taureau shear zone has been coeval, within uncertainty, with NNE-directed extension along the Tawachiche shear zone. The average directions of tectonic transport on both shear zones are almost at right angle from each other (Fig. 2.14A).) Regional foliation conformable to discontinuities and an increase in finite strain towards normal-sense shear zones are structural characteristics that are however common to channel flow, diapirism and MCC formation.

Extrusion of mid-crustal material by channel flow involves a melt-weakened ductile layer bounded by a thrust shear zone below and a normal shear zone above (Godin et al. 2006). If such a mechanism occurred in the Mauricie area, only the top shear zone (normal-sense of shear in this case) has been recognized. An important characteristic of channel flow is the syn-convergent nature of the exhumation. Normal-sense shear zones of the Mauricie

area were active at ~1065-1035 Ma, a time period commonly accepted as a main compressional pulse of the Grenville orogen (i.e. Ottawan phase at 1090-1020 Ma; Rivers et al. 1997). However, the regional deformational strain in areas away from both the eastern Taureau and Tawachiche shear zones is attributed to thrusting and has been dated prior to ~1090 Ma (this study; Corrigan and van Breemen, 1997); evidence for contraction coeval with extension in the Mauricie area is therefore lacking (see below). Channel flow models generally predict a distribution of strain across the whole channel during lateral flow (although it might be concentrated along the bounding shear zones; Godin et al. 2006), but deformation within the interior of the Mékinac-Taureau and Shawinigan domains ceased >20 m.y. prior to extension along the eastern Taureau and Tawachiche shear zones and is clearly related to a different tectonic event. Furthermore, temperature attained in the area (up to 825°C) was largely sufficient for partial melting and weakening of the rocks, but such a temperature was no longer prevalent during extension when temperature was about 700°C and decreasing. This is still above the wet solidus of granitic rocks (Fig. 2.8), but the important solid-state deformation recorded by the leucosome in the shear zone suggests that it was mostly solidified during extension. Therefore, data from the Mauricie area do not support the channel flow hypothesis.

Diapirs are characterized by a radial distribution of stretching lineations, vertical flow in their trunk and horizontal flattening at their apex (e.g. Dixon, 1975). As shown in figure 2.14A, stretching lineations the margins of the Mékinac-Taureau and Shawinigan domains are orthogonal to each other. However, the distribution of these lineations do not correspond to a radial pattern around an hypothetical diapir, but are rather associated with two distinct shear zones located at different structural levels. The interior of the Mékinac-Taureau domain presents a strong foliation dipping away from its core, a feature common to the apex of diapirs. However, relict vertical fabric attesting for vertical flow during diapiric ascent, commonly observed despite the horizontal fabric overprinting (e.g. Gervais et al. 2004), are absent from the interior of the Mékinac-Taureau domain. Furthermore, we have demonstrated that deformation in the interior of the domain and along the bounding shear zones is the result of two distinct tectonic events divided by a >20 m.y. time gap, a timing

irreconcilable with diapirism. Finally, a relatively high buoyancy contrast is required to initiate and maintain diapirism (Teyssier and Whitney (2002). In most cases, this high buoyancy is due to voluminous granite intrusions or partial melting in the core of the diapir. In the Mauricie area, our field observations suggest the opposite: the volume of leucosome is much more important on the margins of the Mékinac-Taureau domain compared to its interior. Furthermore, rocks of the Mékinac-Taureau and the directly overlying Jésuite complex of the Shawinigan domains are of similar composition (i.e. intermediate orthogneiss) and consequently of similar density (e.g. Gibb, 1968). A density contrast in the area can be observed on the Bouguer gravity anomaly map (Geological Survey of Canada), but is associated with plutons of the second pulse of AMGC-type magmatism such as the ~1074 Ma Shawinigan norite, the ~1059 Ma Lejeune complex and the ~1056 Ma Gagnon pluton (Corrigan and van Breemen, 1997). Conclusions about the density of lithological units on the basis of the present gravity pattern should however be avoided. Movement along the eastern Taureau shear zone (i.e. 1064 Ma) started before the emplacement of a majority of these plutons. Furthermore, Corrigan and Hanmer (1997) interpreted this magmatic pulse as the result of convective thinning and extension of the lithosphere. However, the St. Boniface paragneiss contains abundant garnet metapelite and might have a slightly higher density as compared to the underlying Jésuite complex orthogneiss (e.g. Teyssier and Whitney, 2002) at the time of exhumation, but no evidence of normal shearing along the contact between the orthogneiss and paragneiss was observed. Furthermore, the overlying La Bostonnais complex of the Portneuf-Mauricie domain is also composed of felsic to intermediate plutonic rocks, so density contrasts on both sides of the Tawachiche shear zone are also negligible (e.g. Gibb, 1968). Due to poor compatible structural evidence, incompatible timing of deformation and lack of an efficient driving mechanism, diapirism is not proposed as the exhumation process for the Mauricie area.

MCC are characterized by a dome of high-grade metamorphic rocks covered by non-metamorphic upper crustal units (or units that have experienced an earlier metamorphic event). Both domains are separated by a detachment fault that is planar or slightly convex upward on the summit of the dome and dips away from that dome on its flanks (e.g. Wernicke,

1985; Lister and Davis, 1989; Tirel 2006). In the Mauricie area, the Mékinac-Taureau domain underwent high-grade metamorphism before 1084 Ma (1075 MPa and ~825°C; this study) and the Shawinigan domain underwent coeval and slightly lower-grade metamorphism (625-850MPa, 700-775°C, this study; Corrigan and van Breemen, 1997). The Portneuf-Mauricie domain was metamorphosed at ~1400 Ma (300-600 MPa; 550-700°C) and underwent only a limited overprint during the high-grade metamorphism of the two other domains (Corrigan, 1995; Lévesque, 1995; Corrigan and van Breemen, 1997). Evidence supporting low grade Grenvillian metamorphism is however debatable since Corrigan (1995) based this conclusion on U-Pb cooling ages on monazite (concordant) and titanite (discordant). It is now established that high grade metamorphism (temperature in excess of 700°C) does not necessarily resets U-Pb systematics in monazite (e.g. Rubatto et al. 2001; Cherniak et al. 2004) and titanite (e.g. Scott and St-Onge, 1995; Frost et al. 2000). Even if peak metamorphism in the Portneuf-Mauricie domain is the result of Grenvillian metamorphism, pressures conditions of 300-700 MPa, well constrained by Corrigan (1995) and Lévesque (1995), are lower than pressure conditions in the Mékinac-Taureau and Shawinigan domain (this study; Corrigan, 1995; Lévesque, 1995). Corrigan's (1995) conclusion that the Portneuf-Mauricie domain was at a higher structural position during Grenvillian orogeny is probably still valid. Together, these three metamorphic domains are separated by gently dipping (~20-30°) extensional shear zones that were active at ~1065-1035 Ma. In a MCC context, such architecture would correspond to the structurally lower part, away from the center of the MCC dome (Fig 2.14C). Such a mechanism of exhumation best accounts for the timing of deformation in the core of the different domains compared to their bounding shear zones (e.g. Armstrong, 1982; Coney and Harms, 1984). The trend of cooling ages younging towards the core of the dome is a feature uncommon to classic metamorphic core complexes (e.g. Sullivan and Snooke, 2007), but similar cooling trends are nevertheless reported in the literature (e.g. Brun and Sokoutis, 2007). Furthermore, extensional faults and shear zones that are interpreted as synthetic structures related to the main detachment are often observed in the hanging wall of MCC's (e.g. Wernicke, 1985). Such structures are observed in the Shawinigan domain, south of the Taureau shear zone (i.e. structurally above the shear zone; Fig. 2.5B). MCC development is

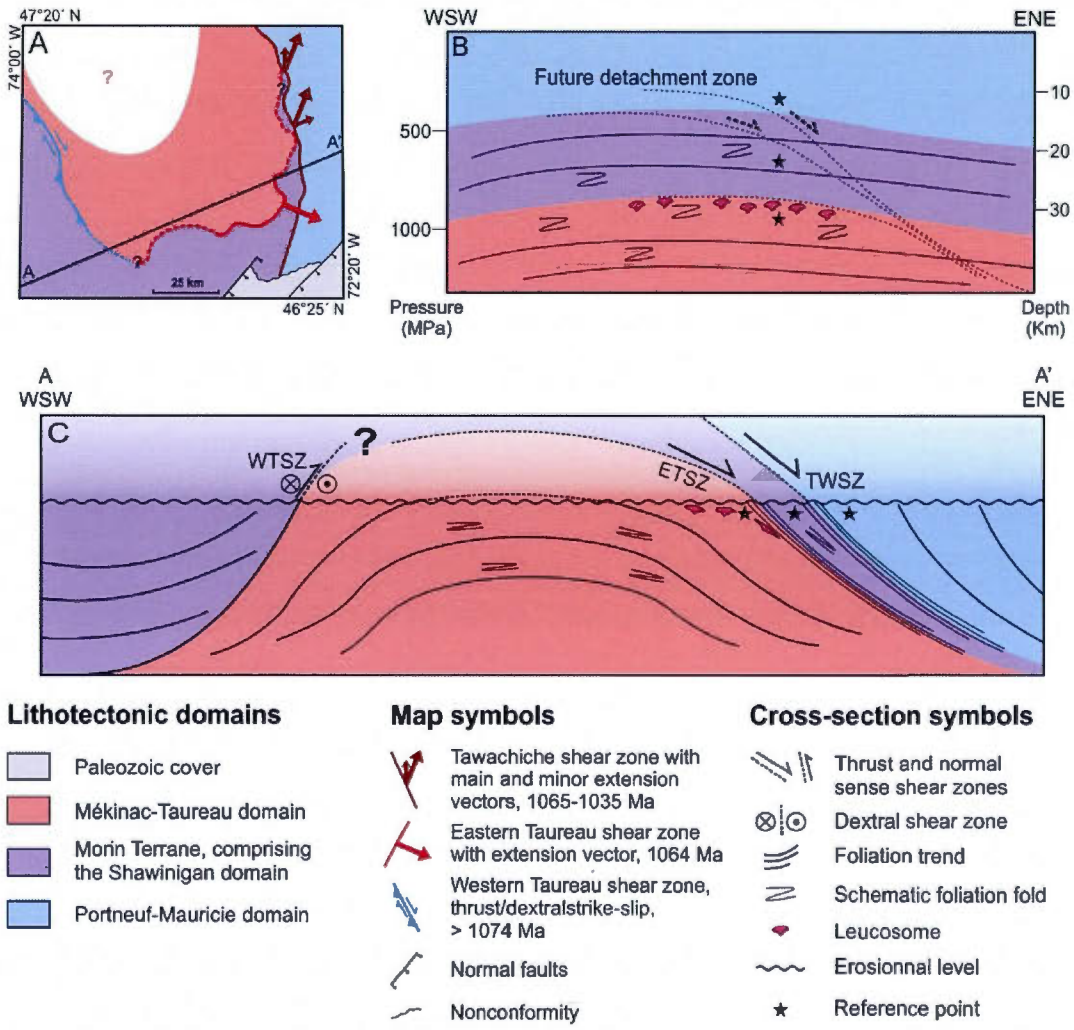

Fig. 2.14 A. Simplified geologic map of lithotectonic domains and major shear zones of the Mauricie area (modified from Nadeau and Brouillette, 1995). Cross section A-A' is shown in figure 2.14C. **B.** Schematic structural profile representing the configuration of thrust-imbricated domains prior to extension. This configuration might have prevailed before 1084 ± 18 Ma, the minimal age constraint determined for peak metamorphism and thrusting in the Mékinac-Taureau domain. The vertical pressure scale is based on values obtained from the Mékinac-Taureau and Shawinigan domains and depth in kilometers is calculated assuming a pressure gradient of 30MPa/km (Winter, 2001). Red pods represent leucosome material at the Mékinac-Taureau and Shawinigan domains interface. The approximate trace of the future detachment zone (i.e. the eastern Taureau and Tawachiche shear zones) is shown on the cross-section. **C.** A-A' cross-section showing the architecture after the 1065-1035 Ma episode of extension. Deformation was localized along both the eastern Taureau and Tawachiche shear zones, responsible for the exhumation of the Mékinac-Taureau and Shawinigan domains as a metamorphic core complex. Reference points (black stars) show how different crustal levels were juxtaposed laterally. WTSZ—western Taureau shear zone, ETSZ—eastern Taureau shear zone, TWSZ—Tawachiche shear zone.

commonly associated with unidirectional direction of extension (e.g. Lister and Davis, 1989; Doughty et al. 2007; Lana et al. 2010), as opposed to what is suggest by available geochronologic data from the Mauricie region (coeval NNE- and ESE-directed extension, within uncertainties). Although uncommon, examples of core complexes with varying direction of extension however exist in nature. Hill et al. (1992) and Hill (1994) described the d'Entrecasteaux Island MCC and argued for the existence of bounding shear zones with directions of shearing at 90°C from one another.

It is also essential to test the driving force of this type of exhumation. It is well known that the majority of MCC develops in extensional regimes through gravitational collapse following crustal thickening (e.g. Coney and Harms, 1984). Crustal thickening in the Mauricie area did occur prior to the onset of extension along the eastern Taureau and Tawachiche shear zones. As stated above, extension in the Mauricie area seems to have happened during a main contractional pulse of the Grenville orogeny. Such timing seems to be incompatible with post-orogenic context, but a review of published geochronological constraints shows that the age of contractional deformation in and around the Mauricie area during the Ottawan phase is uncertain and the subject of debate. To the west, Martignole and Friedman (1998) suggest a minimum age of 1074 ± 4 Ma for thrusting along the western Taureau shear zone. However, no maximum age constraint is provided, leaving open the possibility of an earlier deformation. Furthermore, their isotopic age is defined by a two-point discordia line within a very heterogeneous zircons population (Fig. 9 of Martignole and Friedman, 1998) and should therefore not be considered as a solid base for interpretations on the timing of contractional deformation along the western Taureau shear zone. A second isotopic date was obtained by the same authors on the Labelle shear zone, approximately 175 km away from the Mauricie area. The Labelle shear zone bounds the Morin terrane to the west and has a complex kinematic history (e.g. Martignole and Corriveau, 1991; Zhao et al. 1997). Martignole and Friedman (1998) suggested that the Labelle shear zone represents the western lateral ramp along which the Morin terrane was transported towards the north and provided a 1079 ± 6 Ma minimal age constraint for this thrusting deformation. Further west, the Elzevir terrane is interpreted as part of the orogenic lid that escaped penetrative Grenvillian metamorphism

(Rivers, 2008, 2012) because it did not record any evidence of contraction during the Ottawan phase. East of the Mauricie area, timing constraints for contraction are provided by Hébert et Lacoste (1998) and Hébert et al. (2009) for the St-Fulgence deformation zone which is located to the NW of the Saguenay River, i.e. 200-350 km northeast of the Mauricie area. The St. Fulgence deformation zone is a NE-SW striking transpressional deformation zone that accommodated WNW-directed dextral-oblique thrust between ~1080 and 1030 Ma (Hébert et Lacoste, 1998), with minor displacement until 1010 Ma (Hébert et al. 2009). In the same area, the NE-SW striking Pipmuacan deformation zone accommodated dextral sense of shear at ~1075 Ma (Hébert et al. 2009). No further evidence of Ottawan contraction is recognized yet between the Mauricie and Saguenay area. Evidence of 1060-1030 Ma NW-SE contraction in and around the Mauricie area is therefore ambiguous, which suggests that our region of study might not have been under a compressional tectonic regime during the Ottawan phase of the Grenville orogen. It is possible that contractional deformation could be older in the central Grenville Province than elsewhere, due to diachronous collision for example. Absence of significant contraction during that period could therefore be compatible with post-orogenic collapse and MCC development in the Mauricie area.

2.8.3 Tectonic implications for the Grenville

Recent theory on the evolution of the Grenville Province, concerning more specifically post-Ottawan orogenic collapse, is presented in Rivers (2008, 2012). According to this author, the thickening of the crust during the Ottawan phase (1090-1020 Ma; Rivers, 1997, 2008) led to the formation of a Himalayan-type orogenic plateau in the hinterland of the orogen. Following the Ottawan phase of compression, the collapse of the plateau resulted in the juxtaposition of upper crustal fragments against a series of high-grade mid-crustal core complexes. In the Mauricie area, our study confirms that the Mékinac-Taureau and Shawinigan domains were part of the mid-crust metamorphosed at high-grade in response to crustal thickening. It also confirms that post-thickening extension along the eastern Taureau and Tawachiche shear zones has been responsible for the exhumation of these high-grade metamorphic domains. However, the collision/collapse sequence occurred earlier in the

Mauricie area as documented elsewhere in the Grenville Province in general: high-grade metamorphism is here shown to be pre-1090 Ma, whereas extension was mainly active at 1065-1030 Ma. The reason of that temporal discrepancy is presently enigmatic and should be the focus of further studies. Besides, the directions of extension along the eastern Taureau and Tawachiche shear zones are orthogonal to each other. Even though most extensional shear zones responsible for the juxtaposition of mid- with upper-crust material are generally unidirectional, Rivers (2012) proposed that the quasi-radial overall pattern of extension direction in the Grenville Province is an argument in favor of gravity-driven orogenic collapse. The study of the tectono-metamorphic history of the Mauricie area thus broadly corroborates the orogenic collapse model of Rivers (2008, 2012) for the exhumation of mid-crustal metamorphic core complexes in the Grenville Province.

2.9 Conclusions

Structural analysis, thermobarometry, U-Pb geochronology and $^{40}Ar/^{39}Ar$ thermochronology on selected samples of the Mauricie area provided data essential to the reconstruction of the tectono-metamorphic history of the area:

1) Peak metamorphism in the Mékinac-Taureau domain reached P-T conditions of ~1075 MPa and ~825°C prior to 1084 ± 18 Ma. This metamorphic event is considered as the result of northwestward thrusting and regional-scale crustal thickening.
2) Retrograde conditions varying from 800 to 700 MPa and from 775 to 675°C were recorded in the upper structural levels of the Mékinac-Taureau domain.
3) The Shawinigan domain records P-T conditions varying from 850 to 625 MPa and from 775 to 700°C, values that are equivalent or of a slightly lower metamorphic grade as compared with retrogressed samples from the margin of the Mékinac-Taureau domain.
4) The contact between the Mékinac-Taureau and the Shawinigan domain is marked by a normal-sense shear zone with a top-down-to-the-ESE sense of shear, the eastern Taureau shear zone, that was active at ~1064 ± 12 Ma, during and/or after retrograde metamorphism documented in the Mékinac-Taureau domain.

5) Extension along the eastern Taureau shear zone is coeval, within uncertainty, with NNE-directed extension along the Tawachiche shear zone (Corrigan, 1995; Corrigan and van Breemen, 1997).

6) The area cooled below 550-600°C at ~1000-1030 Ma and below 450°C at ~900-970 Ma.

7) Structural and metamorphic characteristics of the Mauricie area are similar to those expected from the structurally lower levels of a metamorphic core complex formed during post-convergent orogenic collapse. The Mékinac-Taureau and Shawinigan domains were thus probably exhumed by a similar process.

8) Our study supports the orogenic collapse model of Rivers (2008, 2012) for the exhumation of mid-crustal metamorphic core complexes in the Grenville Province, although the sequence of thickening and exhumation is older in the Mauricie area as compared with other parts of the orogen.

Acknowledgments

This work is part of a M.Sc. thesis undertaken by Renaud Soucy La Roche at Université du Québec à Montréal (UQÀM). Renaud Soucy La Roche received graduate scholarships from the Natural Sciences and Engineering Research Council of Canada (NSERC) and the Fonds de recherche du Québec – Nature et Technologies (FRQNT). The project was financed by a NSERC research grant held by Alain Tremblay (PG 105669) and by internal funding provided to Félix Gervais by École Polytechnique de Montréal. Morgann Perrot and Xavier Vasseaud are thanked for field assistance. Lang Shi from the Electron Microprobe Laboratory of the McGill University is thanked for his assistance during the acquisition of mineral chemical compositions for thermobarometry. Michelle Laithier is also thanked for her useful advices on figures conception.

CHAPITRE III

RÉSULTATS SUPPLÉMENTAIRES

3.1 Description des unités

Ce chapitre présente une description plus complète des différentes unités observées sur le terrain et en lame mince, par rapport à la description abrégée fournie dans le manuscrit d'article du chapitre 2. Certains éléments seront repris directement du chapitre 2, mais ils sont essentiels à la mise en contexte des informations additionnelles présentées dans cette section.

3.1.1 Domaine de Mékinac-Taureau

Le domaine de Mékinac-Taureau est principalement composé d'orthogneiss migmatitique à orthopyroxène de composition felsique à intermédiaire. Il comprend aussi des niveaux discontinus de métapélite, de quartzite, de marbre, de gneiss calco-silicaté et de métabasite représentant moins de 1% du volume de ce domaine.

Orthogneiss

La composition de l'orthogneiss varie de felsique à intermédiaire, mais généralement granodioritique, avec la présence locale de gneiss mafique. Les surfaces altérées sont typiquement brunes, tandis que les surfaces fraîches sont vert foncé à cause de l'abondance de plagioclases verdâtres, une couleur typique des orthogneiss à orthopyroxène du faciès granulite (ex : Howie, 1967; Pidgeon et Howie, 1975). Des surfaces plus rosées sont observées dans les gneiss riches en feldspath potassique. Les cristaux sont généralement granoblastiques et leur taille varie de fine à moyenne (1-3 mm). L'orthogneiss montre généralement une gneissossité bien développée, quoiqu'une texture massive soit aussi localement observée. L'orthogneiss felsique à intermédiaire est communément migmatisé, tandis que l'orthogneiss mafique ne l'est que localement. Le volume de leucosome, quelques pourcents seulement dans le cœur du domaine de Mékinac-Taureau, augmente vers le sommet structural du dôme et atteint 20-40% à proximité de la zone de cisaillement Taureau

orientale. Le leucosome forme des bandes stromatiques parallèles à la foliation (Fig. 3.1A) ainsi que des «pochettes» grossières non déformées recoupant la foliation (Fig. 3.1B). Du leucosome piégé entre les boudins formés par les couches plus mafiques (Fig. 3.1A) ou dans les charnières de plis isoclinaux issus de la déformation régionale (Fig. 3.1C) sont aussi observés, suggérant ainsi qu'une première génération de leucosome a été produite pendant la déformation régionale tandis qu'une seconde génération a été produite après cette même déformation. Cette observation pourrait être expliquée par deux évènements métamorphiques différents, ou encore par un épisode de migmatisation formant un continuum pendant et après la déformation régionale (ex. Corrigan, 1995). Cette dernière hypothèse est plus probable étant donné que les deux types de leucosome contiennent le même assemblage minéralogique (voir ci-dessous), indiquant des conditions similaires de formation, et surtout parce qu'il est possible d'observer une relation d'association entre les deux types de leucosome, telle qu'une bande de leucosome stromatique rejoignant et se mêlant à une pochette recoupant la foliation.

L'assemblage minéralogique typique de l'orthogneiss est Pl + Qtz + Kfs + Opx + Hbl + Bt en proportions variables (abréviations d'après Kretz, 1983, voir Liste des abréviations des minéraux). L'apatite et le zircon sont des minéraux accessoires communs tandis que la chlorite rétrograde remplace localement la biotite. Le feldspath potassique est partout perthitique, tandis que la texture anti-perthitique est commune dans le plagioclase. Le quartz forme généralement des rubans granoblastiques polygonaux ou encore des grains isolés polygonaux à ovoïdes avec des frontières de grains suturées. Le clinopyroxène et le grenat sont des constituants mineurs à quelques localités. Les deux types de leucosome (stromatique et pochettes) contiennent le même assemblage minéralogique composé de Qtz + Pl + Opx ± Kfs ± Bt ± Grt ± Cpx ± Hbl. L'orthopyroxène se distingue par son altération brunâtre (Fig. 3.1B) et sa présence dans le leucosome indique que la migmatisation s'est produite au faciès granulite (ex : Percival, 1989, 1991).

À proximité de la zone de cisaillement Taureau orientale, plusieurs textures de déséquilibre métamorphique peuvent être observées dans le gneiss plus mafique. Par

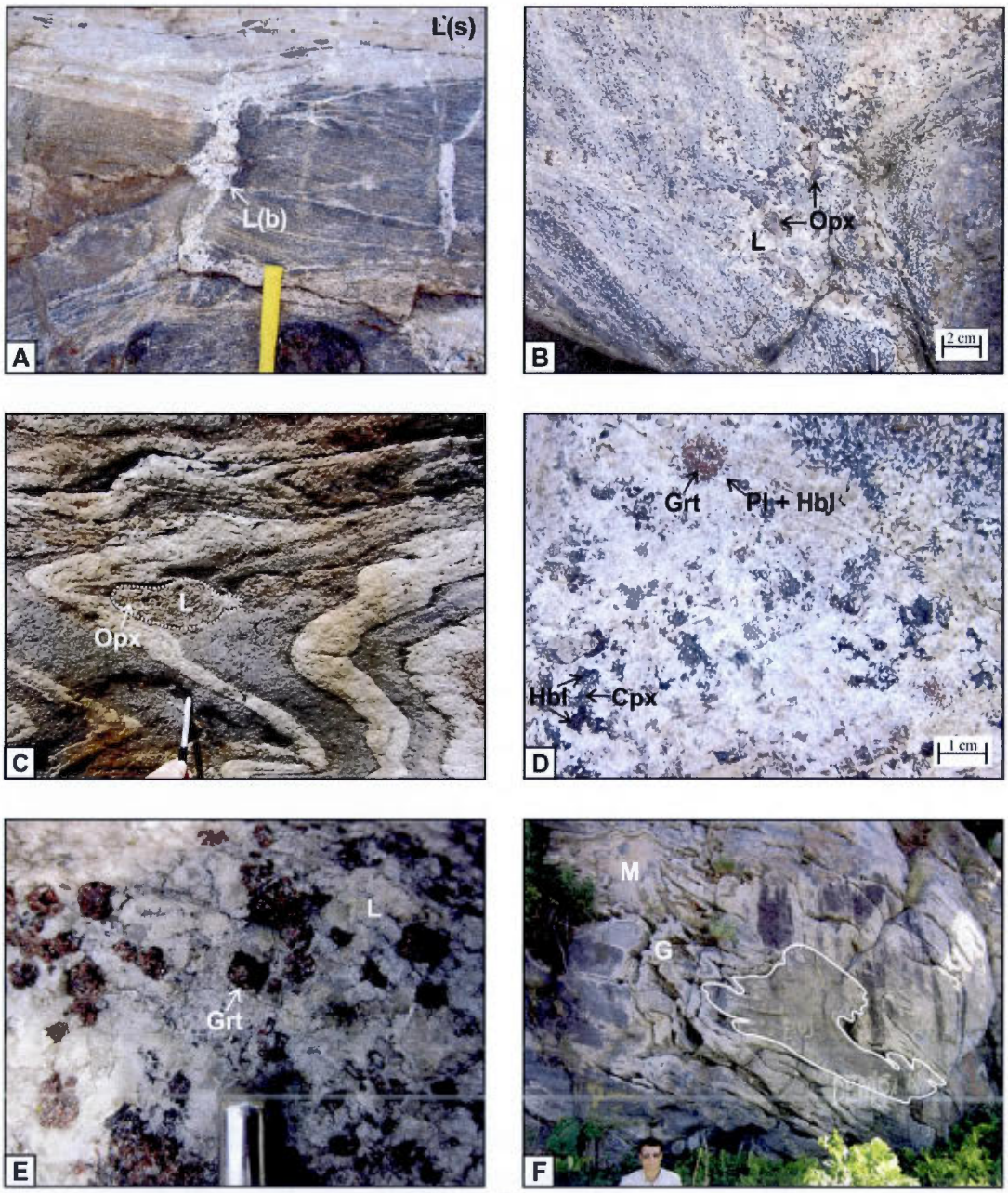

Fig. 3.1. Photographies du domaine de Mékinac-Taureau. **A.** Leucosome pré- à syn-cinématique en couches stomatiques (Ls) et piégé entre des boudins mafiques (Lb). **B.** Leucosome post-cinématique recoupant la foliation et contenant de l'orthopyroxène (L), suggérant une fusion partielle lors du pic métamorphique. **C.** Leucosome pré- à syn-cinématique piégé dans une charnière de plis (L) contenant d'abondants cristaux d'orthopyroxène. **D.** Couronnes réactionnelles de plagioclase et hornblende autour du grenat et clinopyroxène remplacé par de la hornblende dans un leucosome. **E.** Grenat automorphe dans le leucosome des métapélites, indiquant sa formation lors de la fusion partielle. **F.** Couche de marbre (M) et de gneiss calco-silicaté (G) présentant un pli en fourreau.

exemple, le clinopyroxène est fréquemment partiellement remplacé par une couronne de hornblende. Des couronnes réactionnelles composées de plagioclase ont aussi été observées autour de certains grenats (Fig. 3.1D). La présence de telles réactions dans un leucosome contenant du clinopyroxène remplacé par de la hornblende indique que la réaction de décompression :

$$\text{Grt} + \text{Cpx} + \text{liquide de fusion} = \text{Hbl} + \text{Pl} \text{ (Vielzeuf et Schmidt, 2001)} \quad (3.1)$$

s'est produite dans cette roche. De plus, des couronnes réactionnelles de plagioclase et de hornblende ont été observées autour des grenats d'une amphibolite (Fig. 2.6F), suggérant la réaction de décompression suivante :

$$\text{Tschermakite-Hbl} + \text{Grt} + \text{Qtz} = \text{Tremolitic-Hbl} + \text{Pl} \text{ (Schaubs et al. 2002)} \quad (3.2)$$

Paragneiss

Des couches métriques discontinues de paragneiss migmatitique sont dispersées à travers le domaine de Mékinac-Taureau. Elles sont composées principalement de métapélite et localement de quartzite. Les porphyroblastes de grenat et de sillimanite sont caractéristiques des métapélites et peuvent constituer jusqu'à 30% de la roche. L'assemblage minéralogique des métapélites contient Qtz + Pl + Kfs + Bt +Sil + Grt ± Rt ± Ilm ± Zrn ± Mnz. Le grenat est hypidiomorphe et mesure jusqu'à 10 mm, excepté dans le leucosome où il est plus grossier (10-30 mm) et automorphe (Fig. 3.1E). Cela suggère qu'une génération de grenat a été produite pendant la fusion partielle et est demeurée en équilibre durant la cristallisation du leucosome (Powell et Downes, 1990; White et al. 2004). Ce grenat aurait donc été produit par une réaction telle que :

$$\text{Bt} + \text{Sil} = \text{Grt} + \text{Kfs} + \text{liquide de fusion (Spear et al. 1999)} \quad (3.3)$$

Un affleurement à l'intérieur du domaine de Mékinac-Taureau (RS12-021) contient toutefois des grenats parfaitement automorphes, y compris dans le paléosome (Fig. 2.6B). La sillimanite, la biotite, le quartz et les feldspaths sont fréquemment inclus dans ce type de

grenat. La sillimanite forme des prismes fins à moyens (0.1-5mm) qui sont fréquemment courbés autour des porphyroblastes de grenat. Le quartz forme des rubans granoblastiques polygonaux excepté dans un échantillon où des sous-grains sont développés dans les rubans (Fig. 2.5A). La biotite forme de fins cristaux (0.5-2mm) alignés dans la foliation, excepté dans les ombres de pression du grenat là où elle est plus grenue (1-3mm) et moins orientée. Le feldspath potassique présente partout une texture perthitique.

Marbre et gneiss calco-silicaté

Le marbre et les gneiss calco-silicatés forment des couches ayant généralement quelques mètres d'épaisseur, qui sont généralement concordantes avec la foliation régionale. Ils sont couramment associés spatialement avec des paragneiss. Le marbre est blanc à rose en surface fraîche tandis que le gneiss calco-silicaté est plus verdâtre. Toutefois, les deux types de lithologie sont fréquemment altérés en couches récessives brunâtres distinctives. Le marbre pur est grossier (5-30 mm) et massif, mais les abondants minéraux silicatés du gneiss calco-silicaté définissent une forte fabrique parallèle à la foliation régionale. Ces marbres contiennent des fragments arrondis à tordus de l'orthogneiss encaissant et présentent des caractéristiques structurales indiquant une intense déformation ductile telles que des plis en fourreau (Fig. 3.1F). Ces niveaux de marbre ont été interprétés comme des brèches tectoniques par Nadeau et Brouillette (1995). Hanmer (1988) a expliqué la présence de structures similaires par la viscosité relativement basse du marbre à haute température et pression par rapport aux gneiss encaissants. Le marbre impur et les gneiss calco-silicatés contiennent Cal/Dol + Di + Qtz + Ttn + Scp ± Phl ± Ap ± Zrn ± Spl. Le diopside est de forme arrondie et généralement associé au quartz. La scapolite a une composition proche du pôle méionite. Le spinelle forme de rares petits (<0.1 mm) grains xénomorphes. L'olivine est absente de l'assemblage du marbre, ce qui est surprenant considérant le haut grade métamorphique de la région. Toutefois, la composition chimique de la roche, la composition des fluides et leur pression ont une forte influence sur la stabilité des minéraux dans les marbres (Spear, 1993), ce qui pourrait expliquer l'absence d'olivine dans ces roches.

3.1.2 Le domaine de Shawinigan

Le domaine de Shawinigan est composé de deux types d'unités lithologiques en contact tectonique. La partie la plus basse structuralement, en contact avec le domaine de Mékinac-Taureau le long de la zone de cisaillement Taureau orientale, est constituée d'orthogneiss felsique à intermédiaire et nommée le complexe du Jésuite (Nadeau et Brouillette, 1995). Une séquence de roches méta-sédimentaires, le paragneiss de Saint-Boniface, est exposé dans les niveaux structuraux plus élevés de ce domaine. Cette dernière unité est composée de métapélite et localement de quartzite, de marbre et de gneiss calco-silicaté.

Orthogneiss

La composition de l'orthogneiss est essentiellement tonalitique, mais des roches granitiques et plus rarement gabbroïques sont aussi présentes. Les surfaces altérées sont généralement brunâtres tandis que les surfaces fraîches sont grises à verdâtres. Des surfaces fraîches rosâtres sont aussi observées lorsque les roches sont riches en feldspath potassique. Les cristaux des minéraux principaux sont généralement granoblastiques et leur taille varie de fine à moyenne (1-3 mm). L'orthogneiss montre habituellement une gneissossité bien développée, mais peut aussi être massif localement. Des migmatites de type stromatique sont fréquentes dans les gneiss felsiques à intermédiaires, quoiqu'elles ne soient pas aussi importantes que dans les niveaux structuraux supérieurs du domaine de Mékinac-Taureau. L'assemblage minéralogique typique de l'orthogneiss est Pl + Qtz + Hbl + Bt ± Cpx ± Kfs ± Opx ± Ap ± Zrn dans des proportions variables. Le pyroxène est rare et généralement remplacé partiellement par la hornblende (Fig. 3.2A). Le microcline est le feldspath potassique principal et la texture perthitique est rare, ce qui contraste avec le domaine de Mékinac-Taureau dans lequel cette texture est omniprésente. La texture anti-perthitique dans le plagioclase est elle aussi peu commune. Le quartz forme généralement des rubans granoblastiques polygonaux ou des grains isolés polygonaux à ovoïdes avec des frontières de grains suturées.

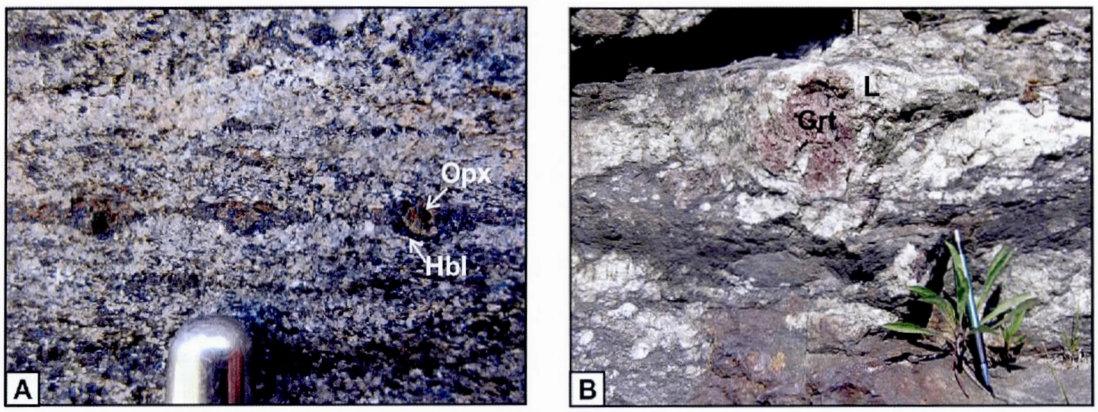

Fig. 3.2. Photographies du domaine de Shawinigan. **A.** Orthopyroxène partiellement remplacé par de la hornblende dans un orthogneiss. **B.** Grenat de 10 cm de diamètre dans un leucosome d'une métapélite.

Paragneiss

Le paragneiss du domaine de Shawinigan est principalement constitué de métapélites et de rares quartzites. Les porphyroblastes de grenat et de sillimanite sont caractéristiques des métapélites et peuvent constituer jusqu'à 40% de la roche. L'assemblage minéralogique des métapélites contient Qtz + Pl + Kfs + Bt ± Sil + Grt + Rt ± Ilm ± Gr ± Tur ± Zrn ± Mnz (Fig. 2.6A). Le grenat est hypidiomorphe et large (1-3 cm, jusqu'à 10 cm dans le leucosome; Fig. 3.2B). Il contient généralement une partie centrale riche en inclusions (Qtz + Ilm; Fig. 2.6C-D). La sillimanite, la biotite, les feldspaths et la tourmaline forment aussi, dans une moindre proportion, des inclusions dans les grenats. Des grenats pauvres en inclusions ont aussi été observés dans un échantillon (RS11-105; Fig. 2.6E). La sillimanite forme des prismes fins à larges (0.1-20mm) qui sont fréquemment boudinés ou courbés autour des porphyroblastes de grenat. Le quartz forme des rubans granoblastiques polygonaux ou des grains aplatis dans la matrice. La biotite forme de fins cristaux (0.5-2mm) alignés dans la foliation, excepté dans les ombres de pression du grenat là où elle est plus grenue (1-4mm) et moins orientée. Le feldspath potassique est la microcline ou la perthite. La tourmaline a été observée dans un affleurement où elle est présente dans le paléosome et le leucosome.

Marbre et gneiss calco-silicatés

Des couches métriques de marbre et de gneiss calco-silicatés associés aux métapélites

sont aussi observées dans le domaine de Shawinigan. Le marbre est généralement blanc, mais prend une teinte verdâtre selon l'abondance des minéraux calco-silicatés. Il est généralement moyennement grenu (0.5-5 mm), massif et ne présente généralement pas l'aspect brèchifié d'origine tectonique typique des marbres du domaine de Mékinac-Taureau. L'assemblage minéralogique typique est Cal/Dol + Ol (Srp) + Di + Phl + Gr ± Zrn ± Qtz. Le diopside et l'olivine forment des grains de forme arrondie de 1 à 2 mm de large. L'olivine est partiellement remplacée par la serpentine, qui y forme parfois un réseau de veines anastomosées. Le quartz est rare et forme des amas xénomorphes.

CONCLUSIONS ET RECOMMANDATIONS

Les analyses structurales, de thermobarométrie classique, de géochronologie U-Pb et de thermochronologie $^{40}Ar/^{39}Ar$ effectuées sur une série d'échantillons de la Mauricie ont fourni des données essentielles à la reconstruction de l'histoire tectono-métamorphique de la région :

1) Le pic métamorphique dans le domaine de Mékinac-Taureau a atteint des conditions de ~1075 MPa et ~825°C avant 1084 ± 18 Ma. Cet évènement métamorphique est considéré comme le résultat d'un chevauchement dirigé vers le nord-ouest et de l'épaississement crustal à l'échelle régionale.
2) Des conditions de métamorphisme rétrograde variant de 800 à 700 MPa et de 775 à 675°C ont été enregistrées dans les niveaux structuraux supérieurs du domaine de Mékinac-Taureau.
3) Le domaine de Shawinigan a enregistré des conditions de pression et de température variant de 850 à 625 MPa et de 775 à 700°C, des valeurs qui sont équivalentes où légèrement inférieures à celles obtenues avec les échantillons rétrogressés des niveaux structuraux supérieurs du domaine de Mékinac-Taureau.
4) Le contact entre les domaines de Mékinac-Taureau et de Shawinigan est marqué par une zone de cisaillement normale vers l'est-sud-est, nommée la zone de cisaillement Taureau orientale. Elle était active autour de 1064 ± 12 Ma, pendant et/ou après le métamorphisme rétrograde documenté dans le domaine de Mékinac-Taureau.
5) L'extension le long de la zone de cisaillement Taureau orientale est contemporaine, à l'intérieur des marges d'erreur, avec l'extension vers le nord-nord-est le long de la zone de cisaillement de Tawachiche (Corrigan, 1995; Corrigan et van Breemen, 1997).
6) La région a refroidi sous 550-600°C à ~1000-1030 Ma et sous 450°C à ~900-970 Ma.
7) Les caractéristiques structurales et métamorphiques de la Mauricie sont similaires à celles observées dans les niveaux structuraux inférieurs des dômes métamorphiques extensifs formés lors de l'effondrement orogénique post-convergent. Les domaines de Mékinac-Taureau et de Shawinigan ont donc probablement été exhumés par un processus similaire.

8) Cette étude appuie le modèle d'effondrement orogénique développé par Rivers (2008, 2012) pour l'exhumation de dômes métamorphiques extensifs dans la Province de Grenville, quoique la séquence d'épaississement et d'exhumation soit plus vieille en Mauricie comparée aux autres sections de cette province géologique.

Toute étude de l'évolution métamorphique et structurale de l'orogénie grenvillienne doit nécessairement inclure l'acquisition de nouvelles données pétrographiques et géochronologiques puisque ces dernières forment les assises d'une meilleure compréhension de cet évènement géologique complexe. Dans la région de la Mauricie, il serait utile de dater plus précisément le pic métamorphique ainsi que la durée du métamorphisme rétrograde documentés dans les domaines de Mékinac-Taureau et de Shawinigan au cours de la présente étude. La datation *in-situ* de minéraux métamorphique (ex : monazite) permettrait probablement d'obtenir des contraintes temporelles sur des réactions métamorphiques précises et de reconstruire une histoire structurale plus complète. Il serait aussi important de dater à nouveau le métamorphisme dans le domaine de Portneuf-Mauricie afin de vérifier l'hypothèse de Corrigan (1995) selon laquelle ce domaine était situé à un niveau structural plus élevé lors de la phase Ottawan. De plus, les données géochronologiques actuelles contraignant la déformation le long des zones de cisaillement Taureau orientale et de Tawachiche pourraient être améliorées par l'acquisition de nouveaux échantillons et l'utilisation de techniques de datation plus précises telles que la spectrométrie de masse par ionisation thermique (TIMS – *chemical abrasion thermal ionization mass spectrometry*). Par exemple, la datation de pegmatites post-cinématiques recoupant la zone de cisaillement Taureau fournirait une limite temporelle inférieure pour cet évènement de déformation. Ces données géochronologiques sont essentielles pour confirmer ou infirmer l'hypothèse selon laquelle la déformation est contemporaine le long de ces deux zones de cisaillement. Finalement, les études supplémentaires devraient aussi se concentrer sur la zone de cisaillement Taureau occidentale. Il serait important de réévaluer la cinématique de ce cisaillement et, surtout, d'obtenir une fourchette d'âges isotopiques plus fiables permettant de contraindre la déformation. Enfin, une étude structurale au sud du domaine de Mékinac-Taureau serait nécessaire afin de comprendre comment les branches occidentales et orientales de la zone de cisaillement Taureau interagissent, quoique la rareté des

affleurements dans cette région rende possiblement cette tâche difficile. Dans une optique plus vaste, il serait important de comprendre pourquoi l'exhumation via des zones de cisaillement normales a commencé plusieurs dizaines de millions d'années plus tôt en Mauricie comparée au reste de la Province de Grenville.

ANNEXE A

PROBLÈMES ASSOCIÉS À LA THERMOBAROMÉTRIE DES MÉTAPÉLITES DE HAUT GRADE

Des précautions particulières doivent être prises lors de l'évaluation des conditions de pression et de température des roches de haut grade métamorphique. La vitesse du processus de diffusion, par lequel les éléments chimiques migrent au sein d'un cristal et entre les cristaux, dépend grandement des minéraux impliqués et de la température (Spear, 1993). En effet, le taux de diffusion du Fe, du Mg, du Ca et du Mn dans le grenat est assez rapide pour modifier le patron de zonation jusqu'au cœur du cristal à partir de températures avoisinant les 500-600°C (Tracy, 1982; Caddick, 2010). Pour les températures où la diffusion est effective, la composition chimique initiale d'un minéral sera modifiée si suffisamment de temps est fourni. Par exemple, la composition chimique d'un grenat de 1000 µm de diamètre sera modifiée en quelques millions d'années si la température atteint 600°C, mais plusieurs dizaines de millions d'années seront nécessaires pour rééquilibrer complètement sa composition chimique même si la température atteint 800°C (Caddick et al. 2010). Dans la biotite, la diffusion sera instantanée si la température est supérieure à 520°C (Spear, 1993). Par contre, les taux de diffusion du Na et du Ca dans le feldspath plagioclase sont très lents pour toutes les températures (Spear et al. 1993). Le feldspath plagioclase a donc tendance à conserver la composition chimique qui était à l'équilibre lors de la formation et ne sera affecté que par des processus de dissolution et reprécipitation (Grove et al. 1984). Puisque les taux de diffusion dans le grenat et la biotite sont relativement rapides sous des conditions du faciès granulite, la composition chimique de ces minéraux est partiellement à complètement rééquilibrée en fonction des conditions ambiantes. Ainsi, la biotite aura une composition chimique homogène représentant les conditions de pic métamorphique tandis que la composition chimique du grenat s'équilibrera de la bordure vers le cœur. Il est donc probable d'observer un plateau compositionnel parfait ou présentant une zonation de croissance relique dans le cœur du grenat. Toutefois, lors du refroidissement, ces hauts taux de diffusions sont aussi responsables de perturbations de la composition chimique du grenat et de la biotite, particulièrement s'ils sont en contact direct. En effet, des échanges de Fe et de Mg

peuvent survenir afin d'équilibrer la composition chimique avec les conditions de pression et de température lors de la rétrogression. Les changements de compositions se font initialement à l'interface des grains de biotite et de grenat et se propagent ensuite vers le cœur de cristaux. La diffusion est plus lente dans le grenat que dans la biotite, dans laquelle ce processus est instantané à l'échelle géologique. Ainsi, le grenat pourra enregistrer l'histoire rétrograde plus précisément que la biotite, qui est rééquilibrée complètement à chaque fois que les conditions de pression et de température sont modifiées, à condition que cette dernière soit en contact avec le grenat. Une interprétation attentive des patrons de zonation dans le grenat est donc nécessaire afin de comprendre les résultats de thermobarométrie calculés avec sa composition chimique.

Si la température n'est pas suffisamment élevée pour que la diffusion soit effective dans le grenat, ce dernier ne sera pas rééquilibré et préservera son patron de zonation de croissance. Dans les métapélites, cette zonation est généralement marquée par une augmentation en Fe et Mg et une diminution en Ca et Mn du cœur vers la bordure (Hollister, 1966). Cette situation est toutefois improbable dans la présente étude puisque les observations pétrographiques suggèrent que les métapélites ont été métamorphisées aux faciès amphibolite supérieure et granulite.

Si la température est suffisante pour permettre la diffusion dans le grenat, celui-ci sera rééquilibré et le patron de zonation de croissance sera partiellement à complètement effacé. Si le grenat atteint des températures élevées pendant un temps suffisamment long et est ensuite refroidi géologiquement instantanément, sa composition chimique sera homogène du cœur vers la bordure. Toutefois, un refroidissement aussi rapide est rare et les observations pétrographiques des grenats suggèrent qu'ils ont presque tous subis de la rétrogression (excepté l'échantillon RS12-021).

Finalement, le scénario le plus plausible implique la rééquilibration du grenat aux conditions de pic métamorphique supérieures à 600°C, suivi par la perturbation de l'équilibre chimique lors de la rétrogression. Dans ce cas, la composition chimique à l'équilibre lors du pic métamorphique sera préservée sous forme de plateau dans le cœur du grenat (ou alors

seulement dans le cœur externe si la rééquilibration Grt-Bt à haute température n'est pas complète) tandis que la bordure présentera une zonation en réponse au déséquilibre lors de la rétrogression. L'épaisseur de la zone perturbée dépend du temps pendant lequel la diffusion opère (c'est-à-dire à partir du pic métamorphique jusqu'au refroidissement sous la température à laquelle la diffusion est effective). Plus le refroidissement est lent, plus la zone perturbée est épaisse.

La perturbation de l'équilibre chimique lors de la rétrogression est le résultat de deux types de réactions principaux: les réactions d'échange et les réactions de transfert net. Les réactions d'échange modifient la composition chimique des minéraux, mais n'affectent pas leurs proportions modales. Les réactions de transfert net sont associées avec la consomption et la production de minéraux, modifiant à la fois leur proportion modale et leur composition chimique. Pour l'assemblage métamorphique des métapélites étudiées, les réactions suivantes peuvent survenir :

Réaction d'échange :

$$Ann + Prp = Alm + Phl \quad (A.1)$$

Réaction de transfert net :

$$Grt + Kfs + H_2O = Sil + Bt + Qtz \text{ (Spear, 1993)} \quad (A.1)$$

$$Grt + Kfs + H_2O = Bt + Sil + Pl \text{ (Spear et Parrish, 1996)} \quad (A.2)$$

$$Grt + Kfs + \text{liquide de fusion} = Bt + Sil \text{ (Spear et al. 1999)} \quad (A.3)$$

En absence d'eau ou de fusion partielle, seule la réaction d'échange peut opérer. Ceci conduira à une augmentation du rapport Fe/(Fe + Mg) dans le grenat et une diminution de ce même rapport dans la biotite (Fig. A.1A). Cela se traduira par une sous-estimation de la température de pic métamorphique. Dans le cas où les réactions de transfert net peuvent opérer elles aussi, il y aura un changement similaire de la valeur Fe/(Fe + Mg) dans le grenat, mais la biotite aura elle aussi une valeur Fe/(Fe + Mg) plus élevé, entrainant une surestimation de la température (Fig. A.1B). Il est aussi important de noter que ces réactions de transfert net consomment le grenat et produisent de la biotite. De plus, lorsque le grenat est consommé, le Mn se concentre à la bordure et crée un pic en X_{sps} caractéristique du métamorphisme rétrograde par une réaction de transfert net (Fig. A.2). Enfin, il est possible

que les réactions d'échange et de transfert net opèrent ensembles et produisent en un rapport Fe/(Fe + Mg) équivalent au rapport initial, donnant une température exacte mais fortuite.

Les précautions prises afin de limiter l'effet de la diffusion pour les mesures de température et de pression dans les systèmes pélitiques sont décrites dans la section 2.5.2 du mémoire.

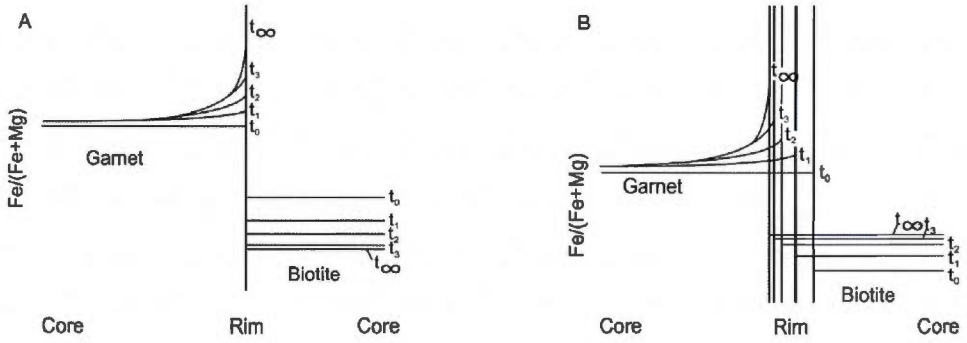

Fig. A.1 Diagrammes montrant l'effet de la rétrogression sur le rapport Fe/(Fe + Mg) dans le grenat et la biotite. Les deux diagrammes montrent que la variation du rapport Fe/(Fe + Mg) se propage de la bordure vers le cœur du grenat tandis qu'il change de façon homogène dans la biotite. **A.** Réaction d'échange qui augmente le rapport Fe/(Fe + Mg) du grenat et le diminue dans la biotite, résultant en une sous-estimation de la température d'équilibre. **B.** Réaction de transfert net qui augmente le rapport Fe/(Fe + Mg) du grenat et de la biotite, résultant en une surestimation de la température d'équilibre (Spear, 1993).

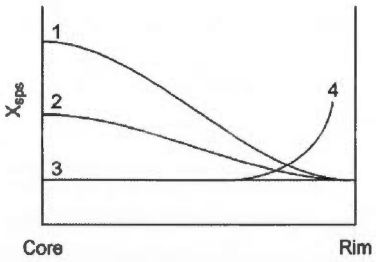

Fig. A.2 Profils de zonation fictifs pour le Mn (X_{sps}) dans le grenat. Le Mn est incorporé préférentiellement dans le grenat, ce qui donne une forme en cloche s'il n'y a pas de diffusion intra-cristalline (1). La diffusion est responsable de l'aplanissement du profil de X_{sps} proportionnellement au grade métamorphique et au temps pendant lequel le grenat est soumis au métamorphisme (2 et 3). La courbe 4 montre le profil de zonation d'un grenat complètement ré-équilibré à haut grade métamorphique, puis soumis à une réaction de transfert net lors du métamorphisme rétrograde (Spear, 1993).

APPENDICE A

COMPOSITIONS CHIMIQUES DES MINÉRAUX ANALYSÉS À LA MICROSONDE

Une copie de ces données est également disponible sur support numérique.

Appendix A. Mineral compositions

	RS11-021												
	Grt C1		Grt C4		Grt C6		Grt C12		Grt C13		Bt		Pl
Wt %[a]	core	rim	core	rim	core	rim	core	rim	core	rim	arm.[b]	ct.[b]	
SiO_2	38,62	38,66	38,97	38,84	38,50	38,48	38,31	38,37	38,39	38,33	36,32	36,78	56,86
TiO_2	0,01	0,02	0,04	0,02	0,08	0,00	0,02	0,00	0,03	0,01	5,86	4,84	0,01
Cr_2O_3	21,61	21,79	21,72	21,67	21,63	21,55	21,63	21,69	21,51	21,51	15,70	15,76	26,89
Al_2O_3	0,01	0,04	0,09	0,00	0,01	0,05	0,05	0,06	0,04	0,06	0,03	0,04	0,01
FeO	27,88	27,29	26,89	26,90	27,67	27,88	27,55	27,29	27,71	27,67	14,71	12,63	0,16
MnO	0,65	0,66	0,67	0,64	0,67	0,70	0,73	0,65	0,71	0,68	0,02	0,01	0,01
MgO	8,49	8,85	8,89	9,03	8,28	8,63	8,36	8,95	8,84	8,50	13,00	15,28	0,00
CaO	2,98	2,72	3,05	2,63	3,11	2,77	3,18	2,62	2,90	2,68	0,03	0,01	9,02
Na_2O	0,01	0,01	0,02	0,00	0,00	0,00	0,00	0,00	0,00	0,00	0,04	0,05	6,22
K_2O	0,03	0,01	0,01	0,00	0,01	0,01	0,02	0,03	0,00	0,01	9,82	10,02	0,28
Total	100,28	100,04	100,34	99,73	99,97	100,06	99,84	99,65	100,14	99,46	95,54	95,42	99,47
Cations per formula unit													
O #[a]	12	12	12	12	12	12	12	12	12	12	6	6	8
Si	2,986	2,985	2,996	3,000	2,985	2,981	2,973	2,976	2,976	2,986	1,479	1,486	2,565
Ti	0,001	0,001	0,003	0,001	0,005	0,000	0,002	0,000	0,001	0,001	0,180	0,147	0,000
Cr	0,000	0,002	0,005	0,000	0,001	0,003	0,003	0,004	0,003	0,004	0,001	0,001	0,001
Al	1,970	1,983	1,968	1,974	1,977	1,968	1,963	1,983	1,981	1,975	0,754	0,750	1,430
Fe	1,803	1,762	1,729	1,738	1,794	1,807	1,795	1,771	1,790	1,803	0,501	0,427	0,006
Mn	0,043	0,043	0,044	0,042	0,044	0,046	0,047	0,043	0,048	0,045	0,001	0,000	0,000
Mg	0,978	1,019	1,019	1,040	0,957	0,997	1,020	1,035	0,968	0,987	0,790	0,920	0,000
Ca	0,247	0,225	0,251	0,217	0,259	0,230	0,241	0,218	0,264	0,224	0,001	0,000	0,436
Na	0,001	0,002	0,003	0,000	0,000	0,000	0,000	0,000	0,000	0,000	0,003	0,004	0,544
K	0,003	0,001	0,001	0,000	0,001	0,001	0,000	0,003	0,002	0,001	0,511	0,516	0,016
Total	8,030	8,023	8,017	8,012	8,022	8,033	8,043	8,032	8,032	8,025	4,220	4,252	4,999
An													44,5
Fe/(Fe+Mg)	0,648	0,634	0,629	0,626	0,652	0,644	0,638	0,631	0,649	0,646	0,388	0,317	
X_{alm}	0,587	0,578	0,568	0,572	0,588	0,587	0,579	0,577	0,583	0,589			
X_{sps}	0,014	0,014	0,014	0,014	0,014	0,015	0,015	0,014	0,016	0,015			
X_{prp}	0,318	0,334	0,335	0,342	0,313	0,324	0,329	0,338	0,315	0,323			
X_{grs}	0,080	0,074	0,083	0,072	0,085	0,075	0,078	0,071	0,086	0,073			

RS12-058

	Grt C5		Grt C9		Bt		Pl
Wt %[a]	core	rim	core	rim	arm.[b]	ct.[b]	
SiO_2	37,96	37,93	38,00	37,53	36,36	35,91	58,29
TiO_2	0,02	0,04	0,01	0,00	4,68	4,60	0,01
Cr_2O_3	21,22	20,89	21,74	21,32	16,62	16,58	26,08
Al_2O_3	0,02	0,00	0,02	0,01	0,04	0,04	0,01
FeO	30,01	31,18	30,16	32,64	14,42	16,16	0,20
MnO	0,69	0,91	0,84	0,95	0,00	0,02	0,01
MgO	7,64	6,25	7,34	5,15	13,87	11,96	0,00
CaO	1,77	1,84	1,89	1,95	0,03	0,02	8,06
Na_2O	0,01	0,01	0,00	0,00	0,07	0,07	6,94
K_2O	0,01	0,01	0,01	0,03	9,74	9,60	0,12
Total	99,36	99,06	100,02	99,58	95,83	94,96	99,71
Cations per formula unit							
O #[a]	12	12	12	12	6	6	8
Si	2,987	3,014	2,973	2,989	1,483	1,472	2,616
Ti	0,001	0,003	0,000	0,000	0,139	0,142	0,000
Cr	0,002	0,000	0,001	0,001	0,001	0,001	0,000
Al	1,968	1,957	2,005	2,001	0,796	0,793	1,378
Fe	1,975	2,072	1,973	2,175	0,546	0,488	0,007
Mn	0,046	0,061	0,055	0,064	0,001	0,000	0,000
Mg	0,897	0,740	0,856	0,612	0,756	0,837	0,000
Ca	0,149	0,157	0,159	0,167	0,001	0,001	0,386
Na	0,001	0,002	0,001	0,000	0,005	0,006	0,605
K	0,001	0,001	0,001	0,003	0,509	0,503	0,007
Total	8,028	8,006	8,025	8,011	4,237	4,243	5,000
An							39,0
Fe/ (Fe+Mg)	0,688	0,737	0,697	0,780	0,420	0,368	
X_{alm}	0,644	0,684	0,648	0,721			
X_{sps}	0,015	0,020	0,018	0,021			
X_{prp}	0,292	0,244	0,281	0,203			
X_{grs}	0,049	0,052	0,052	0,055			

RS12-015

	Grt C5		Grt C7		Grt C10		Bt	
Wt %[a]	core	rim	core	rim	core	rim	arm.[b]	ct.[b]
SiO_2	38,37	37,83	38,15	38,22	38,34	38,30	36,38	36,65
TiO_2	0,03	0,02	0,02	0,02	0,01	0,04	5,51	4,40
Cr_2O_3	21,90	21,84	22,17	21,73	21,79	22,14	17,21	17,04
Al_2O_3	0,01	0,01	0,00	0,01	0,01	0,02	0,06	0,04
FeO	30,18	32,57	29,83	29,87	29,36	31,11	14,04	11,76
MnO	0,21	0,24	0,21	0,22	0,19	0,21	0,01	0,01
MgO	8,84	7,10	9,13	8,90	9,42	8,41	12,89	15,32
CaO	0,76	0,73	0,78	0,57	0,49	0,43	0,01	0,00
Na_2O	0,01	0,00	0,01	0,00	0,00	0,00	0,08	0,10
K_2O	0,01	0,00	0,00	0,02	0,01	0,01	9,72	9,86
Total	100,31	100,34	100,30	99,56	99,63	100,67	95,90	95,17
Cations per formula unit								
O #[a]	12	12	12	12	12	12	6	6
Si	2,972	2,965	2,951	2,979	2,977	2,965	1,467	1,474
Ti	0,001	0,001	0,001	0,001	0,000	0,002	0,167	0,133
Cr	0,001	0,000	0,000	0,001	0,001	0,001	0,002	0,001
Al	1,999	2,018	2,021	1,996	1,995	2,020	0,818	0,808
Fe	1,955	2,135	1,930	1,947	1,907	2,014	0,474	0,396
Mn	0,014	0,016	0,014	0,014	0,013	0,014	0,000	0,000
Mg	1,021	0,829	1,053	1,035	1,090	0,970	0,775	0,918
Ca	0,063	0,061	0,065	0,047	0,041	0,036	0,001	0,000
Na	0,001	0,000	0,002	0,000	0,000	0,000	0,006	0,008
K	0,001	0,000	0,000	0,002	0,001	0,001	0,500	0,506
Total	8,028	8,025	8,038	8,022	8,025	8,023	4,209	4,245
Fe/ (Fe+Mg)	0,657	0,720	0,647	0,653	0,636	0,675	0,379	0,302
X_{alm}	0,641	0,702	0,630	0,640	0,625	0,664		
X_{sps}	0,004	0,005	0,004	0,005	0,004	0,005		
X_{prp}	0,334	0,273	0,344	0,340	0,357	0,320		
X_{grs}	0,021	0,020	0,021	0,016	0,013	0,012		

RS12-27B

	Grt C2a		Grt C2b		Grt C10		Bt		Pl
Wt %[a]	core	rim	core	rim	core	rim	arm.[b]	ct.[b]	
SiO_2	37,63	37,45	37,98	37,63	37,97	37,82	35,45	35,82	58,02
TiO_2	0,04	0,00	0,02	0,03	0,02	0,00	5,45	3,77	0,01
Cr_2O_3	21,11	20,92	21,54	21,26	21,49	21,23	17,23	17,95	26,09
Al_2O_3	0,01	0,03	0,02	0,05	0,02	0,01	0,05	0,04	0,00
FeO	31,91	33,86	31,56	33,55	31,77	32,70	17,03	15,31	0,15
MnO	0,36	0,43	0,32	0,44	0,32	0,35	0,01	0,01	0,01
MgO	6,68	4,97	6,60	5,40	6,49	5,99	10,46	12,68	0,00
CaO	1,73	1,72	2,09	1,89	2,24	1,72	0,01	0,02	7,94
Na_2O	0,00	0,00	0,01	0,01	0,01	0,00	0,12	0,10	6,88
K_2O	0,03	0,01	0,01	0,01	0,01	0,03	9,73	9,64	0,24
Total	99,52	99,40	100,15	100,27	100,34	99,85	95,54	95,34	99,33
Cations per formula unit									
O #[a]	12	12	12	12	12	12	6	6	8
Si	2,981	2,999	2,981	2,981	2,979	2,993	1,459	1,461	2,613
Ti	0,003	0,000	0,001	0,002	0,001	0,000	0,169	0,116	0,000
Cr	0,001	0,002	0,001	0,003	0,001	0,000	0,002	0,001	0,000
Al	1,971	1,975	1,996	1,985	1,988	1,981	0,836	0,863	1,385
Fe	2,114	2,268	2,072	2,223	2,085	2,164	0,586	0,523	0,006
Mn	0,024	0,029	0,021	0,029	0,021	0,024	0,001	0,000	0,000
Mg	0,789	0,594	0,773	0,637	0,760	0,707	0,641	0,771	0,000
Ca	0,147	0,147	0,176	0,161	0,188	0,146	0,001	0,001	0,383
Na	0,000	0,000	0,001	0,001	0,002	0,000	0,010	0,008	0,600
K	0,003	0,001	0,001	0,001	0,001	0,003	0,511	0,502	0,014
Total	8,033	8,014	8,021	8,024	8,027	8,018	4,214	4,246	5,001
An									39,0
Fe/(Fe+Mg)	0,728	0,793	0,728	0,777	0,733	0,754	0,478	0,405	
X_{alm}	0,688	0,747	0,681	0,729	0,683	0,712			
X_{sps}	0,008	0,009	0,007	0,010	0,007	0,008			
X_{prp}	0,257	0,195	0,254	0,209	0,249	0,232			
X_{grs}	0,048	0,048	0,058	0,053	0,062	0,048			

RS11-105

	Grt C3 (1)		Grt C4 (1)		Grt C8 (1)		Grt C12 (1)		Grt C6 (2)		Grt C9 (2)		Grt C1 (3)		Grt C10 (3)		Bt		Pl
Wt %[a]	core	rim	core	rim	core	rim	core	rim	core	rim	core	rim	core	rim	core	rim	arm.[b]	ct.[b]	
SiO_2	37,30	37,06	37,44	36,95	37,39	36,85	37,48	36,71	37,37	37,16	37,26	37,01	37,25	36,86	37,30	37,08	35,18	35,53	62,70
TiO_2	0,02	0,01	0,03	0,00	0,03	0,00	0,01	0,03	0,02	0,00	0,01	0,08	0,02	0,02	0,02	0,00	4,61	3,68	0,02
Cr_2O_3	21,52	21,07	21,29	21,17	21,24	21,03	21,35	20,79	21,33	21,47	21,28	21,08	21,34	21,27	21,42	21,30	17,37	18,35	23,12
Al_2O_3	0,00	0,02	0,02	0,02	0,01	0,04	0,02	0,03	0,01	0,03	0,03	0,00	0,02	0,04	0,02	0,00	0,06	0,05	0,01
FeO	34,53	36,05	34,45	36,28	34,23	36,32	34,31	36,97	34,79	35,45	35,15	36,38	35,20	36,81	35,00	35,37	19,15	18,43	0,14
MnO	0,92	1,08	0,90	1,11	0,98	1,27	0,85	1,09	1,06	1,09	1,05	1,15	0,93	1,19	1,02	1,15	0,03	0,01	0,01
MgO	5,00	3,69	5,15	3,77	5,03	3,48	5,11	3,23	4,85	4,37	4,59	3,45	4,68	3,33	4,60	4,18	9,29	10,03	0,00
CaO	1,05	0,91	1,10	0,89	1,10	0,93	1,31	0,91	0,96	0,94	0,96	0,94	0,95	0,92	0,98	0,92	0,01	0,04	4,37
Na_2O	0,00	0,00	0,01	0,00	0,01	0,01	0,01	0,03	0,01	0,00	0,03	0,01	0,01	0,01	0,02	0,02	0,07	0,10	8,93
K_2O	0,01	0,01	0,02	0,01	0,01	0,02	0,01	0,02	0,02	0,00	0,01	0,02	0,01	0,01	0,01	0,01	9,67	9,58	0,21
Total	100,34	99,90	100,40	100,22	100,02	99,94	100,47	99,81	100,42	100,51	100,37	100,13	100,41	100,44	100,39	100,04	95,44	95,80	99,50
Cations per formula unit																			
O #[a]	12	12	12	12	12	12	12	12	12	12	12	12	12	12	12	12	6	6	8
Si	2,966	2,986	2,975	2,971	2,981	2,977	2,975	2,978	2,975	2,965	2,973	2,981	2,970	2,966	2,975	2,974	1,464	1,463	2,788
Ti	0,001	0,001	0,002	0,000	0,002	0,000	0,001	0,002	0,001	0,000	0,001	0,005	0,001	0,001	0,001	0,000	0,144	0,114	0,001
Cr	0,000	0,001	0,001	0,001	0,000	0,002	0,001	0,002	0,001	0,002	0,002	0,000	0,001	0,003	0,001	0,000	0,002	0,002	0,000
Al	2,017	2,001	1,994	2,007	1,996	2,002	1,997	1,988	2,001	2,019	2,002	2,001	2,005	2,017	2,008	2,014	0,852	0,891	1,212
Fe	2,296	2,429	2,289	2,440	2,282	2,453	2,277	2,508	2,316	2,365	2,346	2,451	2,347	2,477	2,332	2,373	0,667	0,635	0,005
Mn	0,062	0,074	0,061	0,076	0,066	0,087	0,057	0,075	0,071	0,074	0,071	0,079	0,063	0,081	0,069	0,078	0,001	0,001	0,000
Mg	0,592	0,443	0,610	0,452	0,598	0,419	0,604	0,391	0,576	0,520	0,546	0,415	0,556	0,399	0,546	0,499	0,576	0,616	0,000
Ca	0,090	0,078	0,094	0,077	0,094	0,080	0,112	0,079	0,082	0,080	0,082	0,081	0,081	0,079	0,085	0,079	0,001	0,002	0,208
Na	0,001	0,000	0,002	0,000	0,001	0,001	0,002	0,004	0,002	0,000	0,005	0,001	0,001	0,002	0,004	0,004	0,006	0,008	0,770
K	0,001	0,001	0,002	0,001	0,001	0,002	0,001	0,003	0,002	0,000	0,001	0,002	0,001	0,001	0,001	0,001	0,513	0,503	0,012
Total	8,025	8,013	8,028	8,025	8,021	8,023	8,027	8,029	8,026	8,025	8,028	8,016	8,027	8,025	8,022	8,022	4,225	4,233	4,996
An																			21,3
Fe/ (Fe+Mg)	0,795	0,846	0,790	0,844	0,792	0,854	0,790	0,865	0,801	0,820	0,811	0,855	0,809	0,861	0,810	0,826	0,536	0,508	
X_{alm}	0,755	0,803	0,750	0,801	0,751	0,807	0,747	0,821	0,760	0,778	0,770	0,810	0,770	0,816	0,769	0,783			
X_{sps}	0,020	0,024	0,020	0,025	0,022	0,029	0,019	0,025	0,023	0,024	0,023	0,026	0,021	0,027	0,023	0,026			
X_{prp}	0,195	0,146	0,200	0,149	0,197	0,138	0,198	0,128	0,189	0,171	0,179	0,137	0,182	0,131	0,180	0,165			
X_{grs}	0,029	0,026	0,031	0,025	0,031	0,026	0,037	0,026	0,027	0,026	0,027	0,027	0,027	0,026	0,028	0,026			

RS11-82B

	Grt C1		Grt C3		Grt C5		Grt C7		Grt C8		Hbl		Pl	
Wt %[a]	**i. r.**[b]	**rim**	**i. r.**[b]	**rim**	**i. r.**[b]	**rim**	**i. r.**[b]	**rim**	**i. r.**[b]	**rim**	**gr.**[b]	**r. r.**[b]	**gr.**[b]	**r. r.**[b]
SiO_2	38,32	37,93	38,18	37,96	37,92	37,79	~~38,04~~	37,99	38,32	38,05	41,54	41,86	56,28	54,74
TiO_2	0,04	0,08	0,10	0,05	0,08	0,04	~~0,13~~	0,07	0,08	0,09	1,95	1,80	0,02	0,01
Cr_2O_3	20,84	20,47	20,81	20,68	21,21	20,96	~~21,50~~	21,44	21,31	21,01	12,45	12,65	27,43	28,40
Al_2O_3	0,02	0,03	0,02	0,02	0,03	0,07	~~0,04~~	0,02	0,01	0,02	0,03	0,04	0,01	0,00
FeO	23,44	26,14	22,95	26,32	23,10	26,55	~~23,65~~	26,55	23,94	27,02	15,49	14,74	0,24	0,13
MnO	1,18	1,93	0,95	1,75	0,88	1,93	~~1,25~~	1,94	1,52	2,07	0,18	0,14	0,00	0,01
MgO	5,09	5,04	4,55	5,19	4,50	5,31	~~5,20~~	5,37	4,88	4,81	11,04	11,48	0,00	0,00
CaO	10,31	7,33	11,69	7,39	11,52	6,76	~~9,77~~	6,63	9,93	6,64	11,40	11,69	9,43	10,83
Na_2O	0,00	0,00	0,01	0,01	0,01	0,02	~~0,00~~	0,00	0,00	0,00	1,98	1,82	6,02	5,25
K_2O	0,02	0,00	0,01	0,00	0,02	0,01	~~0,02~~	0,01	0,00	0,00	1,20	1,25	0,15	0,13
Total	99,25	98,93	99,28	99,37	99,26	99,44	~~99,60~~	0,01	99,98	99,70	97,27	97,46	99,59	99,51
Cations per formula unit														
O #[a]	12	12	12	12	12	12	~~12~~	12	12	12	6	6	8	8
Si	3,009	3,013	3,001	3,002	2,981	2,987	~~2,976~~	2,980	2,993	3,003	1,637	1,634	2,539	2,479
Ti	0,002	0,005	0,006	0,003	0,005	0,003	~~0,008~~	0,004	0,005	0,005	0,053	0,058	0,001	0,000
Cr	0,001	0,002	0,001	0,002	0,002	0,004	~~0,002~~	0,001	0,000	0,001	0,001	0,001	0,000	0,000
Al	1,929	1,917	1,928	1,928	1,966	1,953	~~1,982~~	1,983	1,961	1,955	0,583	0,577	1,459	1,516
Fe	1,540	1,737	1,508	1,741	1,519	1,755	~~1,548~~	1,742	1,563	1,783	0,482	0,510	0,009	0,005
Mn	0,079	0,130	0,063	0,117	0,059	0,129	~~0,083~~	0,129	0,101	0,138	0,005	0,006	0,000	0,000
Mg	0,596	0,596	0,533	0,612	0,527	0,626	~~0,606~~	0,628	0,568	0,566	0,669	0,647	0,000	0,000
Ca	0,867	0,624	0,985	0,627	0,971	0,572	~~0,819~~	0,557	0,831	0,561	0,490	0,480	0,456	0,526
Na	0,000	0,000	0,002	0,001	0,001	0,003	~~0,000~~	0,000	0,000	0,000	0,138	0,151	0,527	0,462
K	0,002	0,000	0,001	0,000	0,002	0,001	~~0,002~~	0,001	0,000	0,000	0,062	0,060	0,009	0,008
Total	8,025	8,023	8,029	8,031	8,031	8,034	~~8,025~~	8,025	8,022	8,013	4,119	4,125	4,999	4,997
An													46,4	53,2
Fe/ (Fe+Mg)	0,721	0,744	0,739	0,740	0,742	0,737	~~0,718~~	0,735	0,734	0,759	0,419	0,441		
X_{alm}	0,500	0,563	0,488	0,562	0,494	0,569	~~0,506~~	0,570	0,510	0,585				
X_{sps}	0,026	0,042	0,020	0,038	0,019	0,042	~~0,027~~	0,042	0,033	0,045				
X_{prp}	0,193	0,193	0,173	0,198	0,171	0,203	~~0,198~~	0,205	0,185	0,186				
X_{grs}	0,281	0,202	0,319	0,202	0,316	0,186	~~0,268~~	0,182	0,271	0,184				

Notes

a) Wt. % : weight percent; O # : oxygen number in the formula.

b) arm.: armoured; ct: contact with garnet; i. r.: inner rim; gr.: groundmass; r.r.: reaction rim

Data represent average values of multiple measurements used for P-T calculations

crossed-out data was not used for P-T calculations

Experimental Conditions

Microprobe model	JXA JEOL-8900L
Accelaration voltage	15 kV
Beam Current	20 nA
Beam Size	5 um
Correction Method	ZAF

Counting Time	SiO_2	TiO_2	Cr_2O_3	Al_2O_3	FeO	MnO	MgO	CaO	Na_2O	K_2O
(s)	20	20	20	20	20	20	20	20	20	20

Standards										
Garnet	Alm	Rt	Chr	Alm	Alm	Sps	Alm	Alm	Ab	Or
Biotite/Amph	Di	Rt	Chr	Or	Hem	Sps	Di	Di	Ab	Or
Plagioclase	Or	Rt	Chr	Or	Hem	Sps	Di	Di	Ab	Or

Detecion Limits (wt%)										
Garnet	0,04	0,064	0,0616	0,0351	0,0528	0,0439	0,0312	0,0334	0,0263	0,0252
Amphibole	0,0476	0,0774	0,0594	0,0405	0,0453	0,042	0,0372	0,0349	0,0288	0,0311
Biotite	0,0365	0,0662	0,0587	0,032	0,0442	0,0426	0,0304	0,0331	0,0273	0,0262
Plagioclase	0,037	0,0618	0,0583	0,0326	0,0401	0,0379	0,0306	0,031	0,0253	0,026

APPENDICE B

DIAGRAMMES CONCORDIA DES ÂGES U-PB, COMPOSITION CHIMIQUE ET DONNÉES ISOTOPIQUES DES ZIRCONS DES PEGMATITES RS11-098 ET RS12-040

Les données isotopiques et la composition chimique des zircons sont fournies sur support numérique.

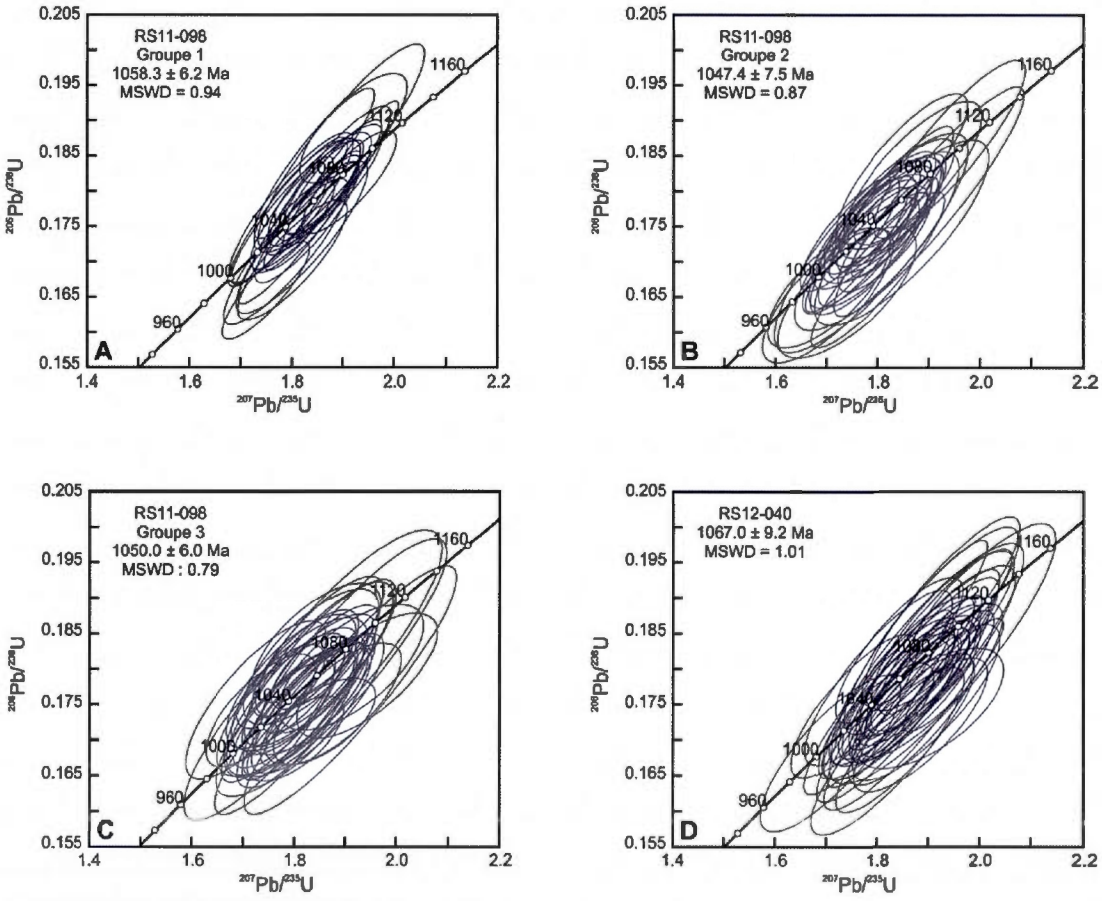

Appendice B. A-C. Diagrammes concordia pour les zircons des groupes 1 à 3 de la pegmatite RS11-098. **D.** Diagrammes concordia pour les zircons de la pegmatite RS12-040. Les ellipses d'erreur sont au niveau 2σ. Les incertitudes sur les ages n'incluent pas les incertitudes de calibration. MSWD : déviation moyenne pondérée au carré (*mean square weighted deviation*).

APPENDICE C

DONNÉES $^{40}AR/^{39}AR$

Les données $^{40}Ar/^{39}Ar$ sont fournies sur support numérique.

APPENDICE D

LOCALISATION DES AFFLEUREMENTS

Localisation des affleurements visités dans la région de la Mauricie, Province géologique du Grenville. Modifiée de Nadeau et Brouillette (1995). Carte en pochette. Le tableau des coordonnées UTM des affleurements est aussi disponible sur support numérique.

Appendice D. Localisation des affleurements

Affleurement	Abscisse (E)[a]	Ordonnée (N)[a]	Affleurement	Abscisse (E)[a]	Ordonnée (N)[a]
RS11-001	657549	5210785	RS11-041	670142	5167646
RS11-002	657793	5196510	RS11-042	669841	5168151
RS11-003	658365	5194824	RS11-043	664986	5167357
RS11-004	658752	5194385	RS11-044	665350	5167853
RS11-005	662770	5192756	RS11-045	665495	5169274
RS11-006	663774	5192044	RS11-046	665569	5169455
RS11-007	668484	5192024	RS11-047	664206	5168106
RS11-008	670691	5190891	RS11-048	663854	5168299
RS11-009	670843	5190296	RS11-049	663215	5168701
RS11-010	677703	5189879	RS11-050	662494	5169018
RS11-011N	665824	5191703	RS11-051	655840	5167924
RS11-011S	666355	5191515	RS11-052	655476	5168293
RS11-012	670360	5179200	RS11-053	676553	5168726
RS11-013	670588	5178975	RS11-054	675576	5168551
RS11-014	670957	5178663	RS11-055	676129	5168644
RS11-015	671176	5177599	RS11-056	674556	5171617
RS11-016	671239	5177225	RS11-057	673949	5171981
RS11-017	671534	5176501	RS11-058	671660	5174314
RS11-018	671816	5176022	RS11-059	671473	5174590
RS11-019	673405	5174204	RS11-060	672256	5173917
RS11-020	673452	5173747	RS11-061	673476	5171619
RS11-021	613584	5173279	RS11-062	673400	5171220
RS11-022	678497	5175346	RS11-063	669966	5171306
RS11-023	680255	5177105	RS11-064	667775	5169143
RS11-024	676499	5201540	RS11-065	668626	5169139
RS11-025	680647	5204584	RS11-066	669139	5169467
RS11-026	682409	5203353	RS11-067	669928	5170962
RS11-027	683091	5202593	RS11-068	679564	5193291
RS11-028	682701	5203202	RS11-069	679558	5193595
RS11-029	683766	5203669	RS11-070	679601	5193683
RS11-030	683950	5203447	RS11-071	677695	5193953
RS11-031	677451	5208506	RS11-071.5	679752	5194152
RS11-032	672707	5184505	RS11-072	679726	5194321
RS11-033	675477	5183134	RS11-073	679683	5194401
RS11-034	676768	5185892	RS11-074	679810	5194872
RS11-035	677122	5186513	RS11-075	680142	5195084
RS11-036	677237	5186660	RS11-076	680452	5195212
RS11-037	678299	5191103	RS11-077	680677	5195167
RS11-038	678870	5192158	RS11-078	682683	5194754
RS11-039	680108	5192584	RS11-079	681109	5195609
RS11-040	669820	5167539	RS11-080	674508	5172780

Affleurement	Abscisse (E)[a]	Ordonnée (N)[a]	Affleurement	Abscisse (E)[a]	Ordonnée (N)[a]
RS11-081	680666	5178824	RS11-123	650555	5137333
RS11-082	680747	5178829	RS11-124	651577	5166535
RS11-083	680757	5178833	RS11-125	653348	5164730
RS11-084	680744	5178877	RS11-126	654472	5164366
RS11-085	680747	5178867	RS11-127	656185	5164088
RS11-086	680720	5178843	RS11-128	655859	5163668
RS11-087	676295	5168733	RS11-129	654722	5162807
RS11-088	676545	5168830	RS11-130	649113	5163205
RS11-089	680697	5178880	RS11-131	642529	5157786
RS11-090	680684	5178899	RS11-132	639974	5160894
RS11-091	680674	5178912	RS11-133	642261	5163735
RS11-092	680749	5178819	RS11-134	643153	5165387
RS11-093	680023	5179184	RS11-135	642090	5164245
RS11-094	679980	5179243	RS11-136	636958	5163925
RS11-095	679804	5179318	RS11-137	635789	5169484
RS11-096	680739	5178828	RS11-138	634384	5166566
RS11-097	680761	5178847	RS11-138.5	632241	5167503
RS11-098	680719	5178838	RS11-139	630707	5167354
RS11-099	678056	5167844	RS11-140	636265	5161847
RS11-100	677664	5170545	RS11-141	632499	5159747
RS11-101	669837	5168353	RS11-142	631530	5159967
RS11-102	669876	5168481	RS11-143	630698	5160626
RS11-103	669901	5168529	RS11-144	627384	5159486
RS11-104	670467	5169460	RS11-145	625546	5158634
RS11-105	670199	5158530	RS11-146	624652	5161522
RS11-106	665569	5169455	RS11-147	622021	5159133
RS11-107	665851	5169324	RS11-148	621989	5160735
RS11-108	678873	5169324	RS11-149	625172	5166371
RS11-109	678988	5192473	RS11-150	628911	5158258
RS11-110	679380	5193010	RS11-151	627415	5155101
RS11-111	679806	5193010	RS11-152	625687	5154651
RS11-112	679806	5193117	RS11-153	623666	5156502
RS11-113	685301	5177182	RS11-154	623434	5150342
RS11-114	665887	5191666	RS11-155	626065	5148977
RS11-115	666117	5191538	RS11-156	626105	5148561
RS11-116	666201	5191524	RS11-157	626097	5148831
RS11-117	676547	5169360	RS11-158	626096	5148917
RS11-118	676237	5169333	RS11-159	619762	5152722
RS11-119	676023	5169336	RS11-160	619110	5154302
RS11-120	680666	5178824	RS11-161	620413	5157636
RS11-121	676332	5168907	RS11-162	629678	5157332
RS11-122	676531	5168764	RS11-163	616650	5162518

Affleurement	Abscisse (E)[a]	Ordonnée (N)[a]
RS11-164	611275	5162234
RS11-165	611429	5161134
RS11-166	606381	5160985
RS11-167	607111	5162671
RS11-168	603054	5164910
RS11-169	602139	5166129
RS11-170	601545	5165099
RS11-171	603758	5168092
RS11-172	598473	5170082
RS12-001	657816	5196071
RS12-002	656004	5196350
RS12-003	654527	5196309
RS12-004	649291	5200527
RS12-005	638770	5205132
RS12-006	636331	5209827
RS12-007	636176	5210707
RS12-008	635886	5212435
RS12-009	627712	5214264
RS12-010	640367	5202582
RS12-011	638851	5200181
RS12-012	637798	5197865
RS12-013	644090	5195827
RS12-014	647173	5194881
RS12-015	671945	5175943
RS12-016	672817	5184413
RS12-017	685041	5179857
RS12-018	666017	5180809
RS12-019	666344	5180912
RS12-020	665871	5180627
RS12-021	665257	5180592
RS12-022	665289	5180834
RS12-023	665249	5181164
RS12-024	665113	5181550
RS12-025	654622	5168659
RS12-026	663615	5168361
RS12-027	667295	5153814
RS12-028	672324	5159886
RS12-029	675472	5163591
RS12-030	674879	5163204
RS12-031	675158	5166737
RS12-032	670542	5178981
RS12-033	660751	5197009
RS12-034	677126	5163900
RS12-035	677002	5161940
RS12-036	675813	5160122
RS12-037	676831	5170281
RS12-038	672752	5186449
RS12-039	674543	5172883

a) UTM NAD 83, zone 18N

BIBLIOGRAPHIE

Allaz, J. (2008). *Metamorphic evolution in the northern Central Alps: linking ^{39}Ar-^{40}Ar dating with thermobarometry* (Dissertation de doctorat). Universität Bern, Bern, Suisse.

Allaz, J., Engi, M., Berger, A. et Villa, I.M. (2011). The Effects of Retrograde Reactions and of Diffusion on ^{40}Ar–^{39}Ar Ages of Micas. *Journal of Petrology, 52*(4), 691-716.

Armstrong, R.L. (1982). Cordilleran metamorphic core complexes-from Arizona to southern Canada. *Annual Review of Earth and Planetary Sciences, 10*, 129.

Barton, J.M.Jr. et Doig, R. (1972). Rb-Sr Isotopic studies of the Lac Croche Complex, Grenville Province, Quebec. *Canadian Journal of Earth Sciences, 9*(9), 1180-1186.

Beaumont, C.J., Jamieson, R.A., Nguyen, M.H. et Lee, B. (2001). Himalayan tectonics explained by extrusion of a low-viscosity crustal channel coupled to focused surface denudation. *Nature, 414*(6865), 738-742.

Beaumont, C.J., Nguyen, M. H., Jamieson, R. A. et Ellis, S. (2006). Crustal flow modes in large hot orogens. *Geological Society, London, Special Publications, 268*(1), 91-145.

Béland, J. (1961). *Région de Shawinigan*, (97- carte 1327). Québec : Ministère des Richesses naturelles du Québec.

Berman, R.G. (1988). Internally-consistent thermodynamic data for stoichiometric minerals in the system K2O-Na2O-CaO-MgO-FeO-Fe2O3-Al2O3-SiO2-TiO2-H2O-CO2-O. *Journal of Petrology, 29*(2), 445-522.

Berman, R.G. (1990). Mixing properties of Ca-Mg-Fe-Mn garnets. *American Mineralogist, 75,* 328-344.

Berman, R.G. (1991). Thermobarometry using multi-equilibrium calculations: a new technique, with petrological applications. *Canadian Mineralogist, 29*(4), 833-855.

Berman, R.G. (2007). winTWQ (version 2.3): A software package for performing internally-consistent thermobarometric calculations. *Geological Survey of Canada, Open File, 5462* (revised).

Berman, R.G., Aranovich, L.Y., Rancourt, D.G. et Mercier, P.H.J. (2007). Reversed phase equilibrium constraints on the stability of Mg-Fe-Al biotite. *American Mineralogist, 92*, 139-150.

Bernier, L.R. et MacLean, W.H. (1993). Lithogeochemistry of a metamorphosed VMS alteration zone at Montauban Grenville Province, Quebec. *Exploration and Mining Geology, 2*(4), 367- 386.

Brun, J. P., & Sokoutis, D. (2007). Kinematics of the southern Rhodope core complex (North Greece). *International Journal of Earth Sciences, 96*(6), 1079-1099.

Brun, J.P., Sokoutis, D. et van den Driessche, J. (1994). Analogue modeling of detachment fault systems and core complexes. *Geology, 22*(4), 319-322.

Caddick, M.J., Konopasek, J. et Thompson, A.B. (2010). Preservation of garnet growth zoning and the duration of prograde metamorphism. *Journal of petrology, 51*(11), 2327-2347.

Calvert, A.T., Gans, P.B. et Amato, J.M. (1999). Diapiric ascent and cooling of a sillimanite gneiss

dome revealed by $^{40}Ar/^{39}Ar$ thermochronology: the Kigluaik Mountains, Seward Peninsula, Alaska. *Geological Society, London, Special Publications, 154*(1), 205-232.

Cherniak, D.J., Watson, E.B., Grove, M. et Harrison, T.M. (2004). Pb diffusion in monazite: a combined RBS/SIMS study. *Geochimica et Cosmochimica Acta, 68*(4), 829-840.

Coney, P.J. et Harms, T.A. (1984). Cordilleran metamorphic core complexes: Cenozoic extensional relics of Mesozoic compression. *Geology, 12*(9), 550-554.

Corfu F., Hanchar, J.M., Hoskin, P.W.O. et Kinny, P. (2003). Atlas of zircon textures. *Reviews in Mineralogy and Geochemistry, 53(1)*, 469-500.

Corrigan, D. 1995. *Mesoproterozoic evolution of the south-central Grenville orogen: structural, metamorphic, and geochronologic constraints from the Mauricie transect* (Ph.D. thesis). Carleton University, Ottawa.

Corrigan, D., et Hanmer, S. (1997). Anorthosites and related granitoids in the Grenville orogen: A product of convective thinning of the lithosphere? *Geology, 25*(1), 61-64.

Corrigan, D. et van Breemen, O. (1997). U-Pb age constraints for the lithotectonic evolution of the Grenville Province along the Mauricie transect, Québec. *Canadian Journal of Earth Sciences, 34*(3), 299-316.

Dahl, P.S. (1996). The effects of composition on retentivity of argon and oxygen in hornblende and related amphiboles: a field-tested empirical model. *Geochimica et Cosmochimica Acta, 60*(19), 3687-3700.

Davidson, C., Schmid, S.M., et Hollister, L.S. (1994). Role of melt during deformation in the deep crust. *Terra Nova, 6*(2), 133-142.

Dewey, J.F. (1988). Extensional collapse of orogens. *Tectonics, 7*(6), 1123-1139.

Dewey, J.F. et Burke, K.C. (1973). Tibetan, Variscan, and Precambrian basement reactivation: products of continental collision. *The Journal of Geology 81*(6), 683-692.

Dixon, J. M. (1975). Finite strain and progressive deformation in models of diapiric structures. *Tectonophysics, 28*(1), 89-124.

Dodson, M.H. (1973) Closure temperature in cooling geochronological and petrological systems. *Contributions to Mineralogy and Petrology, 40*(3), 259-274.

Doig, R. (1991). U-Pb zircon dates of Morin Anorthosite suite rocks, Grenville Province, Quebec. J*ournal of Geology, 99*(5), 729-738.

Doughty, P.T., Chamberlain, K.R., Foster, D.A. et Grant, S.S. (2007). Structural, metamorphic, and geochronologic constraints on the origin of the Clearwater core complex, northern Idaho. *Geological Society of America Special Papers, 433*, 211-241.

England, P. et Jackson, J. (1987). Migration of the seismic-aseismic transition during uniform and nonuniform extension of the continental lithosphere. *Geology, 15*(4), 291-294.

England, P. et Molnar, P. (1990). Surface uplift, uplift of rocks, and exhumation of rocks. *Geology, 18*(12), 1173-1177.

Essene, J.E. (1989). The current status of thermobarometry in metamorphic rocks. *Geological Society, London, Special Publication, 43*(1), 1-44.

Ferguson, L.J. (1974). *The sapphirine-bearing and associated rocks north of Grand Mère,*

Québec, (B.Sc. thesis). Carleton University, Ottawa.

Ferriss, E.D.A., Essene, E.J., et Becker, U. (2008). Computational study of the effect of pressure on the Ti-in-zircon geothermometer. *European Journal of Mineralogy, 20*(5), 745-755.

Ferry, J.M. et Watson, E.B. (2007). New thermodynamic models and revised calibrations for the Ti-in-zircon and Zr-in-rutile thermometers. *Contributions to Mineralogy and Petrology, 154*(4), 429-437.

Fortier, S.M. et Giletti, B.J. (1989). An empirical model for predicting diffusion coefficients in silicate minerals. *Science, 245*(4925), 1481-1484.

Friedman, R.M. et Martignole, J. (1995). Mesoproterozoic sedimentation, magmatism, and metamorphism in the southern part of the Grenville Province (western Quebec): U-Pb geochronological constraints. *Canadian Journal of Earth Sciences, 32*(12), 2103-2114.

Frost, B.R., Chamberlain, K.R. et Schumacher, J.C. (2001). Sphene (titanite): phase relations and role as a geochronometer. *Chemical Geology,172*(1), 131-148.

Fuhrman, M.L. et Lindsley, D.H. (1988). Ternary-feldspar modeling and thermometry. *The American Mineralogist, 73*(3-4), 201-216.

Gapais, D., Cagnard, F., Gueydan, F., Barbey P. et Ballèvre M. (2009). Mountain building and exhumation processes through time: inferences from nature and models. *Terra Nova, 21*(3), 188-194.

Gautier, E. (1993). *Géochimie et pétrologie du Complexe de La Bostonnais et du gabbro du Lac Lapeyrère* (Mémoire de maîtrise). Université Laval, Québec, Canada.

Geological Survey of Canada. Superior-Grenville Provinces - 400m - MAG - Residual Total Field - Provinces Supérieur-Grenville - Composante résiduelle. [Carte]. Base Canadienne de données aéromagnétiques. Comission géologique du Canada. Utilisation d'ArcMap (version 10). [logiciel SIG].

Geological Survey of Canada. Canada 2 km_ Bouguer - Bouguer. [Carte]. Base Canadienne de données gravimétriques. Comission géologique du Canada. Utilisation d'ArcMap (version 10). [logiciel SIG].

Gervais, F. et Brown, R. L. (2011). Testing modes of exhumation in collisional orogens: Synconvergent channel flow in the southeastern Canadian Cordillera. *Lithosphere, 3*(1), 55-75.

Gervais, F., Nadeau, L. et Malo, M. (2004). Migmatitic structures and solid-state diapirism in orthogneiss domes, eastern Grenville Province, Canada. *Geological Society of America Special Papers, 380*, 359-378.

Gibb, R.A. (1968). The densities of Precambrian rocks from northern Manitoba. *Canadian Journal of Earth Sciences, 5*(3), 433-438.

Godin, L., Grujic, D., Law, R.D. et Searle, M.P. (2006). Channel flow, ductile extrusion and exhumation in continental collision zones: an introduction. *Geological Society, London, Special Publications, 268*(1), 1-23.

Grove, T.L., Baker, M.B., et Kinzler, R.J. (1984). Coupled CaAl-NaSi diffusion in plagioclase feldspar: Experiments and applications to cooling rate speedometry. *Geochimical et*

Cosmochimica Acta, 48(10), 2112-2121.

Hanmer, S. (1988). Ductile thrusting at mid-crustal level, southwestern Grenville Province, *Canadian Journal of Earth Sciences, 25*(5), 1049- 1059.

Hanmer, S. et Passchier, C. (1991). *Shear-sense indicators: A review*. Ottawa: Geological Survey of Canada.

Harrison, T.M. (1981). Diffusion of ^{40}Ar in hornblende. *Contribution to Mineralogy and Petrology, 78*(3), 324-331.

Harrison, T.M., Duncan, I. et McDougall, I. (1985). Diffusion of ^{40}Ar in biotite: temperature, pressure and compositional effects. *Geochimica et Cosmochimica Acta, 49*(11), 2461-2468.

Hauzenberger, C.A., Robl, J. et Stüwe, K. (2005). Garnet zoning in high pressure granulite-facies metapelites, Mozambique belt, SE-Kenya constraints on the cooling history. *European journal of mineralogy, 17*(1), 43-55.

Hayden L.A., Watson E.B. (2007). Rutile saturation in hydrous siliceous melts and its bearing on Ti thermometry of quartz and zircon. *Earth and Planetary Sciences Letters, 258*(3), 561-568

Hébert, C., Lacoste, P. (1998). *Géologie de la région de Jonquière-Chicoutimi (22D/06)*. Québec: Ministère des Ressources naturelles.

Hébert, C., van Breemen, O., Cadieux, A.M. et Gosselin, C. (2009). *Région du réservoir Pipmuacan, (SNRC 22E): synthèse géologique*. Québec: Ministère des ressources naturelles et de la faune.

Henry, D.J., Guidotti, C.V. et Thomson, J.A. (2005). The Ti-saturation surface for low-to-medium pressure metapelitic biotites: Implications for geothermometry and Ti-substitution mechanisms. *American Mineralogist, 90*(2-3), 316-328.

Herd, K., Ackerman, D., Windley, B.F., et Rondot, J. (1986). Sapphirine-garnet rocks, St. Maurice area, Québec: petrology and implications for tectonics and metamorphism. *Geological Association of Canada, Special Paper, 31*, 241-253.

Hill, E.J. (1994). Geometry and kinematics of shear zones formed during continental extension in eastern Papua New Guinea. *Journal of Structural Geology, 16*(8), 1093-1105.

Hill, E.J., Baldwin, S.L. et Lister, G.S. (1992). Unroofing of active metamorphic core complexes in the D'Entrecasteaux Islands, Papua New Guinea. *Geology, 20*(10), 907-910.

Hocq, M. et Dufour S. (2002). Compilation Géologique – *Réservoir Taureau*. Québec : Ministère des Ressources Naturelles et de la Faune.

Hodges, K.V., Burchfiel, B.C., Royden, L.H., Chen, Z. et Liu, Y. (1993). The metamorphic signature of contemporaneous extension and shortening in the central Himalayan orogen: data from the Nyalam transect, southern Tibet. *Journal of Metamorphic Geology, 11*(5), 721-737.

Holdaway, M.J. (2001). Recalibration of the GASP geobarometer in light of recent garnet and plagioclase activity models and versions of the garnet-biotite geothermometer. *American Mineralogist, 86*(10), 1117-1129.

Hollister, L.S. (1966). Garnet zoning : an interpretation based on the Rayleigh Fractionation

model. *Science 154*(3757), 1647-1651.

Hoskin, P.W.O. et Black, L.P. (2000). Metamorphic zircon formation by solid-state recrystallization of protolith igneous zircon. *Journal of Metamorphic Geology, 18*(4), 423-439.

Hoskin, P.W.O. et Shaltegger, U. (2003). The composition of zircon and igneous and metamorphic petrogenesis. *Reviews in Mineralogy and Geochemistry, 53*(1), 27-62.

Howie, R.A. (1967). Charnockites and their colour. *Journal of the Geological Society of India 8*, 1-7.

Hynes, A. et Rivers, T. (2010). Protracted continental collision evidence from the Grenville Orogen. *Canadian Journal of Earth Sciences, 47*(5), 591-620.

Indares, A., Dunning, G., Cox, R., Gale, D., et Connelly, J. (1998). High-pressure, high-temperature rocks from the base of thick continental crust: geology and age constraints from the Manicouagan Imbricate Zone, eastern Grenville Province. *Tectonics, 17*(3), 426-440.

Jamieson, R.A., Beaumont, C., Nguyen, M.H., et Culshaw, N.G. (2007). Synconvergent ductile flow in variable-strength continental crust: numerical models with application to the western Grenville orogen. *Tectonics, 26*(5), TC5005-1-23.

Jamieson, R.A., Beaumont, C., Warren, C.J., et Nguyen, M.H. (2010). The Grenville Orogen explained? Applications and limitations of integrating numerical models with geological and geophysical data. *Canadian Journal of Earth Sciences, 47*(4), 517-539.

Jourdan, F. et Renne. P.R. (2007). Age calibration of the Fish Canyon sanidine $^{40}Ar/^{39}Ar$ dating standard using primary K-Ar standards. *Geochimimica Cosmochimica Acta, 71*(2), 387-402.

Jourdan, F., Verati, C. et Féraud. G. (2006). Intercalibration of the Hb3gr $^{40}Ar/^{39}Ar$ dating standard. *Chemical Geology, 231*(3), 77-189.

Kohn, M.J. et Spear, F. (2000). Retrograde net transfer reaction insurance for pressure-temperature estimates. *Geology, 28*(12), 1127-1130.

Kretz, R. (1983). Symbols for rock-forming minerals. *American Mineralogist, 68*, 277-279.

Lana, C., Kisters, A. et Stevens, G. (2010). Exhumation of Mesoarchean TTG gneisses from the middle crust: Insights from the Steynsdorp core complex, Barberton granitoid-greenstone terrain, South Africa. *Geological Society of America Bulletin, 122*(1-2), 183-197.

Leake, B.E. (1978). Nomenclature of amphiboles. *Canadian Mineralogist, 14*(4), 501-520.

Lee, J.Y., Marti, K., Severinghaus, J.P., Kawamura, K., Yoo, H.S., Lee, J.B. et Kim, J.S. (2006). A redetermination of the isotopic abundances of atmospheric Ar. *Geochimica et Cosmochimica Acta, 70*(17), 4507-4512.

Lemieux, É.B. (1992). *Analyse structurale de la partie nord du groupe de Montauban, province de Grenville* (Mémoire de maîtrise). Université Laval, Québec, Canada.

Lévesque, S. (1995). *Zonation metamorphique et évolution thermique de la region Portneuf-Mauricie, orogène de Grenville* (Mémoire de maîtrise). Université Laval, Québec.

Lister, G.S., et Davis, G.A. (1989). The origin of metamorphic core complexes and detachment faults formed during Tertiary continental extension in the northern Colorado River region,

USA. *Journal of Structural Geology*, *11*(1), 65-94.

Ludwig, K.R. (2003). *User's Manual for Isoplot 3.00.* Berkeley: Geochronology Center.

MacLean, W.H., Stamatelopoulou-Seymour, K. et Prahbu, M.K. (1982). Sr, Y, Zr, Nb, Ti, and REE in Grenville amphibolites at Montauban-les-Mines, Quebec. *Canadian Journal of Earth Sciences, 19*(4), 633 -644.

Mäder, U.K., Percival, J.A. et Berman, R.G. (1994). Thermobarometry of garnet-clinopyroxene-hornblende granulites from the Kapuskasing structural zone, *Canadian Journal of Earth Sciences, 31*(7), 1134-1145.

Mark, D.F., Stuart, F.M. et De Podesta, M. (2011). New high-precision measurements of the isotopic composition of atmospheric argon. *Geochimica et Cosmochimica Acta*, *75*(23), 7494-7501.

Martignole, J. (1975). *Le Précambrien dans le sud de la province tectonique de Grenville (Bouclier Canadien)* (Thèse de doctorat d'état). Université Paul Sabatier, Toulouse.

Martignole, J. et Corriveau, L. (1991). Lithotectonic studies in the Central Metasedimentary Belt of the southern Grenville Province: Lithology and structure of the Saint Jovite map area, Québec. *Geological Survey of Canada, Current research, part C*, 77-87.

Martignole, J. et Friedman, R. (1998). Geochronological constraints on the last stages of terrane assembly in the central part of the Grenville Province. *Precambrian Research, 92*(2), 145-164.

Martignole J. et Nantel, S. (1982). Geothermobarometry of cordierite-bearing metapelites near the Morin anorthosite complex, Grenville Province, Quebec. *Canadian Mineralogist 20*(3), 307-318.

McLelland, J., Daley, J.S., et McLelland, J.M. (1996). The Grenville orogenic cycle (ca. 1350-1000 Ma): an Adirondack perspective. *Tectonophysics, 265*(1-2), 1-28.

Nadeau, L. et Brouillette, P. (1994). Structural map of the La Tuque area (NTS 31P), Grenville Province, Quebec. *Geological Survey of Canada, Open File 2938*, échelle 1 : 250 000.

Nadeau, L. et Brouillette, P. (1995). Structural map of the Shawinigan area (NTS 31I), Grenville Province, Quebec. *Geological Survey of Canada, Open File 3012*, échelle 1 : 250 000.

Nadeau, L., Brouillette, P. et Hébert, C., (1999). New observations on relict volcanic features in medium-grade gneiss of the Montauban group, Grenville Province, Quebec. *Geological Survey of Canada, Current Research, E*, 149-160.

Nadeau, L., Brouillette, P. et Hébert, C., (1992). Geology and structural relationships along the east margin of the St.Maurice tectonic zone, north of Montauban, Grenville orogen, Quebec. *Geological Survey of Canada, Current Research, C,* 139-146.

Nadeau, L., Brouillette, P. et Hébert, C. (2008, mai). *Arc magmatism, continental collision and exhumation: the mesoproterozoic evolution of the south-central Grenville Province, Portneuf-Mauricie region, Quebec*. Livret d'excursion du congrès annuel de la Geological Association of Canada – Mineralogical Association of Canada, Québec.

Nadeau, L., Brouillette, P. et Hébert, C. (2009). *Geological compilation map of the Portneuf-St.Maurice region, Grenville Province, Quebec* (GM 63830). Québec : Ministère des

Ressources Naturelles et de la Faune.

Nadeau, L. et Corrigan, D. (1991). Preliminary notes of the geology of the St-Maurice tectonic zone, Grenville orogen, Quebec. *Geological Survey of Canada, Current research,* E, 245-255.

Nadeau, L. et Van Breemen, O. (2001). U-Pb Zircon Age and Regional Setting of the Lapeyrère Gabbronorite, Portneuf-Mauricie Region, South Central Grenville Province, Quebec. *Geological Survey of Canada, Current research, part F6,* 1-8.

Nadeau, L. et van Breemen, 0. (1994, mai). *Do the 1.45-1.39 Ga Montauban group and the La Bostonnais complex constitute a Grenvillian accreted terrane?* Communication présentée au congrès annuel de la Geological Association of Canada – Mineralogical Association of Canada, Waterloo, résumé 19: A81.

Passchier, C. W., et Trouw, R.A.J. (2005). *Microtectonics* (2e éd.). Berlin : Springer.

Pattison, D.R.M. (1992). Stability of andalusite and sillimanite and the Al_2SiO_5 triple point: constraints from the Ballachulish aureole, *The Journal of Geology, 100*(4), 423-446.

Pan, Y. (1997). Zircon- and monazite-forming metamorphic reactions at Manitouwadge, Ontario. *The Canadian Mineralogist, 35*(1), 105-118.

Peck, W.H., DeAngelis, M.T., Meredith, M.T. et Morin, E. (2005). Polymetamorphism of marbles in the Morin terrane, Grenville Province, Quebec. *Canadian Journal of Earth Sciences, 42*(10), 1949-1965.

Peck, W.H. (2012). Reconnaissance geochronology and geochemistry of the Mont-Tremblant gneiss of the Morin terrane, Grenville Province, Québec. *Geosphere, 8*(6): 1356-1365.

Percival, J.A. (1989). A regional perspective of the Quetico metasedimentary belt, Superior Province, Canada. Canadian Journal of Earth Sciences, 26(4), 677-693.

Percival, J.A. (1991). Orthopyroxene-poikilitic tonalites of the Desliens igneous suite, Ashuanipi granulite complex, Labrador-Quebec, Canada. Canadian Journal of Earth Sciences, 28(5), 743-753.

Pidgeon, R.T. et Howie, R.A. (1975). U-Pb Age of Zircon from a Charnockitic Granulite from Pangnirtung on the East Coast of Baffin Island. *Cananadian Journal of Earth Sciences 12*(6), 1046-1047.

Powell, R. et Downes, J. (1990). Garnet porphyroblast-bearing leucosomes in metapelites: mechanisms, phase diagrams, and an example from Broken Hill, Australia. Dans *High-temperature metamorphism and crustal anatexis (p. 105-123).* Netherlands: Springer.

Renne, P.R., Balco, G., Ludwig, R.L., Mundil, R. et Min. K. (2011). Response to the comment by W.H. Schwarz et al. on "Joint determination of ^{40}K decay constants and $^{40}Ar^*/^{40}K$ for the Fish Canyon sanidine standard, and improved accuracy for $^{40}Ar/^{39}Ar$ geochronology" by PR Renne et al. (2010). *Geochimica et Cosmochimica Acta, 75*(17), 5097-5100.

Renne, P.R., Mundil, R., Balco, G., Min, K. et Ludwig R.L. (2010). Joint determination of ^{40}K decay constants and $^{40}Ar^*/^{40}K$ for the Fish Canyon sanidine standard, and improved accuracy for $^{40}Ar/^{39}Ar$ geochronology. *Geochimica et Cosmochimica Acta 74*(18), 5349-5367.

Rey, P.F., Teyssier, C. et Whitney, D.L. (2009). Extension rates, crustal melting, and core complex dynamics. *Geology, 37*(5), 391-394.

Rey, P.F., Vanderhaeghe, O. et Teyssier, C. (2001). Gravitational collapse of the continental crust: Definition, regimes and modes. *Tectonophysics, 342*(3), 435-449.

Ring, U., Brandon, M.T., Lister, G.S. et Willet, S.D. (1999). Exhumation Processes. *Geological Society, London, Special Publications, 154,* 1-27.

Rivers, T. (1997). Lithotectonic elements of the Grenville Province: review and tectonic implications. *Precambrian Research, 86*(3), 117-154.

Rivers, T. (2008). Assembly and preservation of lower, mid and upper orogenic crust in the Grenville Province – Implications for the evolution of large, hot long-duration orogens. *Precambrian Research, 167*(3), 237-259.

Rivers, T. (2009). The Grenville Province as a large hot long-duration collisional orogen – insights from the spatial and thermal evolution of its orogenic fronts. *Geological Society, London, Special Publication 327*(1), 405-444.

Rivers, T. (2012). Upper-crustal orogenic lid and mid-crustal core complexes: signature of a collapsed orogenic plateau in the hinterland of the Grenville Province. *Canadian Journal of Earth Sciences, 49*(1), 1-42.

Rivers, T., Martignole, J., Gower, C.F. et Davidson, A. (1989). New tectonic divisions of the Grenville Province, southeast Canadian shield. *Tectonics, 8*(1), 63-84.

Robinson, P., Spear, F.S., Schumacher, J.C., Laird, J., Klein, C., Evans, B.W. et Doolan, B.L. (1982). Phase relations of metamorphic amphiboles: natural occurrence and theory. *Reviews in Mineralogy and Geochemistry, 9*(1), 1-211.

Roddick, J.C. (1983). High precision intercalibration of $^{40}Ar/^{39}Ar$ standards. *Geochimica et Cosmochimica Acta, 47*(5), 887-898.

Rondot, J. (1962). *Région de Matawin – Lac Chat est (comtés de Laviolette et de Portneuf)* (DPV-373). Québec: Ministère des Richesses naturelles du Québec.

Rosenberg, C.L., et Handy, M.R. (2005). Experimental deformation of partially melted granite revisited: implications for the continental crust. *Journal of Metamorphic Geology, 23*(1), 19-28.

Rubatto, D., Williams, I.S. et Buick, I.S. (2001). Zircon and monazite response to prograde metamorphism in the Reynolds Range, central Australia.*Contributions to Mineralogy and Petrology, 140*(4), 458-468.

Ruffet, G., Féraud, G. et Amouric, M. (1991). Comparison of $^{40}Ar/^{39}Ar$ conventional and laser dating of biotites fram the North Trégor Batholith. *Geochimica et Cosmochimica Acta, 55*(6), 1675-1688.

Ruffet, G., Féraud, G., Ballèvre, M. et Kiénast, J.R. (1995). Plateau ages and excess argon on phengites: a $^{40}Ar/^{39}Ar$ laser probe study of alpine micas (Sesia zone). *Chemical Geology, 121*(11), 327-343.

Ruppel, C., Royden, L. et Hodges, K.V. (1988). Thermal modeling of extensional tectonics: application to pressure-temperature-time histories of metamorphic rocks. *Tectonics, 7*(5),

947-957.

Sappin, A.A., Constantin, M., Clark, T. et van Breemen, O. (2009). Geochemistry, geochronology, and geodynamic setting of NiCu PGE mineral prospects hosted by mafic and ultramafic intrusions in the Portneuf-Mauricie Domain, Grenville Province, Quebec. *Canadian Journal of Earth Sciences*, *46*(5), 331-353.

Schaubs, P.M., Carr, S.D. et Berman, R.G. (2002). Structural and metamorphic constraints on ca. 70Ma deformation of the northern Valhalla complex, British Columbia: implications for the tectonic evolution of the southern Omineca belt. *Journal of structural geology*, *24*(6), 1195-1214.

Schrijver, K. (1973). Correlated changes in mineral assemblages and in rock habit and fabric across an orthopyroxene isograd, Grenville Province, Quebec. *American Journal of Science, 273*(2), 171-186.

Scott, D.J. et St-Onge, M.R. (1995). Constraints on Pb closure temperature in titanite based on rocks from the Ungava orogen, Canada: Implications for U-Pb geochronology and PTt path determinations. *Geology*, *23*(12), 1123-1126.

Selleck, B.W., McLelland, J.M. et Bickford, M.E. (2005). Granite emplacement during tectonic exhumation: The Adirondack example. *Geology, 33*(10), 781-784.

Sláma, J., Košler, J, Condon, D.J., Crowley, J.L., Gerdes, A., Hanchar, J.M., Horstwood, M.S.A., Morris, G.A., Nasdala, L., Norberg, N., Schaltegger, U., Schoene, B., Tubrett, M.N. et Whitehouse, M.J. (2008). Plešovice zircon — A new natural reference material for U-Pb and Hf isotopic microanalysis. *Chemical Geology, 249*(1), 1-35.

Snoke, A.W., Tullis, J. et Todd, V.R. (1998). *Fault-related Rocks: A Photographic Atlas*. Princeton: Princeton University Press.

Spear, F.S. (1993). *Metamorphic phase equilibria and pressure-temperature-time paths*. Washington, D.C.: Mineralogical Society of America.

Spear, F.S. et Florence, F.P. (1992). Thermobarometry in granulites: pitfalls and new approaches. *Precambrian Research*, *55*(1), 209-241.

Spear, F.S., Kohn, M.J. et Cheney, J.T. (1999). P-T paths from anatectic pelites. *Contributions to Mineralogy and Petrology, 134*(1), 17-32.

Spear, F.S. et Parrish, R.R. (1996). Petrology and cooling rates of the Valhalla Complex, British Columbia, Canada. *Journal of Petrology, 37*(4), 733-765.

Storm, L.C. et Spear, F.S. (2005). Pressure, temperature and cooling rates of granulite facies migmatitic pelites from the southern Adirondack Highlands, New York. *Journal of Metamorphic Geology*, *23*(2), 107-130.

Sullivan, W. A., & Snoke, A. W. (2007). Comparative anatomy of core-complex development in the northeastern Great Basin, USA. *Rocky Mountain Geology,42*(1), 1-29.

Sun, S.S. et McDonough, W.F. (1989). Chemical and isotopic systematics of oceanic basalts: implications for mantle composition and processes. Geological Society, London, *Special Publications, 42*(1), 313-345.

Teyssier, C. et Whitney, D.L. (2002). Gneiss domes and orogeny. *Geology, 30*(12), 1139-1142.

Tirel, C. (2004). *Dynamique de l'extension des domaines continentaux épaissis: dômes métamorphiques et écoulement de la croûte ductile* (Thèse de doctorat). Université de Rennes, Rennes.

Tirel, C., Brun, J.P. et Burov, E. (2004). Thermomechanical modeling of extensional gneiss domes. *Geological Society of America Special Papers, 380*, 67-78.

Tirel, C., Brun, J.P. et Burov, E. (2008). Dynamics and structural development of metamorphic core complexes. *Journal of Geophysical Research: Solid Earth 113*(B04403), 1-25.

Tirel, C., Brun, J.P. et Sokoutis, D. (2006). Extension of thickened and hot lithospheres: Inferences from laboratory modeling. *Tectonics, 25*(1), TC1005.

Tracy, R.J. (1982). Compositional zoning and inclusions in metamorphic minerals. R*eviews in Mineralogy and Geochemistry, 10*(1), 355-397.

Tracy, R.J., Robinson, P. et Thompson, A.B. (1976). Garnet composition and zoning in the determination of temperature and pressure of metamorphism, central Massachusetts. *American Mineralogist*, 61, 762-775.

Turner, G., Huneke, J.C., Podosek, F.A. et Wasserburg G.J. (1971). $^{40}Ar/^{39}Ar$ ages and cosmic ray exposure age of Apollo 14 samples. *Earth and Planetary Science Letters, 12*(1), 19-35.

Vielzeuf, D. et Schmidt, M.W. (2001). Melting relations in hydrous systems revisited: application to metapelites, metagreywackes and metabasalts. *Contributions to Mineralogy and Petrology, 141*(3), 251-267.

Villa, I.M. (1998). Isotopic closure. *Terra Nova, 10*(1), 42-47.

Villa, I.M., Grobéty, B., Kelley, S.P., Trigila, R. et Wieler, R. (1996). Assessing Ar transport paths and mechanisms for McClure Mountains Hornblende. *Contribution to Mineralogy and Petrolology, 126*(1-2), 67-80.

Villa, I.M. et Puxeddu, M. (1994). Geochronology of the Larderello geothermal field: new data and the "closure temperature" issue. *Contributions to Mineralogy and Petrology, 115*(4), 415-426.

Watson, E.B. et Harrison, T.M. (2005). Zircon thermometer reveals minimum melting conditions on earliest Earth. *Science, 308*(5723), 841-844.

Watson, E.B., Wark D.A., Thomas J.B. (2006). Crystallization thermometers for zircon and rutile. *Contribution to Mineralogy and Petrolology, 151*(4), 413-433.

Wernicke, B. (1985). Uniform-sense normal simple shear of the continental lithosphere. *Canadian Journal of Earth Sciences, 22*(1), 108-125.

Winter, J.D. (2001). *An introduction to igneous and metamorphic petrology.* New York: Prentice Hall.

White, R.W., Powell, R. et Halpin, J.A. (2004). Spatially-focussed melt formation in aluminous metapelites from Broken Hill. *Journal of Metamorphic Geology, 22*(9), 825-845.

Yardley, B.W.D. (1977). An empirical study of diffusion in garnet. *American Mineralogist, 62*, 793-800.

York, D. (1968). Least squares fitting of a straight line with correlated errors. *Earth and planetary science letters, 5*, 320-324.

Zhao, X., Ji, S. et Martignole, J. (1997). Quartz microstructures and c-axis orientations in high-grade gneisses and mylonites around the Morin anorthosite (Grenville Province). *Canadian Journal of Earth Sciences, 34*(6), 819-832.